CYCLIC INJECTION, STORAGE, AND WITHDRAWAL OF HEATED WATER IN A SANDSTONE AQUIFER AT ST. PAUL, MINNESOTA

Field observations, preliminary model analysis, and aquifer thermal efficiency

By R. T. Miller

U.S. Geological Survey Open-File Report 89-261

Prepared in cooperation with the

UNIVERSITY OF MINNESOTA
and the MINNESOTA GEOLOGICAL SURVEY

U.S. DEPARTMENT OF THE INTERIOR

MANUEL LUJAN, JR. Secretary

U.S. GEOLOGICAL SURVEY

Dallas L. Peck, Director

For additional information
write to:

District Chief
U.S. Geological Survey
702 Post Office Building
St. Paul, Minnesota 55101

Copies of this report can be
purchased from:

U.S. Geological Survey
Books and Open-File Reports Section
Federal Center
Box 25425
Denver, Colorado 80225

CONTENTS

ILLUSTRATIONS

ILLUSTRATIONS --Continued

ILLUSTRATIONS--Continued

TABLES

CONVERSION FACTORS AND ABBREVIATIONS

Multiply metric units	By	To obtain inch-pound units
liter per second (L/s)	15.85	gallon per minute
meter (m)	3.281	foot
meter per day (m/d)	3.281	foot per day
square meter per day (m^2/d)	10.76	square foot per day
Joules per meter per day per degree Celsius [((J/m)/d)/°C]	1.605×10^{-4}	British thermal unit per foot per day per degree Fahrenheit
Joules per cubic meter per degree Celsius [(J/m^3)/°C]	1.492×10^{-5}	British thermal unit per cubic foot per degree Fahrenheit
kilopascal (kPa)	0.1450	pound per square inch

TEMPERATURE

degree Celsius (°C)	°F = 9/5 °C + 32	degree Fahrenheit (°F)

Sea level: In this report "sea level" refers to the National Geodetic Vertical Datum of 1929 (NGVD of 1929)--a geodetic datum derived from a general adjustment of the first-order level nets of both the United States and Canada, formerly called Sea Level Datum of 1929.

CYCLIC INJECTION, STORAGE, AND WITHDRAWAL OF HEATED WATER IN A SANDSTONE AQUIFER AT ST. PAUL, MINNESOTA

Field observations, preliminary model analysis, and aquifer thermal efficiency

By R. T. Miller

ABSTRACT

In May 1980, the University of Minnesota began a project to evaluate the feasibility of storing heated (150 °C (degree Celsius)) water in the deep (180 to 240 m (meters)) Franconia-Ironton-Galesville aquifer and later recovering it for space heating. The Aquifer Thermal-Energy Storage (ATES) system was doublet-well design in which the injection/withdrawal wells were spaced approximately 250 m apart. High-temperature water from the University's steam-generation facilities supplied heat for injection. Water was pumped from one of the wells through a heat exchanger, where heat was added or removed. Water then was injected back into the aquifer through the other well. The experimental plan for testing the ATES system consisted of a series of short-term hot-water injection, storage, and withdrawal cycles. Each cycle was 24-days long, and each injection, storage, and withdrawal step of the cycle was 8 days.

The Franconia-Ironton-Galesville aquifer is a consolidated sandstone, approximately 60 m thick, the top of which is approximately 180 m below the land surface. It is confined above by the St. Lawrence Formation--a dolomitic sandstone 8-m thick--and below by the Eau Claire Formation--a shale 30-m thick. Initial hydraulic testing with inflatable packers indicated that the aquifer has four hydraulic zones with distinctly different values of relative horizontal hydraulic conductivity. The thickness of each zone was determined by correlating data from geophysical logs, core samples, and the inflatable-packer tests.

A comprehensive network for data collection, storage, and analysis has been designed to monitor temperature and pressure changes during the ATES test cycles. A total of 22 pressure transducers and 56 thermocouples monitor pressures and temperatures in the aquifer and in the upper and lower confining units.

Temperature and pressure measurements were collected in observation well nests at distances of approximately 7 or 14 m from the production wells. All pressure and temperature data were transmitted by buried cables from the observation wells to a central data logger, where results of the measurements were viewed independently or stored on computer magnetic tape for later analysis. Interactive computer programs were available to display data stored on magnetic tapes as individual measurements or as plots of pressure and temperature versus time.

Analyses of step-drawdown and constant-discharge aquifer tests indicate that the Franconia-Ironton-Galesville aquifer is anisotropic in the horizontal plane. Major and minor transmissivities are 101.5 and 44.6 m^2/d (meters squared per day), respectively, for the Ironton and Galesville Sandstones

and 40.0 and 24.0 m^2/d, respectively, for the upper part of the Franconia Formation. The average transmissivity of the entire Franconia-Ironton-Galesville aquifer is about 98 m^2/d. Effective porosity ranges from 25 to 31 percent, and the average storage coefficient is 4.5×10^{-5}.

Two computer models have been constructed to simulate the movement of ground water and heat. The first is a nonisothermal, isotropic, single-phase, radial, ground-water flow and thermal-energy-transport model that was constructed to examine the sensitivity of model results to various hydraulic and thermal properties. The model also was used to study the potential for buoyancy flow within the aquifer and the effect of various cyclic injection/withdrawal schemes on the relative thermal efficiency of the aquifer. The second model is a fully three-dimensional ground-water flow and thermal-energy-transport model that was constructed to incorporate the anisotropy of the aquifer.

In the first model, the sensitivity analysis assumed 8 days of injection of 150 °C water at 18.9 L/s (liters per second), 8 days of storage, and 8 days of withdrawal of hot water at 18.9 L/s. The analysis indicates that, for practical ranges of hydraulic and thermal properties, the ratio of horizontal to vertical hydraulic conductivity is the least important property and thermal dispersivity is the most important property used to compute temperature and aquifer thermal efficiency.

Buoyancy flow was examined for several values of hydraulic conductivity and ratios of horizontal to vertical hydraulic conductivities. For the assumed base values of hydraulic and thermal properties, buoyancy flow was negligible. The greatest simulated buoyancy flow resulted from simulations in which horizontal hydraulic conductivity was increased to ten times the base value and in which the vertical hydraulic conductivity was set equal to the horizontal hydraulic conductivity.

The effects of various injection/withdrawal rates and durations on computed values of aquifer relative-thermal efficiency and final well-bore temperature were studied for five 1-year hypothetical test cycles of injection and withdrawal. The least-efficient scheme was 8 months injection of 150 °C water at 18.9 L/s and 4 months of withdrawal of hot water at 18.9 L/s. The most efficient scheme was obtained with 6 months of injection of 150 °C water at 18.9 L/s and 6 months of withdrawal of hot water at 37.8 L/s. The hypothetical simulations indicate that the calibrated model of the doublet-well system will be a valuable tool for use by the University in selecting a highly efficient system operation.

In the second model, analytical solutions of anisotropic hydraulic flow around the doublet-well system were obtained to provide fluid-flux boundary conditions around the heat-injection well in three dimensions. This information simplifies simulation of the doublet-well system because only the heat-injection well needs to be simulated.

This second model was calibrated with data from an 8-day ambient-temperature injection test at 18.9 L/s. Boundary-flux conditions were examined for nonisothermal conditions by simulating 8 days of injection of 150 °C water at 18.9 L/s.

Results of simulations using both models indicate that the flux-boundary conditions are adequate for simulations of short-term heat-injection testing.

INTRODUCTION

During the past decade, the concept of Aquifer Thermal-Energy Storage (ATES) has received increasing attention regarding its potential to decrease energy consumption and environmental pollution. Kazmann (1971), Meyer and Todd (1973), Hausz (1974), and Meyer and others (1976) were among the first to discuss the ATES concept. Most of these discussions, however, were restricted to economic and institutional concerns. Injection of heated or cooled fluids into aquifers had been practiced for many years (Leggett and Brashears, 1938; Guyton, 1946), but field experiments designed to evaluate the feasibility of the ATES concept for long-term, large-scale energy storage were not described until 1975 (Werner and Kley, 1977), and the first demonstration project in the United States did not begin until 1976 (Molz and others, 1978). There have been many other contributions to understanding and evaluating the ATES concept and they are described or summarized in Mercer and others (1980), Tsang (1979), and Lawrence Berkeley Laboratory (1978).

In May 1980, the University of Minnesota started a project to evaluate use of a deep, confined, sedimentary bedrock aquifer located beneath the St. Paul Campus for thermal-energy storage. The project was funded by the U.S. Department of Energy through Battelle Pacific Northwest Laboratories. Other participants in the project include the Minnesota Geological Survey, the Minnesota Energy Agency, Orr-Schelen-Mayeron and Associates, National Biocentrics, Inc., and the U.S. Geological Survey. The project was designed to evaluate the feasibility and effects of storing high-temperature (150 °C) water in the Franconia-Ironton-Galesville aquifer beneath the St. Paul Campus, and to later recover the heat for water and space heating.

The University of Minnesota test facility was doublet-well system with a spacing of approximately 250 m. Initial testing of the ATES system was with a series of hot-water injection, storage, and withdrawal cycles. Each cycle was 24-days long and the injection, storage, and withdrawal steps of the cycle were each 8-days long. During the injection and withdrawal steps, water was pumped from the Franconia-Ironton-Galesville aquifer from one of the wells, transported through a heat exchanger where it was heated or cooled, and then injected back into the aquifer through the other well. The ATES site, underlying geology, and doublet-well system are shown diagrammatically in figure 1.

The specific objectives of the U.S. Geological Survey in evaluating the ATES concept were to (1) develop an understanding of the ground-water-flow system in the vicinity of the site, (2) identify the hydraulic properties of the ground-water-flow system that are most important with respect to thermal-energy storage and identify data-collection needs for monitoring and evaluation of aquifer-system performance, (3) develop a method to evaluate flow and thermal-energy transport for various cyclic injection and withdrawal schemes and aid selection of an efficient well-system design, and (4) aid in the collection of hydraulic and thermal data during injection/withdrawal tests

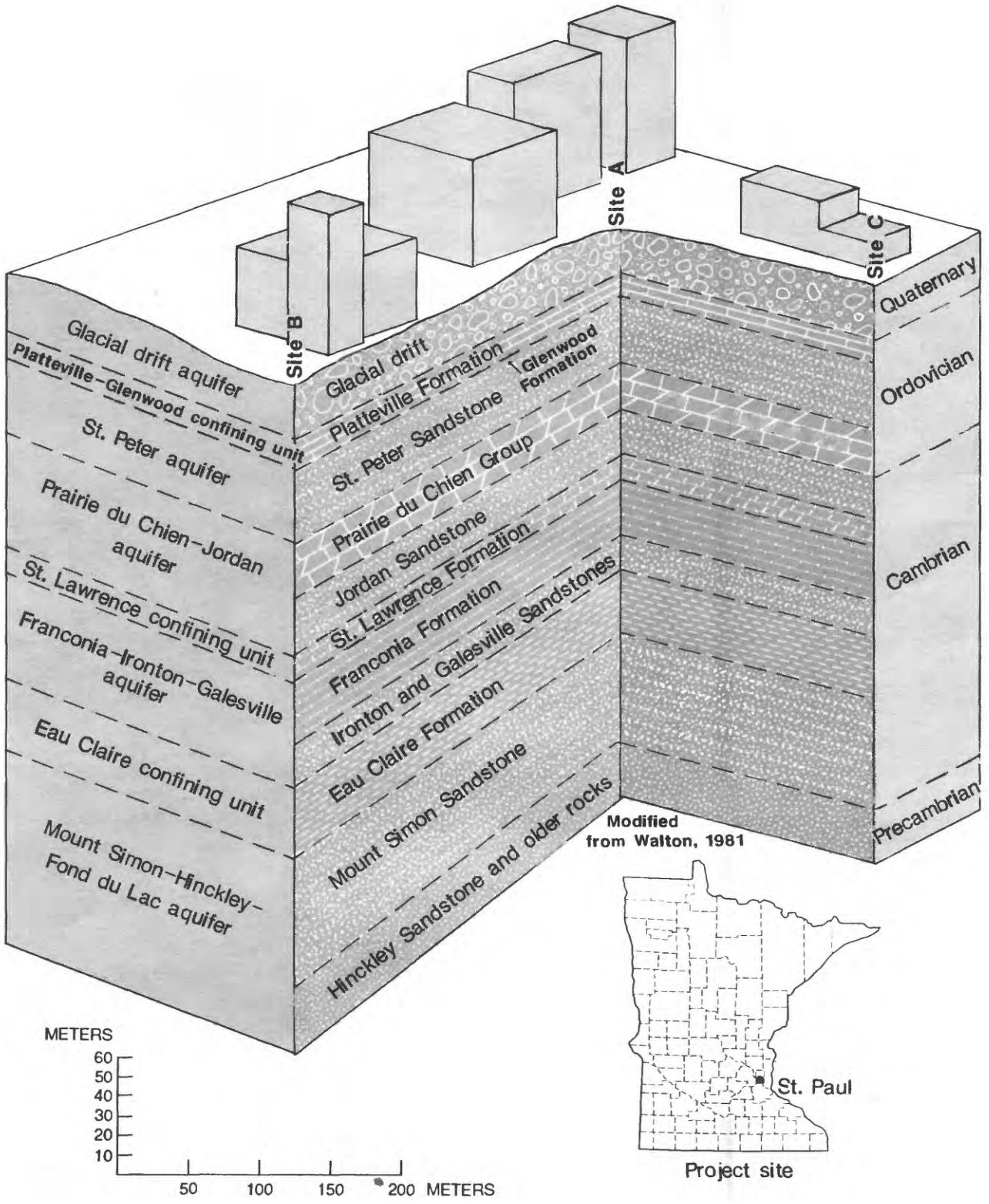

Figure1.--Location and block diagram of the Aquifer Thermal-Energy Storage site.

and the design a data-processing system to facilitate entry of the data into computer storage.

Purpose and Scope

This report describes the (1) analysis of field observations for aquifer characterization and observation network design, (2) preliminary model analysis to determine model sensitivity to hydraulic and thermal characteristics and to facilitate final model design, and (3) aquifer thermal efficiency.

This report is one in a series that describes the potential for thermal-energy storage within the Franconia-Ironton-Galesville aquifer located beneath the St. Paul campus of the University of Minnesota.

Methods

To meet the objectives described in this report, data from previous studies were collected and the analytical solutions to ground-water flow and thermal-energy transport were used in the design of the production and observation well network. Geophysical logging, packer testing, aquifer tests, step-drawdown tests, and injection tests were conducted in the production well, and in some observation wells, to obtain information on aquifer hydraulic properties.

A nonisothermal, isotropic, single-phase, radial-flow, ground-water flow and thermal-energy transport model was constructed to (1) examine the sensitivity of various hydrologic and thermal properties of the aquifer and (2) investigate the relative efficiency of the ATES system for different injection and withdrawal rates and duration. A three-dimensional, anisotropic, single-phase, nonisothermal ground-water flow and thermal-energy transport model also was constructed for calibration with ambient temperature injection/withdrawal field-test data.

Hydrogeologic Setting

The St. Paul Metropolitan Area is underlain by a stratified sequence of Proterozoic and early Paleozoic sedimentary formations consisting of porous sandstone and fractured dolomite that can be grouped into four major regional aquifers. The aquifers generally are separated by semipermeable sandstone, siltstone and shale formations. The major aquifers are the St. Peter, Prairie du Chien-Jordan, Franconia-Ironton-Galesville, and Mount Simon-Hinckley-Fond du Lac (fig. 1).

The St. Peter aquifer consists of the St. Peter Sandstone. The St. Peter Sandstone is composed of a light-yellow or white, massive, quartzose, fine- to medium-grained, well-sorted and friable sandstone. Thin beds of siltstone and shale near the base of the St. Peter Sandstone form a lower confining layer. The upper confining layer, consisting of the Glenwood and Platteville Formations, overlies the St. Peter Sandstone and is in direct contact with glacial drift. The St. Peter aquifer is approximately 45 m below land surface and is

50-m thick. Transmissivity ranges from 220 to 280 m^2/d and the storage coefficient ranges from 9.75×10^{-3} to 9.0×10^{-5}. Porosity ranges from 0.28 to 0.30. The hydraulic gradient is estimated to be 0.006 and the pore velocity is estimated to be 0.18 m/d (Norvitch and others, 1973).

The Prairie du Chien-Jordan aquifer consists of the Prairie du Chien Group and the Jordan Sandstone (fig. 1). The Prairie du Chien Group is predominantly a light brownish-gray or buff, sandy, thin- to thick-bedded dolomite that is vuggy and fractured and contains some thin layers of interbedded grayish-green shale. The underlying Jordan Sandstone is a white to yellow, quartzose, fine- to coarse-grained sandstone that is massive or thick to thin bedded and varies from friable to well cemented. Despite the differing lithologies, the Prairie du Chien Group and Jordan Sandstone function as one aquifer because there is no regional confining bed between them. At the test site the aquifer is approximately 105 m below land surface and is 64-m thick. The average transmissivity is approximately 1,235 m^2/d, with a porosity of 0.3. The hydraulic gradient has been estimated to be approximately 0.005 and the estimated pore velocity is 0.3 m/d (Norvitch and Walton, 1979).

The St. Lawrence Formation is 170 m below land surface and is approximately 8-m thick. It is a gray and greenish-gray, laminated, thin-bedded, dolomitic siltstone, silty dolomite, and shale. The porosity ranges from 15 to 20 percent and transmissivities range from 1 to 10 m^2/d.

The Franconia-Ironton-Galesville aquifer consists of the Franconia Formation, and the Ironton and Galesville Sandstones. The Franconia Formation is a gray to greenish, glauconitic, very fine- to coarse-grained quartz sandstone with some interbedded greenish-gray micaceous shale and nonglauconitic sandstone layers. The Ironton Sandstone is white, medium-grained, moderately well-sorted quartz arenite that contains some silt-sized material. The Galesville Sandstone consists of a white to light-gray slightly glauconitic, well to moderately-well sorted, mostly medium-grained quartzose sandstone. The approximate depth and thickness of the Franconia-Ironton-Galesville aquifer beneath the site are 180 and 61 m, respectively. The transmissivity has been reported to be approximately 35 m^2/d and the storage coefficient ranges from 10^{-4} to 10^{-6} (Norvitch and Walton, 1979). Average porosity is approximately 0.25 with a hydraulic gradient of 0.002 and estimated pore velocity is 0.05 m/d (Norvitch and others, 1973).

The Eau Claire Formation consists of interbedded siltstone, shale, and fine silty sandstone with a few thin layers of dolomite. The approximate depth and thickness of the formation beneath the site are 241 and 30 m, respectively. Transmissivity ranges from 0.5 to 5 m^2/d and porosity ranges from 28 to 35 percent (Norvitch and others, 1973).

The Mount Simon-Hinckley-Fond du Lac aquifer consists of the Mount Simon, Hinckley, and Fond du Lac Sandstones. The Mount Simon Sandstone is fine to coarse grained, contains very thin beds of shale, and commonly is gray, white, or pink in color. The Hinckley Sandstone is fine to coarse grained and pale red to light pink in color. The Fond du Lac Sandstone is characterized by lenticular beds of fine to medium grained arkosic sandstone interbedded with mudstone. It is dark red to pink in color. The top of the aquifer is at a depth of approximately 271 m and the aquifer is approximately 60-m thick. The transmissivity is approximately 250 m^2/d and the storage coefficient is about

6×10^{-5} (Norvitch and others, 1973). The porosity averages 0.25, the hydraulic gradient is 0.0025, and the pore velocity is approximately 0.03 m/d (Norvitch and others, 1973).

Aquifer Selection

The selection of an aquifer for heat-storage testing was based on the following criteria: (1) minimal water use from the aquifer in the Twin Cities Area, (2) adequacy of the confining units above and below the aquifer to contain the injected heated water, and (3) the hydrogeologic properties and natural gradients occurring within the aquifer and their effect to control the movement of heat.

The Franconia-Ironton-Galesville aquifer was selected based on the above criteria for the following reasons: (1) the aquifer is little used in the St. Paul area for water supply owing to its relatively low transmissivity and the availability of adequate supplies at shallower depths, (2) it is well confined above by the St. Lawrence Formation, a shale approximately 8-m thick, and below by the Eau Claire Formation, a siltstone and shale approximately 30-m thick, and (3) natural ground-water movement is slow due to low hydraulic gradients and transmissivity. Thus the potential is good for heat in the aquifer to be contained near the injection well.

Location of Production and Observation Wells

The minimum spacing between injection/withdrawal wells in a doublet-well energy-storage system is directly related to the farthest distance heat will move from the injection well. If breakthrough of the thermal front from the injection well to the withdrawal well occurs during injection, the efficiency of the system will be reduced because the heat being injected simply will be circulated within the aquifer system and will not be stored.

Gringarten and Sauty (1975) describe an analytical solution for determining the minimum well spacing for temperature breakthrough in a doublet-well system as a function of injection rate, duration, thermal properties of the aquifer and the confining beds, and porosity of the aquifer. The assumptions in their solution are:

1. The aquifer is of infinite areal extent, oriented horizontally, and of uniform thickness. It is confined above and below by layers that are impermeable and of infinite vertical extent.

2. Flow is steady, with a constant injection rate equal to the withdrawal rate, and all wells fully penetrate the aquifer.

3. Initially, the water and rock in all layers are at the same temperature. At time $t = 0$, the temperature of the injected water is set equal to T_i, and maintained constant thereafter. Thermal equilibrium is assumed to take place instantaneously between rock and water.

4. There is no heat transfer by conduction in the horizontal directions in the aquifer or confining layers. All heat transport is by forced convection in the horizontal direction in the aquifer and by vertical conduction above and below the aquifer.

5. Aquifer thermal and hydraulic characteristics are constant and differences in viscosity between injected and native water are insignificant.

Gringarten and Sauty (1975, p. 4962) express the minimum distance, D, between the two wells as:

$$D = \left\{ \frac{2Q\Delta t}{\left(\phi+(1-\phi)\frac{\rho_R C_R}{\rho_W C_W}\right)h + \left[\left(\phi+(1-\phi)\frac{\rho_R C_R}{\rho_W C_W}\right)^2 h^2 + 2\frac{K_R \rho_R C_R}{(\rho_W C_W)^2}\Delta t\right]^{1/2}} \right\}^{1/2} \quad (1)$$

where:

Q = injection rate [L^3/T] (cm^3/s),

Δt = duration of injection [T] (s),

ϕ = aquifer porosity [dimensionless],

$\rho_R C_R$ = heat capacity of upper confining layer [$(E/L^3)/t$] ($(cal/cm^3)/°C$),

$\rho_W C_W$ = heat capacity of water [$(E/L^3)/t$] ($(cal/cm^3)/°C$),

K_R = thermal conductivity of upper confining layer [$((E/L)/T)/t)$] ($((cal/cm)/s)/°C$), and

h = aquifer thickness [L] (cm).

The unit of energy used, by Gringarten and Sauty (1975) in equations 1 and 4 is calories, which will be used in this part of the report to remain consistent with their original work. To convert to the more commonly used energy unit, joule, used in the remainder of this report, multiply calorie by 4.187.

The minimum doublet-well spacing for the Franconia-Ironton-Galesville aquifer was determined for an injection rate of 75.6 L/s (liters per second) and duration of 4 months. The injection rate corresponds to an operational rate four times the short-term testing rate. The duration is the approximate time surplus heat energy would be available from the University steam-generating plant. The hydraulic and thermal properties needed for equation 1 are listed in table 1. The thermal properties were obtained from Clark (1966).

Table 1.--*Hydraulic and thermal properties for determination of minimum doublet-well spacing and observation well locations*

Porosity of Franconia-Ironton-Galesville aquifer	= 0.25
Heat capacity of Franconia-Ironton-Galesville aquifer	= 0.5743 $(cal/cm^3)/°C$
Heat capacity of St. Lawrence Formation	= 0.4324 $(cal/cm^3)/°C$
Heat capacity of water	= 1.00 $(cal/cm^3)/°C$
Thermal conductivity of St. Lawrence Formation	= 6.5×10^{-3} $((cal/cm)/s)/°C$
Thickness of Franconia-Ironton-Galesville aquifer	= 61 m

Substituting values from table 1 into equation 1 results in a minimum well spacing of approximately 150 m. To accommodate physical restrictions of well locations and to take advantage of existing underground utility corridors at the test site, the final production well spacing was chosen as 250 m. With this spacing a reduction in aquifer efficiency due to temperature breakthrough, as described by Gringarten and Sauty (1975), was not a problem.

Observation wells were located by assuming that the flow of injected water was radially outward from the production wells and could be described as a cylinder whose volume is described as

$$V = Qt = \pi r^2 h \phi \qquad (2)$$

where:

V = volume $[L^3]$ (m^3),

Q = rate of injection $[L^3/T]$ (m^3/s),

t = duration of injection [T] (s),

r = distance of injected water from well bore [L] (m),

h = aquifer thickness [L] (m), and

ϕ = aquifer porosity [dimensionless].

Assuming heat is transported mainly by convection with the injected water, the approximate location of the temperature front can be calculated from equation 2 by solving for r

$$r = \left(\frac{Qt}{\pi h \phi}\right)^{1/2} \tag{3}$$

Substituting the test-injection rate of 18.9 L/s and the aquifer thickness and porosity from table 1, equation 3 was solved for the approximate location of the temperature front for various times during the proposed test cycles. The temperature fronts were calculated to be approximately 11.7 and 16.5 m from the injection well for times of 4 and 8 days respectively. Based on these distance approximations and physical space limitations around the test site, radial distances of 7 and 14 m from the injection well were proposed for observation well locations.

Although equation 3 indicates that temperature fronts may pass the proposed 7- and 14-m observation well locations, the equation gives no indication of the magnitude of temperature that might be observed. Gringarten and Sauty (1975, p. 4958) give an analytical solution for one-dimensional heat flow within a streamtube in a doublet-well flow field. The assumptions in their equation are the same as those described on page 7 and 8 for calculating the minimum well spacing for a doublet-well system. The water temperature within the streamtube may be described as

$$\frac{T_o - T(S,t)}{T_o - T_i} = \operatorname{erfc}\left[\frac{(\rho_W C_W)^2}{K_R \rho_R C_R}\left(\frac{q}{S}\right)^2\left(t - \frac{\rho_A C_A}{\rho_W C_W}\frac{hS}{q}\right)\right]^{-1/2} \tag{4}$$

where:

$T(S,t)$ = temperature of the aquifer within a streamtube at some time, t, after injection started [t] (°C),

T_o = initial aquifer and confining-layer temperatures before injection [t] (°C),

T_i = temperature of injected water [t] (°C),

q = flow rate within streamtube [L^3/T] (m^3/hr),

S = area of streamtube [L^2] (m^2),

$\rho_A C_A$ = heat capacity of aquifer [$(E/L^3)/t$] ($(cal/cm^3)/°C$), and

erfc = complimentary error function = (1-erf)

and the remaining variables have been defined previously. Assuming that flow near the injection-well bore is radial, and that the drawdown effects of the withdrawal well are negligible near the injection well, the area of a streamtube at the two proposed observation well distances of 7 and 14 m can be solved as part of the area of a circle;

$$S = \frac{\pi r^2}{N} \tag{5}$$

where:

S = area of streamtube [L^2] (m^2),

r = radial distance from well [L] (m), and

N = total number of streamtubes [dimensionless].

Equation 4 was solved for temperatures at radial distances of 7 and 14 m for injection times of 4 and 8 days, an injection rate of 18.9 L/s, (68 m^3/hr (cubic meters per hour)) and a temperature of 150 °C. Variables for equation 4 are listed in table 1. The number of streamtubes for equation 5 was selected as 68, which reduces the flow rate per streamtube, q, to 1 m^3/hr. The initial aquifer/confining layer temperature is assumed to be 10 °C. The calculated values are shown in table 2.

Table 2.--*Calculated temperature values for radial distances of 7 and 14 meters at the end of 4 and 8 days of injection*

Time (days)	Distance (meters)	
	7	14
4	137 °C	127 °C
8	149 °C	146 °C

Table 2 indicates that appreciable temperature changes will occur at the two selected observation well distances during the 8-day injection test. Therefore, radial distances of 7 and 14 m were selected for observation well locations near both the injection and withdrawal wells (fig. 2).

The location of observation well CM1, chosen as a future site for another injection or withdrawal well, is approximately 280 m from production well A.

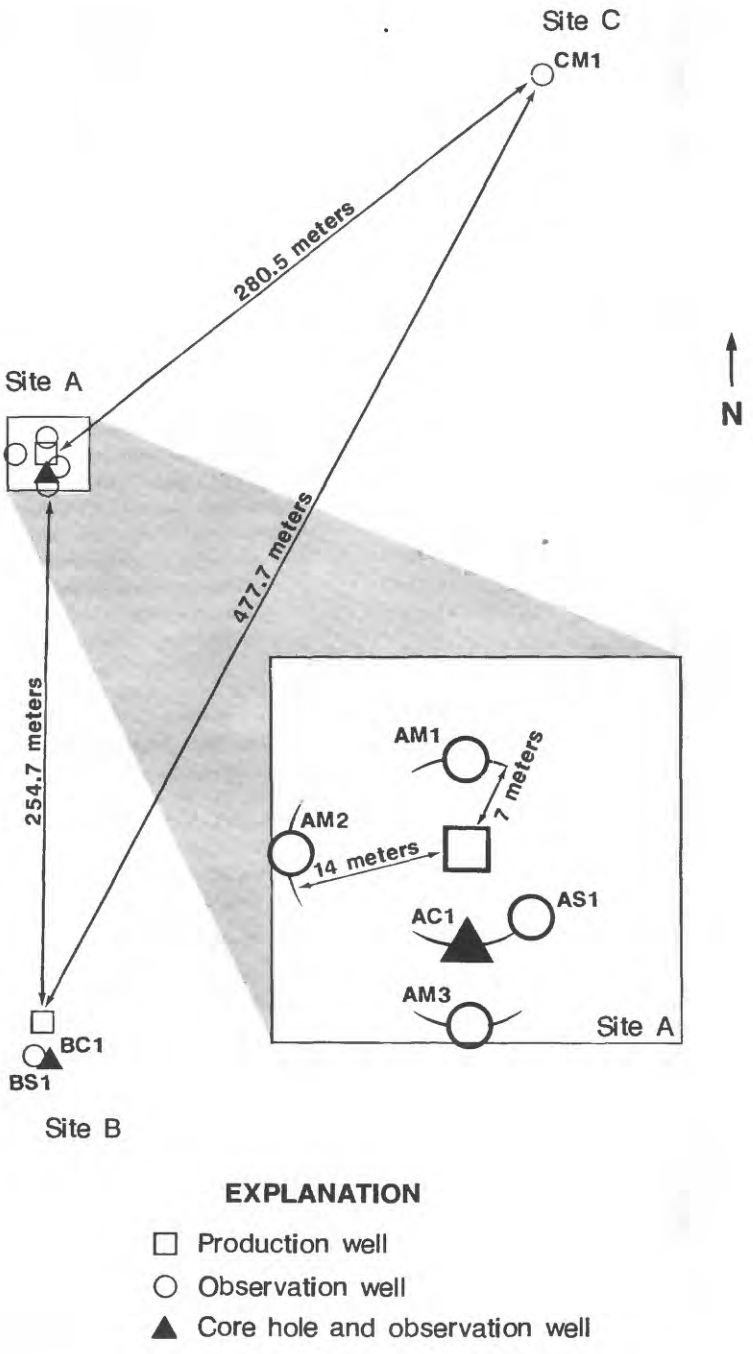

Figure 2.--Plan view of the Aquifer Thermal-Energy Storage site.

Instrumentation of Observation Wells

Measurement points in each observation well were located to obtain information on temperature and pressure in either the (1) injection zone (Franconia-Ironton-Galesville aquifer), (2) upper or lower confining beds (St. Lawrence and Eau Claire Formations), or (3) upper or lower aquifers (Jordan and Mt. Simon Sandstones). Measurement instrumentation also was designed for easy removal and replacement in case of failure. Observation wells were completed as piezometer nests using combinations of 2.54-, 3.18-, or 5.08-cm (centimeter) diameter well casings, depending on the type of instrumentation. Figure 3 illustrates the completion of individual observation wells and the location of measurement points in them. The average distance between temperature-measurement points in observation wells with 5.08-cm-diameter casings is 6.5 m to minimize the potential for thermal convection within the well casing.

Pressure transducers and thermocouples were used for all pressure and temperature measurements respectively. The pressure transducers were sealed gages with a pressure range of 0 to 1,724 kPa (kilopascals) and a compensated temperature range of 10 to 121 °C. Accuracy was $\pm$2 percent of the full-scale output over the compensated temperature range, or a maximum of $\pm$34 kPa at 121 °C. Electrical output signal was 4 to 20 milliamperes over the full scale.

Temperatures were measured using type 'T' (copper versus copper-nickel) teflon-coated thermocouples. The temperature range was from 0 to 315 °C with an accuracy of $\pm$0.4 percent for full scale or a maximum error of 1.3 °C at 315 °C. Electrical output signal was 0 to 15.76 millivolts over the full scale.

A total of 22 pressure and 58 temperature-measurement instruments were located at sites A and B. All data were transmitted via buried cables to a central data processor and stored on computer magnetic tape and paper tape. Data-reduction and display programs were constructed to manipulate the raw data. Data recorded for each measurement point could be retrieved in the form of time/measurement tables or graphical plots of time versus the measurement. Czarnecki (1983) discusses the data-reduction programs and describes their use.

FIELD OBSERVATIONS

Geophysical Logging

Geophysical logs were made of the 12.38-cm-diameter core holes at sites A and B and of the 20.32-cm-diameter test hole at site C. The logs obtained included natural gamma, temperature, specific conductance, caliper, single-point resistivity, self-potential, and flowmeter. These data were used in conjunction with the core samples to determine aquifer and confining-bed lithology. Figure 4 illustrates natural gamma logs for core holes at sites A and B and the test hole at site C and the self-potential and specific-conductance logs for the core hole at site A. Figure 5 illustrates the stratigraphy described from cores collected at sites A and B (Marcus Hoyer, Minnesota Geological Survey, written commun., 1980).

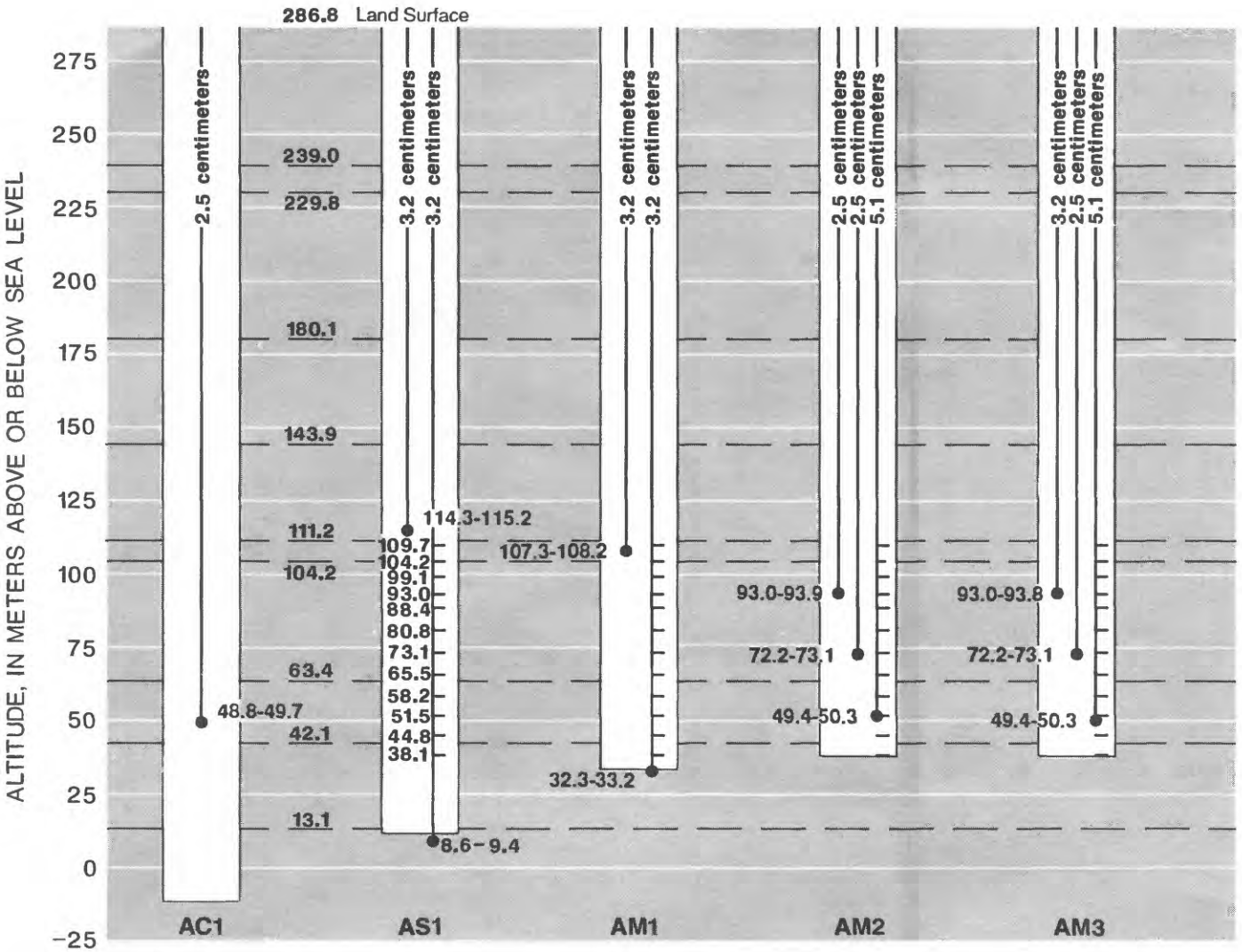

EXPLANATION

- ● Pressure measurement point with altitude, in meters
- – Temperature measurement point with altitude, in meters

Figure 3.--Depths of observation well screened

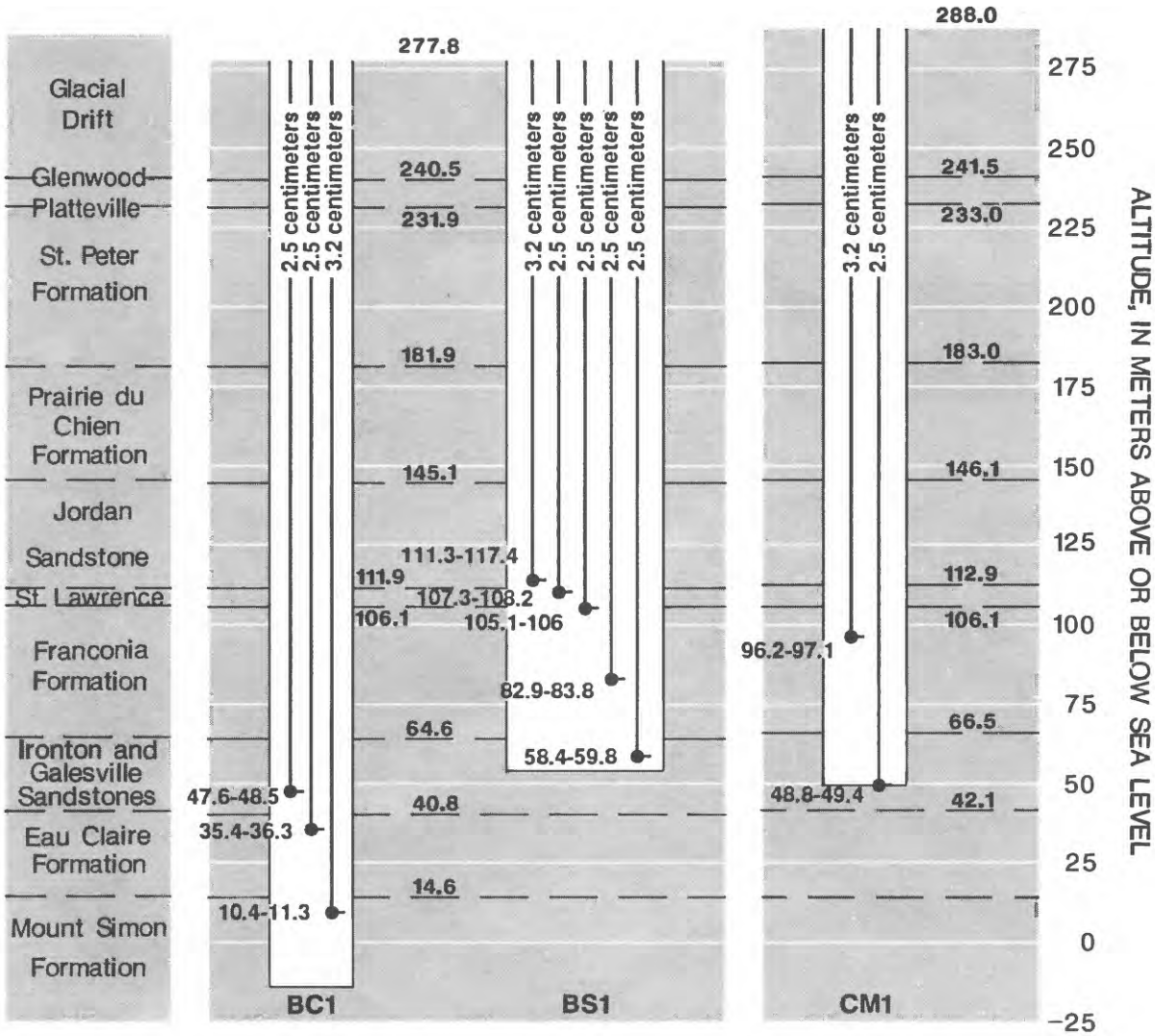

intervals and measurement point locations.

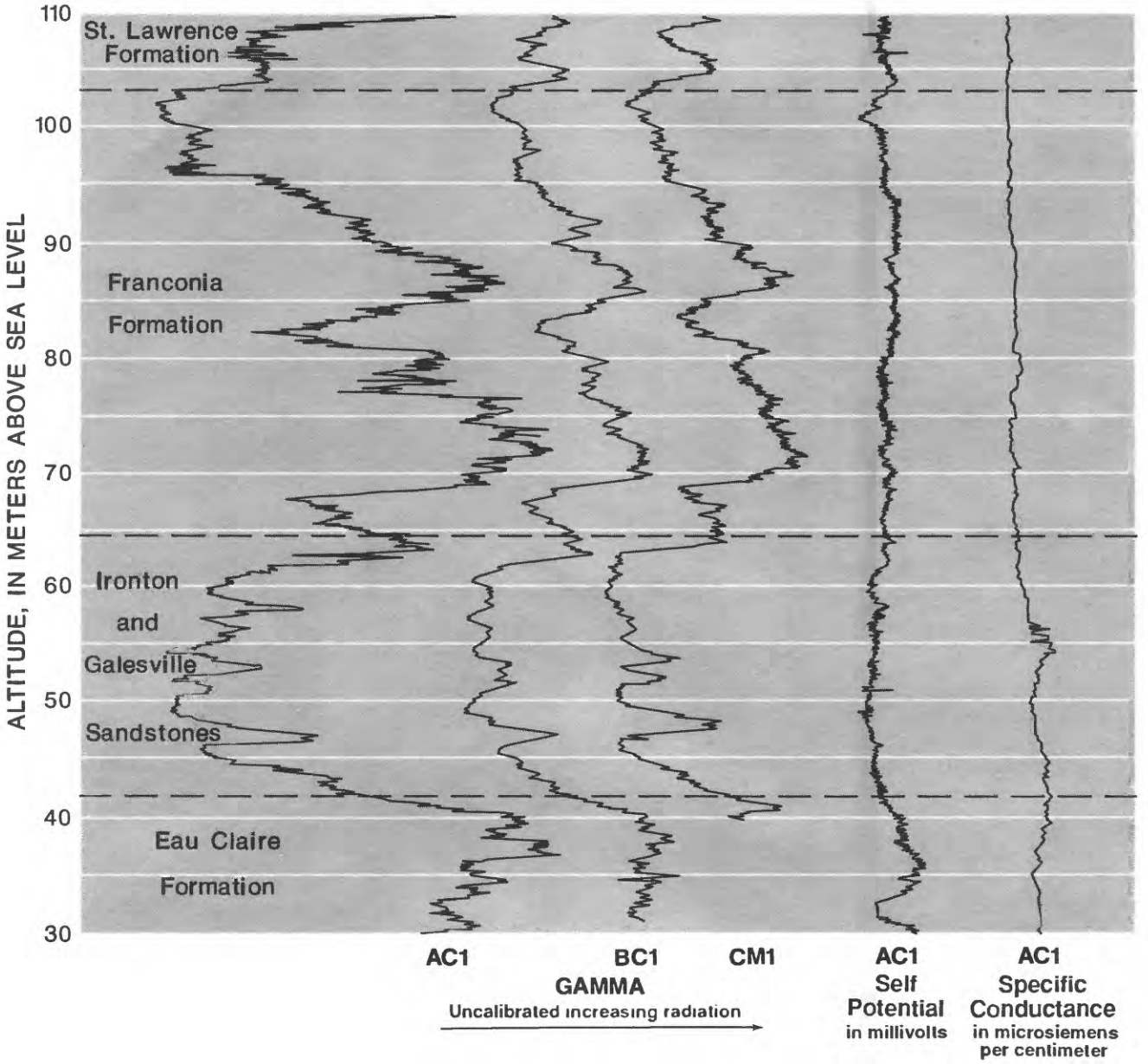

Figure 4.--Bore-hole geophysical logs of self potential, specific conductance, and natural gamma for core hole AC1 and natural gamma for core hole BC1 and observation well CM1.

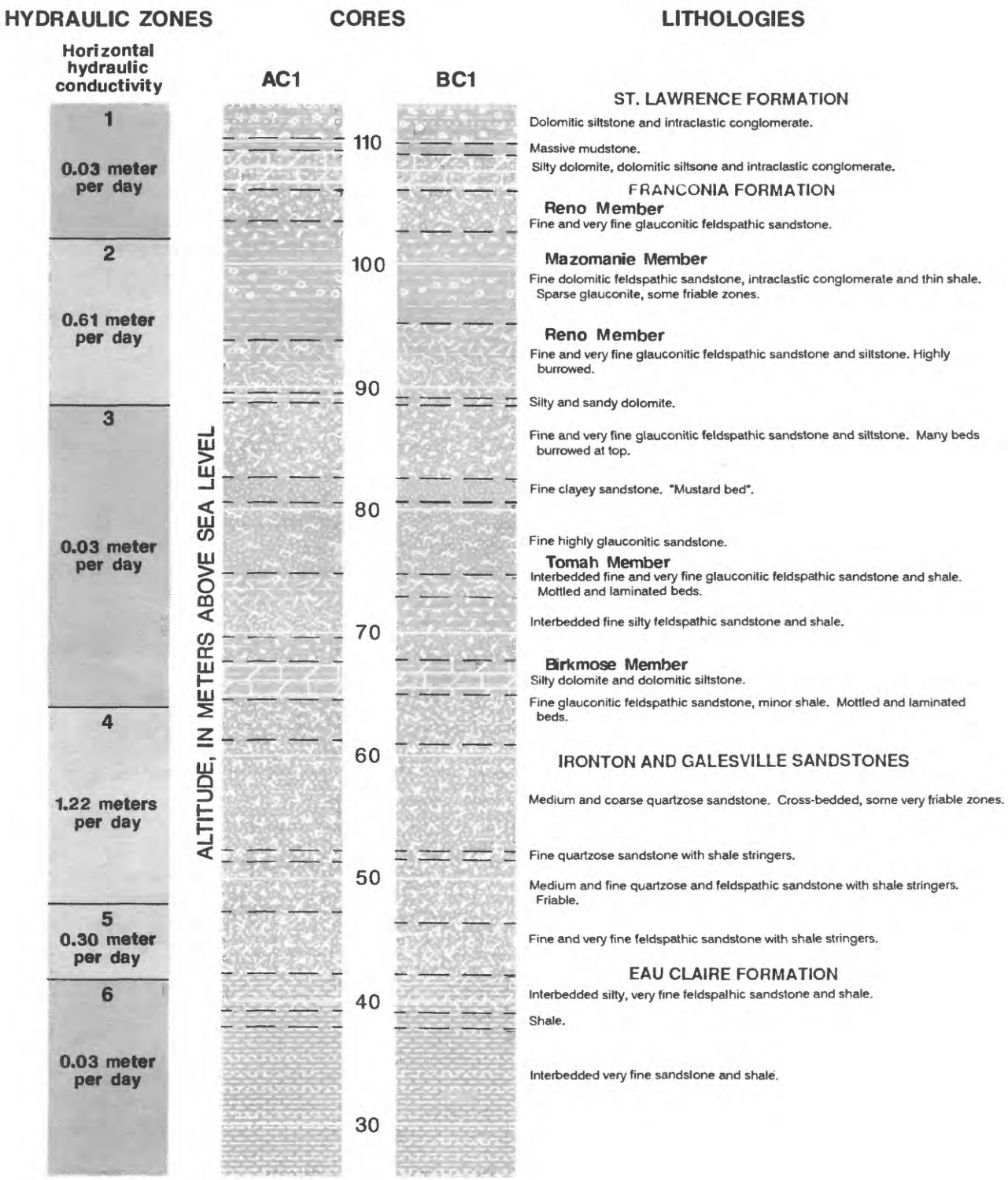

Figure 5.--Lithologies and hydraulic conductivities described from cores collected at core holes AC1 and BC1.

The similarity between the respective geophysical logs and core samples at sites A, B, and C indicate stratigraphic uniformity within the study area for the Franconia-Ironton-Galesville aquifer and the upper and lower confining beds. These data also indicate that the aquifer and confining beds are oriented horizontally. The natural gamma logs from sites A, B, and C indicate the presence of continuous, thin shale beds that also were correlated with the core samples. The natural-gamma logs also indicate a thick shale layer in the lower part of the Franconia Formation from approximately 70 to 80 m in elevation. This area corresponds to the lower Reno Member, Tomah Member, and Birkmose Member of the Franconia Formation. Geophysical-logging techniques also were used to estimate porosity variations, which will be discussed in the section on hydraulic properties.

Packer Testing

Data from inflatable straddle-packer tests in core holes at sites A and B were analyzed to determine values of relative horizontal hydraulic conductivity. Figure 6 illustrates the intervals tested in core holes AC1 and BC1, respectively.

A 7.62-cm-diameter submersible pump was installed midway between the two inflatable packers. Packer testing consisted of inflating the two packers to form a sealed interval and pumping within the straddled interval at a constant rate. Pressures within the straddled interval were measured during pumping to determine the relative horizontal hydraulic conductivity for the interval. Pressures also were measured directly above and below the interval to determine whether a proper seal between the packer and the wall of the core hole had been obtained. Pumping time for straddled intervals ranged from 5 to 20 minutes, depending on the observed rate of pressure change within the straddled interval and on the measured pumping rate. Values of relative horizontal hydraulic conductivity and transmissivity for each straddle interval were obtained based on the analysis of specific-capacity data.

Table 3 summarizes the specific-capacity, transmissivity, and relative horizontal hydraulic conductivity data and test interval for straddle-packer interval tests 1-8 in core hole AC1 and 1-18 in core hole BC1. Calculated values of transmissivity were determined from the specific capacity data for each straddle-packer interval with the methods described by Theis, Brown, and Meyer (1963) using a computer program developed by Czarnecki and Craig (1985). A storage coefficient of 2×10^{-4} was assumed for all straddle-packer intervals.

Analysis of results of the straddle-packer tests indicated the occurrence of four hydraulic zones within the Franconia-Ironton-Galesville aquifer. Visual inspection of cores and analysis of bore-hole-geophysical logs previously described were used to support and better define the location and thickness of each zone. Figures 5 and 7 shows the hydraulic zonation of the Franconia-Ironton-Galesville aquifer and the upper and lower confining beds according to values of relative hydraulic conductivity.

Table 3.--*Specific capacity, transmissivity, relative hydraulic conductivity, and interval tested for inflatable packer tests on core holes AC1 and BC1*

[(L/s)/m, liters per second per meter; m^2/d, square meters per day; m, meters; m/d, meters per day; <, less than]

Core hole	Test number	Specific capacity (L/s)/m	Transmissivity (m^2/d)	Interval tested (m)	Relative horizontal hydraulic conductivity (m/d)
AC1	1	0.007	<0.186	11.0	<0.017
AC1	2	.007	<.186	11.0	<.017
AC1	3	.117	10.2	11.0	.927
AC1	4	.051	4.18	11.0	.380
AC1	5	---- no discharge after 5 minutes pumping ----			
AC1	6	.373	32.5	126.5	.250
AC1	7	.373	28.8	75.3	.382
AC1	8	.032	3.53	11.0	.320
BC1	1	---- no discharge after 5 minutes pumping ----			
BC1	2	.039	3.26	6.40	.509
BC1	3	.269	26.6	73.2	.363
BC1	4	.168	15.9	6.4	2.48
BC1	5	.153	14.5	6.4	2.25
BC1	6	.109	10.0	6.4	1.57
BC1	7	.149	14.1	60.0	.578
BC1	8	.261	25.7	48.8	.527
BC1	9	.008	.576	6.4	.089
BC1	10	.002	.123	6.4	.019
BC1	11	.002	.123	6.4	.019
BC1	12	---- no discharge after 5 minutes pumping ----			
BC1	13	.012	.873	6.4	.136
BC1	14	.159	15.1	6.4	2.36
BC1	15	.035	2.87	6.4	.449
BC1	16	.002	.123	6.4	.019
BC1	17	.143	13.5	6.4	2.11
BC1	18	.594	61.9	97.5	.635

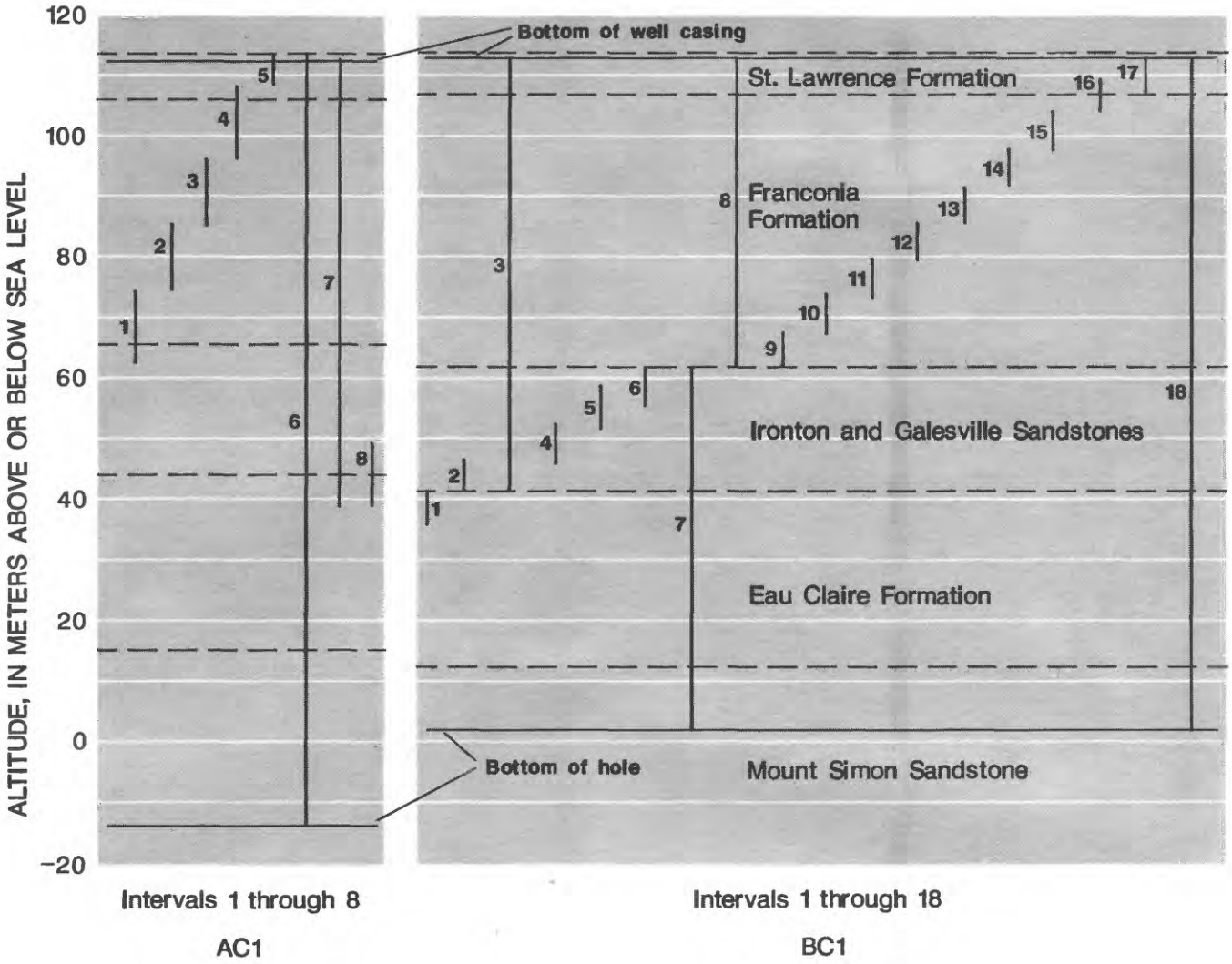

Figure 6.--Packer-test intervals for core holes AC1 and BC1.

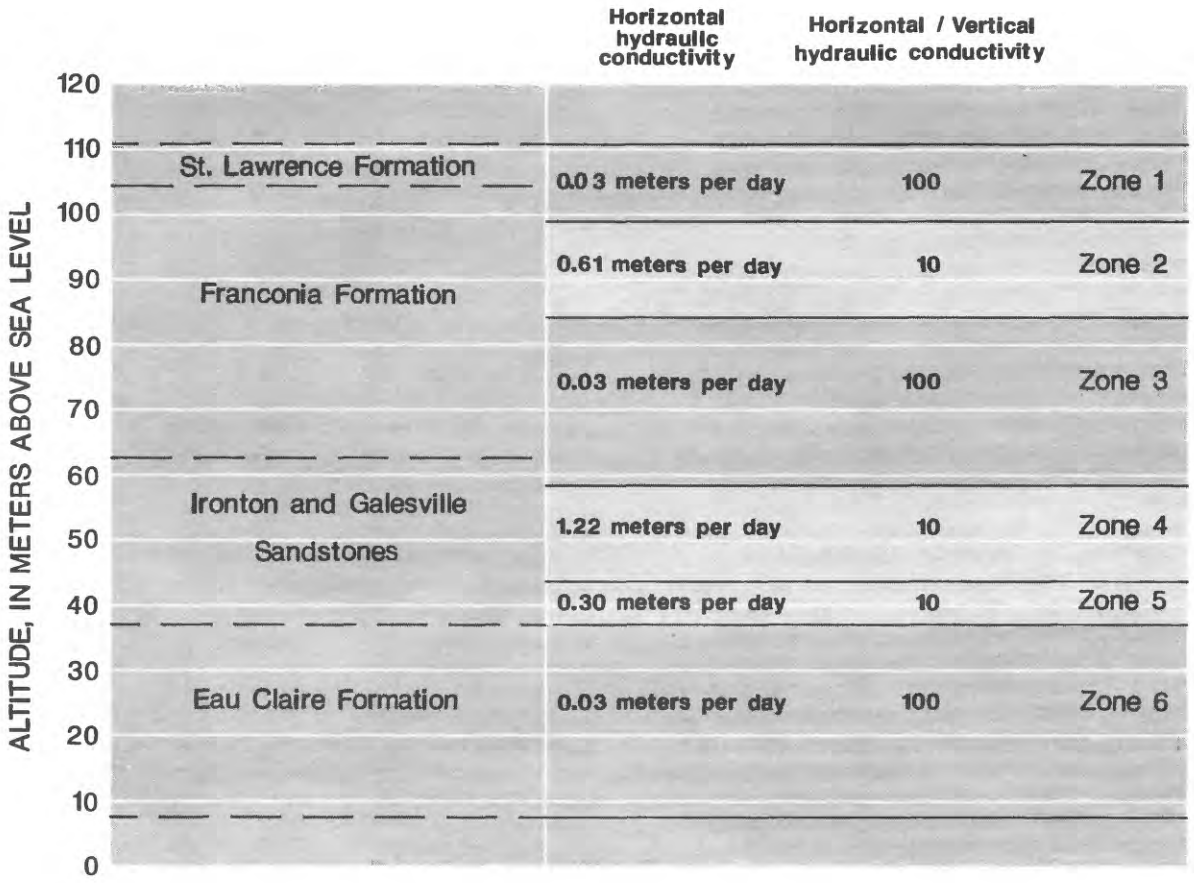

Figure 7.--Hydraulic zonation from the St. Lawrence Formation through the Eau Claire Formation based on interpretation of data from core holes AC1 and BC1.

Production Well Completion and Well-Efficiency Testing

Based on the hydraulic zonation established from the analysis of geophysical logs and from inflatable straddle-packer testing, production wells A and B were screened in two intervals, the upper 14 m of the Franconia Formation and the 21 m of the Ironton and Galesville Sandstones. Figure 8 illustrates the screened intervals and well completion for production wells A and B. The screen is wire-wound, stainless steel, 10-slot size that has been specially heat treated to withstand metal fatigue due to repeated contact with 150 °C temperature water and is set in a uniform gravel pack with an approximate grain size of 0.1 cm. The well is steel cased from land surface to the top of the well screen in several steps from 1.3-m to 30.5-cm inside diameter. A high-temperature silica cement was used to grout between the casing and the well bore.

Step-drawdown tests were made in production wells A and B immediately after well construction. Analysis of the data indicates that production well B is more efficient than production well A. Since the hydrogeologic properties are similar at both sites, the difference in well efficiencies probably is due to slightly different screen settings within the aquifer and the effectiveness of the development of each well.

Production well A was developed using the pump and surge method for approximately 8 hours. Production well A was pumped at a maximum rate of 53.5 L/s during development. The maximum drawdown observed after 3.0 hours of continuous pumping was approximately 75 m below the predevelopment static water level. After approximately 18 hours of recovery the water level was within 0.09 m of the predevelopment water level. This was considered to be sufficient recovery to conduct a step-drawdown test. Pumping durations and rates for the step-drawdown test were as follows: 202 minutes at 16.8 L/s; 164 minutes at 30.3 L/s; 104 minutes at 36.8 L/s; and 133 minutes at approximately 63 L/s. The paddle-wheel type flow meter stopped working at the beginning of the last step and the pumping rate had to be estimated. The last step was not used in analysis of the test.

Production well B also was developed by the pump-and-surge method for approximately 10 hours. The maximum rate pumped during development of production well B was 53.6 L/s for approximately 4.75 hours, maximum drawdown measured was approximately 78 m below the predevelopment static level. After approximately 12 hours of recovery, the water level was within 0.06 m of the predevelopment water level, which was considered to be sufficient recovery to conduct a step-drawdown test. Pumping durations and rates for the step-drawdown test were as follows: 258 minutes at 13.9 L/s; 217 minutes at 24 L/s; and 190 minutes at 46.4 L/s. The drawdowns for step-drawdown tests of production wells A and B are illustrated in figure 9.

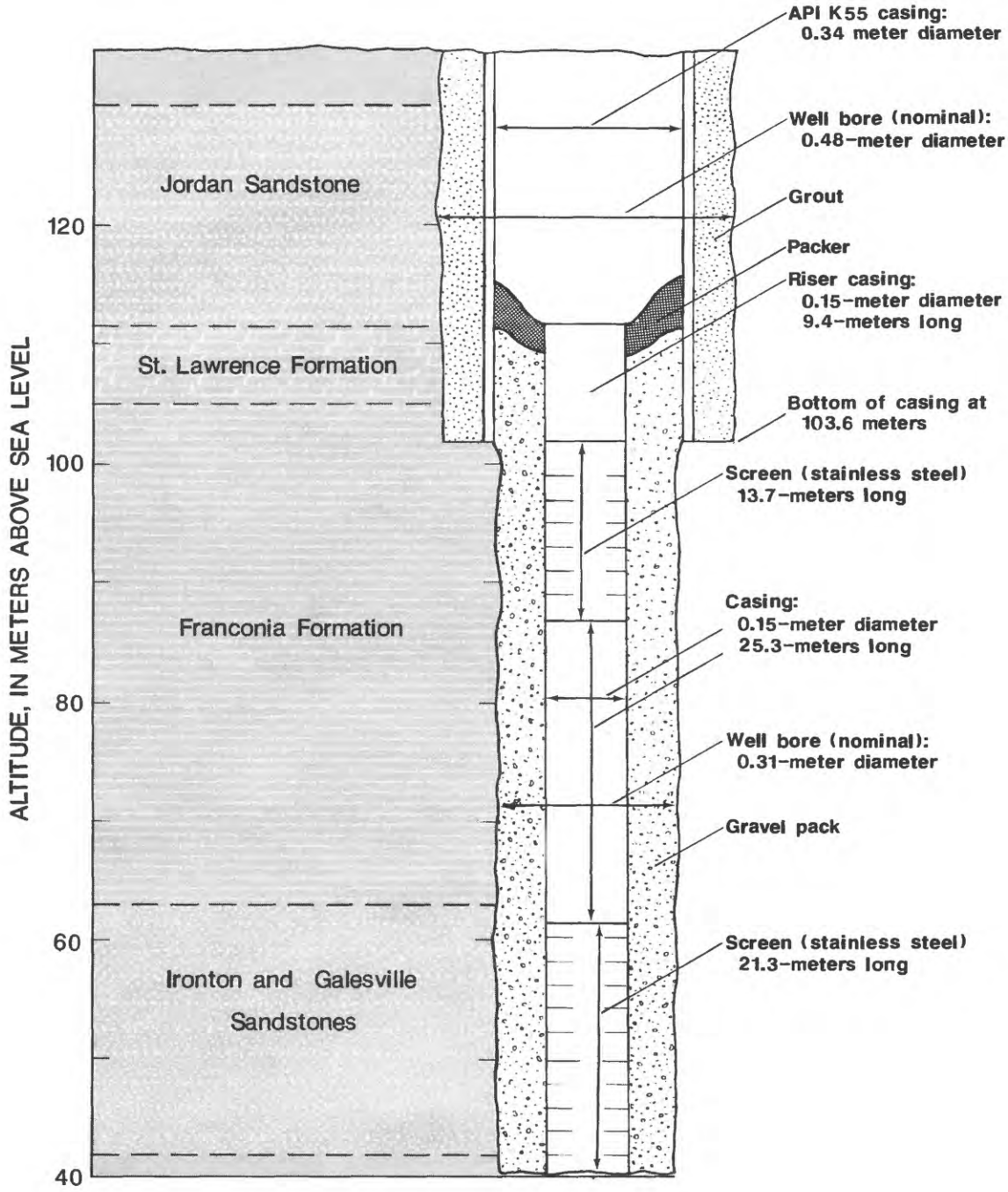

Figure 8.--Well completion and screened intervals for production wells A and B.

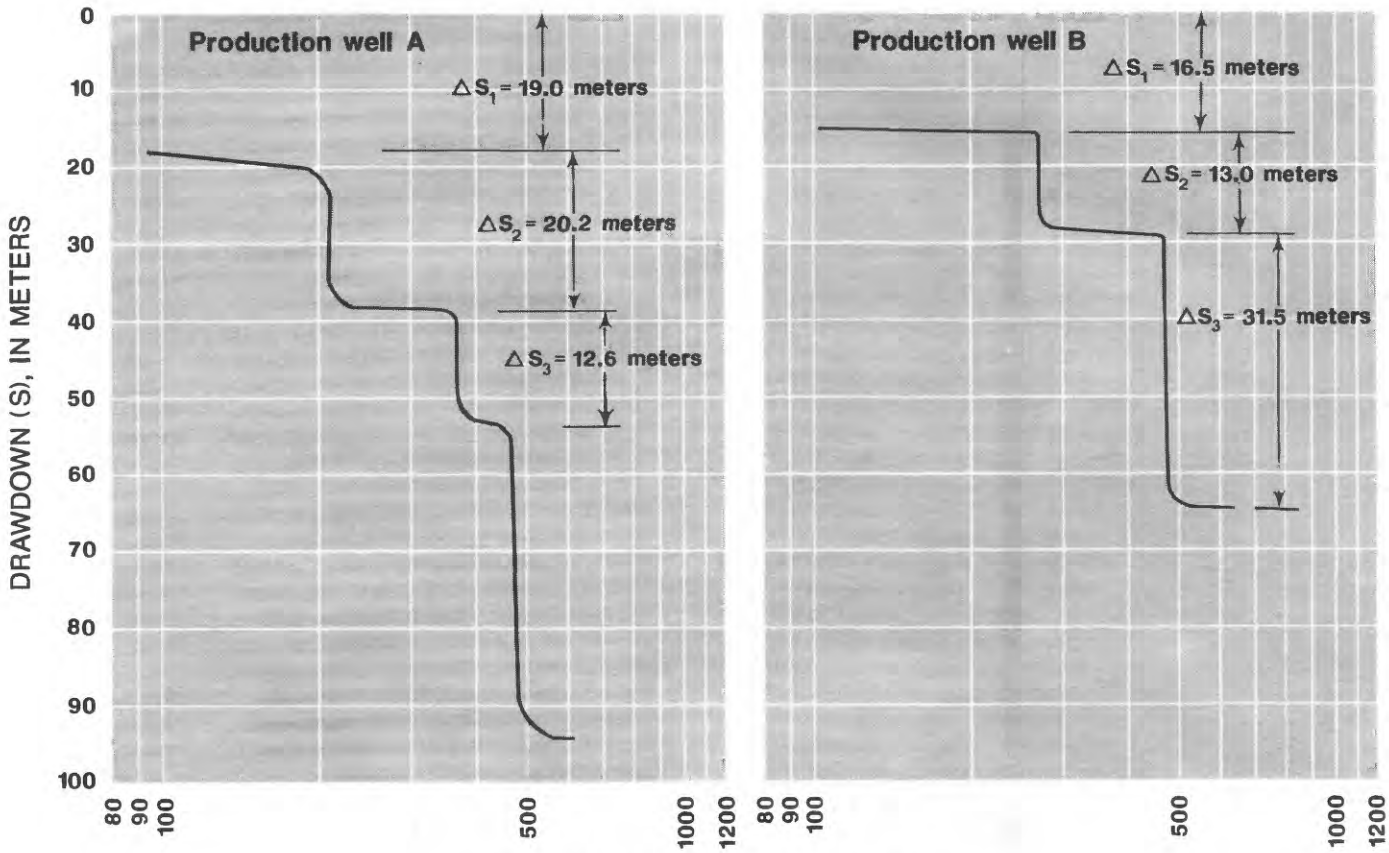

Production well A

Step	Q	ΔS	S_t	S_t/Q
1	16.842	19.0	19.0	1.128
2	30.278	20.2	39.2	1.295
3	36.839	12.6	51.8	1.406

Production well B

Step	Q	ΔS	S_t	S_t/Q
1	13.878	16.5	16.5	1.189
2	23.970	13.0	29.5	1.231
3	46.395	31.5	61.0	1.315

{Q, discharge in liters per second;
ΔS, drawdown in meters;
S_t, total drawdown in meters;
S_t/Q, total drawdown/discharge in meters per liter per second}

Figure 9.--Drawdowns for the step-drawdown tests conducted on production wells A and B.

Two methods were used to analyze data from the step-drawdown tests; a graphical method and an optimization technique. The basic formula in the step-drawdown test is (Rorabaugh, 1953; Labadie and Helweg, 1975, p. 439):

$$S = BQ + CQ^N \tag{6}$$

where

S = drawdown in the well [L] (m),

B = head-loss coefficient due to laminar flow in the aquifer,

C = head-loss coefficient due to turbulent flow in the well bore,

N = exponent that indicates the severity of turbulent head loss, and

Q = discharge of well [L^3/T] (L/s).

For the graphical method, the value of N was assumed to equal 2 (Rorabaugh, 1953). Values of S/Q and Q were plotted on rectangular coordinate paper. A straight line was drawn between the plotted points and extended to the intersection of the S/Q axis. The intersection value corresponds to the coefficient B and the slope of the line corresponds to the coefficient C. This method and the resulting coefficients, B and C, for the tests on production wells A and B are shown in figure 10. Substituting the values of B and C into equation 6 yields, for production well A,

$$S = 0.854Q + 0.0154Q^2 \tag{7}$$

and at site B,

$$S = 1.132Q + 0.0037Q^2 \tag{8}$$

Labadie and Helweg (1975) describe another method for calculating the coefficients of B, C, and N. They use a minimizing optimization technique that uses Cramer's Rule and a one-dimensional grid search to determine the coefficients. The parameter-determination problem described by equation 6 is formulated as an optimization problem of the following form (Labadie and Helweg, 1975, p. 440):

$$\text{Minimize } E(B,C,N) = \min_{B,C,N} \sum_{i=1}^{M} \left[\left(BQ_i + CQ_i^N \right) - S_i \right]^2 \tag{9}$$

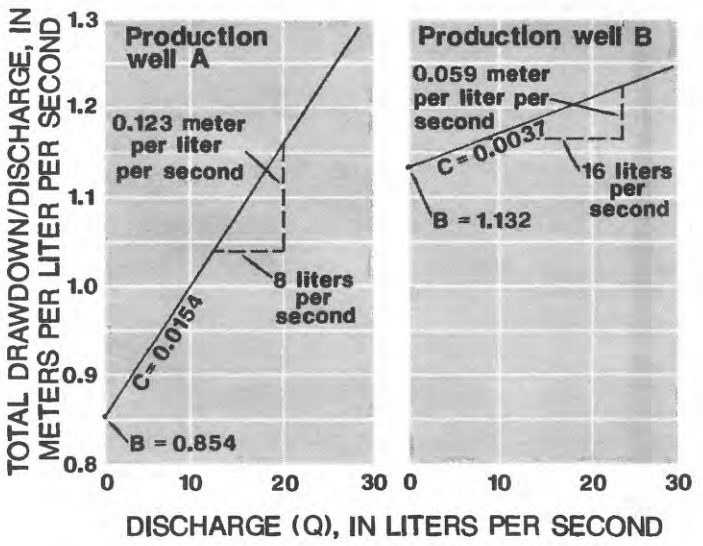

(B, head-loss coefficient due to laminar flow in the aquifer in meters per liter per second
C, (slope, head-loss coefficient due to turbulent flow near the well in meters)

Figure 10.--Relation of discharge to drawdown divided by discharge for step-drawdown test data from production wells A and B.

where

M = total number of pumping steps, i = 1,2,...,M [dimensionless],

Q_i = discharge during step i of the test [L^3/T] (L/s),

S_i = drawdown observed after step i of the test [L] (m), and

E(B,C,N) = the squared fitting error as a function of chosen B,C,N for given step-drawdown test data.

Using this method to solve for values of B, C and N and substituting these values into equation 6 yields, for production well A,

$$S = 1.046Q + 3.982\times10^{-4} Q^{2.888} \quad (10)$$

and for production well B,

$$S = 1.117Q + 7.899\times10^{-3} Q^{1.839} \quad (11)$$

Comparison of the calculated drawdowns for various pumping rates from the two methods using equations 7, 8, 10, and 11 for production wells A and B are shown in table 4.

Rorabaugh (1953) defined well efficiency as the ratio of the theoretical drawdown to the theoretical drawdown in the well minus the effects of turbulence. Well efficiencies can be calculated for various pumping rates from equation 6 by setting the head-loss coefficient, C, equal to zero and computing efficiency as BQ/S. The minimization equations 10 and 11 were used to calculate values of BQ and S for production wells A and B respectively. Table 5 summarizes values of BQ, S, and efficiency (BQ/S) for various pumping rates for the wells.

The lower efficiencies computed for production well A at the greater pumping rates could be due to improper well construction or poor well development, as less time was spent developing production well A compared to production well B. The efficiency may improve during further testing. Regardless, the total drawdown computed for both wells are close for the planned short-term test cycle rate of 18.9 L/s. A well efficiency of approximately 90 percent for a rate of 18.9 L/s is not expected to affect system performance significantly during hot-water testing.

Table 4.--*Calculated drawdowns for various pumping rates for production wells A and B*

Rate (liters per second)	Drawdown (meters)			
	Site A		Site B	
	Graphical (equation 7)	Minimization (equation 10)	Graphical (equation 8)	Minimization (equation 11)
6.3	6.0	6.7	7.3	7.3
12.6	13.2	13.8	14.9	14.9
18.9	21.6	21.7	22.7	22.9
25.2	31.3	30.8	30.9	31.1
31.5	42.2	41.4	39.3	39.7
37.9	54.5	54.1	48.2	48.7

Table 5.--*Well efficiencies for production wells A and B*

Rate (liters per second)	Site A			Site B		
	S (meters)	BQ (meters)	Efficiency (percent)	S (meters)	BQ (meters)	Efficiency (percent)
6.3	6.7	6.6	98.8	7.3	7.0	96.8
12.6	13.8	13.2	95.6	14.9	14.0	94.4
18.9	21.7	19.8	91.1	22.9	21.1	92.3
25.2	30.8	26.4	85.6	31.1	28.1	90.4
31.5	41.4	32.9	79.6	39.7	35.2	88.7
37.9	54.1	39.6	73.3	48.7	42.3	87.0

Hydraulic Properties

Estimates of Transmissivity from Step-Drawdown Data

Using the methods described by Harrill (1970), transmissivity was approximated using recovery data from the step-drawdown test of production well B. Harrill's method is a modified form of the Theis recovery formula (Theis, 1935). On semilogarithmic paper, residual drawdown, S is plotted against the corresponding step-drawdown-test value of

$$\frac{t_1\left(\frac{\Delta Q_1}{Q_n}\right)t_2\left(\frac{\Delta Q_2}{Q_n}\right)\ldots t_n\left(\frac{\Delta Q_n}{Q_n}\right)}{t'} \qquad (12)$$

where

$t_1, t_2, \ldots t_n$ = elapsed times since the pump was turned on or discharge increased at each step, in days

t' = the elapsed time since the pump was turned off, in days

$Q_1, Q_2, \ldots Q_n$ = the well discharge rates for each step in liters per day, and

$\Delta Q_1, \ldots \Delta Q_2, \Delta Q_n$ = the incremental increases in discharge between steps in liters per day.

The value of S is plotted on the arithmetic scale. After the value of t' is sufficiently large, the observed data fall on a straight line. If the value of equation 12 is chosen over one log cycle, its logarithm is unity and the transmissivity, in m^2/d, may be computed from:

$$T = \frac{1.83\times10^{-4}Q_n}{S} \qquad (13)$$

where S is the change in residual drawdown in meters per log cycle of time (Harrill, 1970). Figure 11 illustrates the semilogarithmic plot of recovery data from the step-drawdown test at site B. Values of S and transmissivity were computed as 6.7 m and 109.5 m^2/d, respectively.

The lack of a reliable determination of pumping rate during the fourth step of the step-drawdown test for production well A made calculation of the transmissivity by Harrill's (1970) method impossible. Instead, an approximation of the transmissivity was obtained using specific-capacity data computed from the first step. A specific capacity of 0.93 (L/s)/m (liters per second per meter) was calculated after 1 hour of pumping. Using this value, a transmissivity of 97.5 m^2/d was computed based on curves from Walton (1970, p. 317). This value is in agreement with the 109.5 m^2/d calculated for production well B.

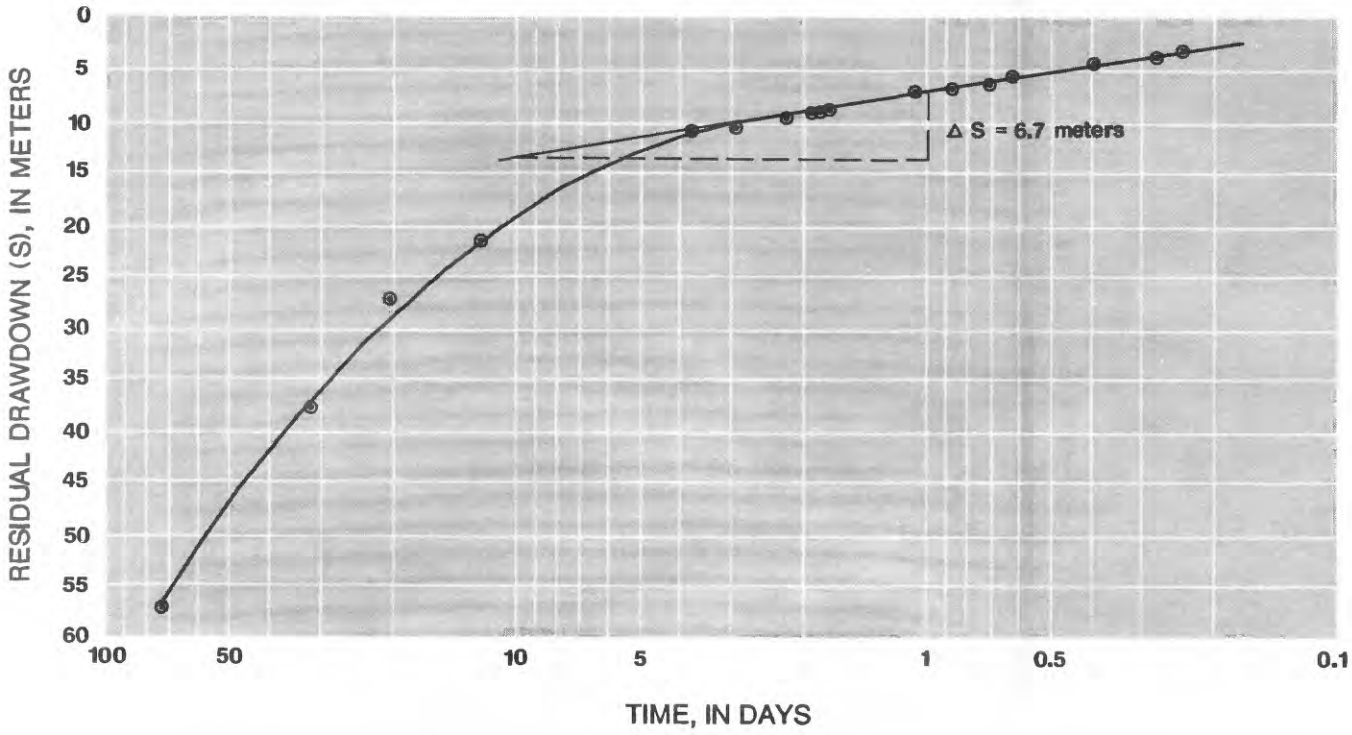

Figure 11.--Recovery of ground-water levels following the step-drawdown test at production well B.

Estimates of Transmissivity and Areal Anisotropy from Constant-Rate Aquifer Tests

Two methods were used to analyze the aquifer-test data. The first method, described by Lohman (1972), was used to approximate the transmissivity and storage coefficient of a leaky confined aquifer with vertical movement. The second method, described by Papadopulos (1966), was used to estimate aquifer anisotropy.

A constant-rate aquifer test was conducted using production well A. The well was pumped for approximately 4.5 days at an average rate of 21.5 L/s. The pumping rate varied for the first 20 minutes of the test from 28.4 to 22.7 L/s due to manual adjustment of a discharge-control valve. Pumping was interrupted twice during the latter part of the aquifer test for periods of no longer than 15 minutes due to freezing of water in an automatic-cutoff pump-control pressure switch. These interruptions in pumping had negligible effects on analysis of the test data.

Time divided by radius squared was plotted versus drawdown on logarithmic graph paper for selected observation points in the upper part of the Franconia Formation and the Ironton and Galesville Sandstones. The resulting curves were matched against type curves developed by Cooper (1963). Match points were chosen and values of transmissivity and storage coefficient were calculated as described by Lohman (1972). Table 6 summarizes the transmissivity and storage coefficient calculated for the selected observation points.

Table 6.--*Transmissivity in square meters per day (m^2/d) and storage coefficient at selected observation points*

Observation well number	Aquifer hydraulic zone	Transmissivity (m^2/d)	Storage coefficient (dimensionless)
AM2	Upper part of the Franconia Formation	27.9	3.9×10^{-5}
AM2	Ironton and Galesville Sandstones	41.2	2.68×10^{-5}
AM3	Ironton and Galesville Sandstones	70.6	1.16×10^{-5}
CM1	Upper part of the Franconia Formation	28.8	1.04×10^{-5}
BC	Upper part of the Franconia Formation	45.1	4.28×10^{-5}
BC	Ironton and Galesville Sandstones	80.4	3.46×10^{-5}

Averaging the transmissivity and storage-coefficient values in table 6 for each hydraulic zone gives a transmissivity for the Ironton and Galesville Sandstones of approximately 64.0 m^2/d and a storage coefficient of 2.4×10^{-5}

and a transmissivity for the upper part upper part of the Franconia Formation of 33.9 m^2/d and a storage coefficient of 3.1×10^{-5}. Summing the two transmissivity values yields a total transmissivity of 97.9 m^2/d for the Franconia-Ironton-Galesville aquifers, which is in very close agreement with the value of 97.5 m^2/d for the aquifer at site A calculated from analysis of specific-capacity data. The average storage coefficient is 2.75×10^{-5}.

The degree of anisotropy of the aquifer in the x-y areal plane was determined using the type-curve method described by Papadopulos (1966) for non-steady flow to a well in an infinite anisotropic aquifer. Miller (1984) describes in detail the determination of the x-y areal plane anisotropy for the Franconia-Ironton-Galesville aquifer and examines the sensitivity of the results to errors in observation well locations. Miller's determination of the x-y areal anisotropy is summarized below.

A rectangular-coordinate system was designed with the surface location of production well A as the origin, the x axis being a line east-west through the surface position of observation well AM2, and the y axis a line north-south through the surface positions of observation wells AM1, AC1, and AM3. Figure 12 illustrates this coordinate system and shows the locations of observation wells at land surface and at the depth below land surface of the observation point. Horizontal deviations with respect to depth are not shown for observation well AC1 because of the questionable results of the deviation survey on this well. Horizontal deviation surveys with respect to depth were not available for observation wells BS1, BC1, and CM1, but it is likely that they have similar deviations with depth.

Knowing the relative coordinates of three or more observation points it is possible, using the methods outlined by Papadopulos, to calculate values for the principal axes of a transmissivity ellipse and a corresponding direction of the principal axes related to a known rectangular coordinate system. Values for the Ironton and Galesville Sandstones were calculated, with drawdown data from observation wells AM2, AM3, BC1, and CM1, and for the upper part of the Franconia Formation with data from, observation wells AM2, BS1, and BC1 (fig. 12).

When data from more than three observation wells are available, they can be grouped into combinations of three. Data from the four observation wells in the Ironton and Galesville Sandstones were grouped into four sets, each containing data from three wells. Table 7 summarizes the grouping and assigns a corresponding set number.

Table 8 summarizes the calculated major and minor transmissivity values their corresponding directions, and the storage coefficients for the Ironton and Galesville Sandstones and the upper part of the Franconia Formation. The direction angles (θ) are measured from the x-axis in figure 12 to the major axis of transmissivity, being positive in a counterclockwise direction. Summing the respective average major and minor transmissivities for the Ironton and Galesville Sandstones and the upper part of the Franconia Formation

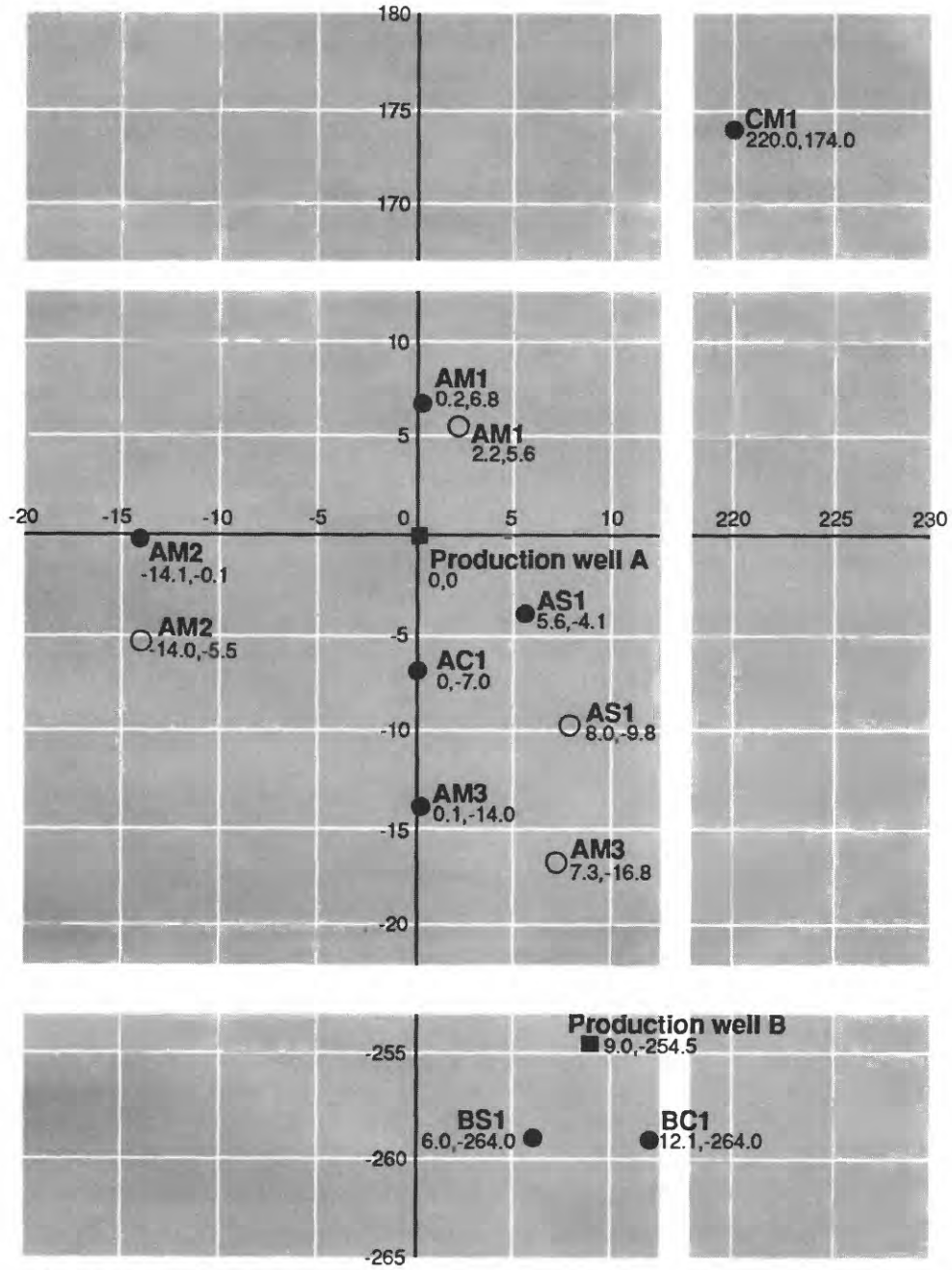

Coordinate system distances are measured in meters from production well A

EXPLANATION

- ● Observation well
- ○ Well deviation at 234.7 meters below land surface

Figure 12.--Arbitrary coordinate system, in meters, indicating location and known deviation of production wells A and B and observation wells AC1, AM1, AM2, AM3, AS1, BC1, BS1, and CM1.

Table 7.--*Observation-well combinations and corresponding set numbers used for determining aquifer anisotropy*

Aquifer hydraulic zone	Set number	Observation wells in set
Ironton and Galesville Sandstones	1	AM2, AM3, BC1
Do.	2	AM2, AM3, CM1
Do.	3	AM2, BC1, CM1
Do.	4	AM3, BC1, CM1
Upper part of the Franconia Formation	1	AM2, BS1, BC1

Table 8.--*Computed values of transmissivity, in square meters per day (m^2/d), storage coefficient, and direction of major axis of transmissivity by set number*

Aquifer hydraulic zone	Set number	Transmissivity (m^2/d)		Storage coefficient	θ (degrees)*
		Major	Minor		
Ironton and Galesville Sandstones	1	115.2	37.2	2.7×10^{-5}	64
Do.	2	124.5	34.4	4.4×10^{-5}	71
Do.	3	71.5	60.4	5.9×10^{-5}	67
Do.	4	94.8	46.5	4.8×10^{-5}	76
	Average	101.5	44.6	4.5×10^{-5}	
Upper part of the Franconia Formation	1	40.0	24.0	3.7×10^{-5}	68

*The direction of the major axis of transmissivity, θ, is an angle measured from the x-axis positive in a counterclockwise direction.

and calculating the harmonic mean for the total average transmissivity yields a value of approximately 104.8 m^2/d. This value is in very close agreement with the transmissivity, 97.9 m^2/d, calculated with the method described by Lohman (1972) and 109.5 m^2/d calculated with the step-drawdown recovery method described by Harrill (1970). Values of storage coefficient calculated with this method also are similar to those calculated by the method of Lohman (1972) and given in table 6.

Estimates of Effective Porosity

The porosity of the Franconia-Ironton-Galesville aquifer and the St. Lawrence Formation and Eau Claire Formation confining beds were estimated from a combination of neutron bore-hole geophysical logs and from laboratory determinations of effective porosity of core samples.

Figure 13 shows a comparison between the natural-gamma, gamma-gamma-density logs for observation well AM1 and the laboratory-determined value of effective porosity of core samples from core hole AC1. The neutron log indicates distinct zonation of the aquifer as relative values of porosity are indicated by general shifts in the log.

At the approximate altitude from 98 to 104 m, the neutron log indicates a shift toward higher porosity. Examination of the gamma-gamma-density log at the same altitude also indicates a large shift to the right. Examination of well-driller's records suggests that the shift probably is caused by cement grout installed by the driller during observation well completion. The effective porosity determined from laboratory analysis of core samples opposite the zone indicates no large increase in porosity, suggesting that the neutron-porosity log may not be representative of the aquifer in this area; thus, this part of the log was disregarded in determining approximate porosity values.

To determine approximate effective-porosity values, a linear regression was performed on laboratory values of effective porosity, in percent, and the corresponding neutron value, in cps (counts per second), shown in figure 13. The resulting linear equation for approximating effective porosity from neutron-log values is:

$$\phi = -0.0169x + 41.68 \qquad (14)$$

where

ϕ = effective porosity, and

x = neutron-log value, in cps.

The average effective porosity was determined for the aquifer and confining layers using equation 14; values ranged from 25 to 31 percent.

Ambient-Temperature Water-Injection Testing

Ambient-temperature water-injection testing was conducted on production well A at different injection rates to determine the ability of the aquifer to accept injected water and to obtain pressure data for isothermal-model cali-

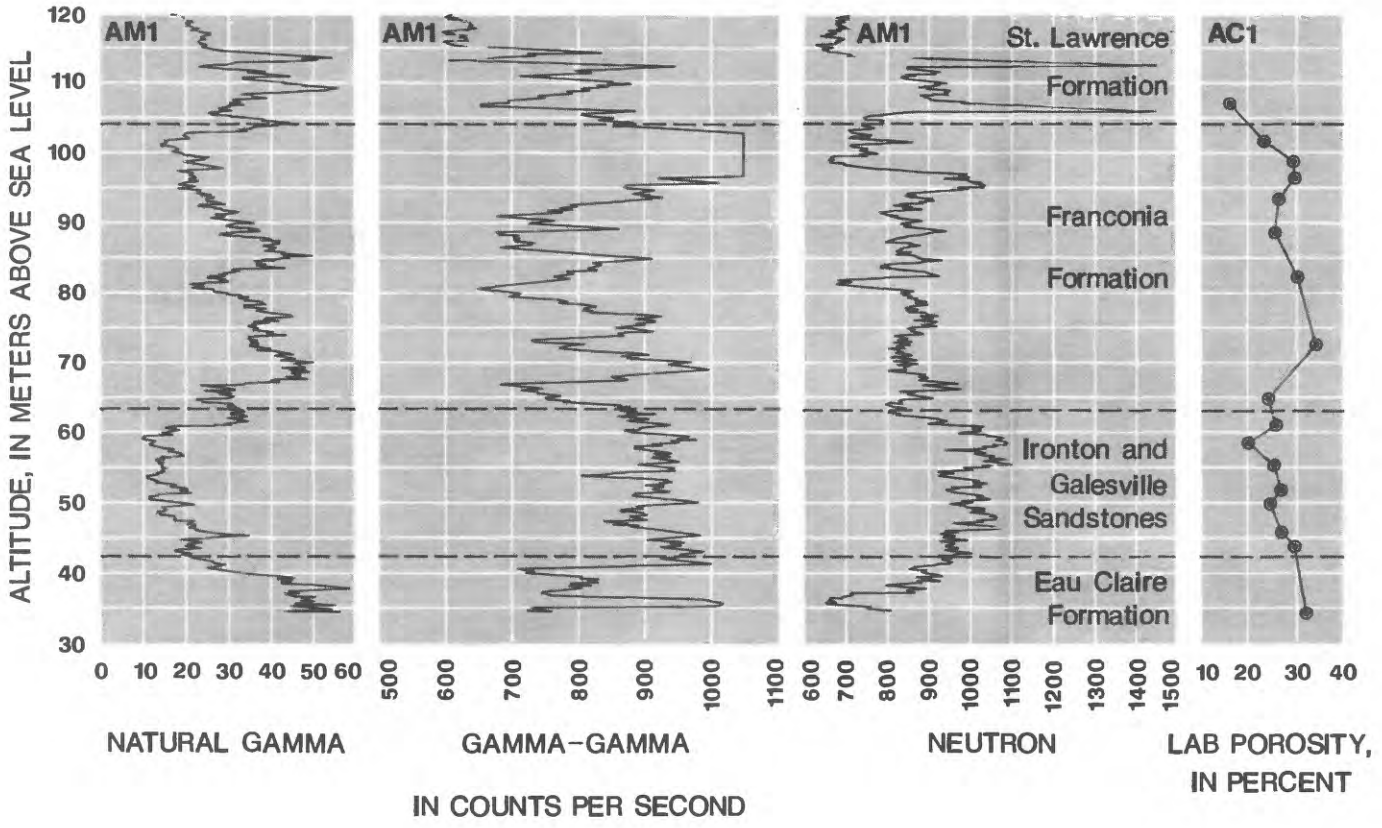

Figure 13.--Comparison of natural gamma, neutron porosity, and gamma-gamma density logs and laboratory-determined values of effective porosity.

bration. Injection of water into production well A was designed to occur within the annular space between the well casing and pump-discharge column. Artificial recharge work by Sniegocki (1963), Foxworthy and Bryant (1967), Foxworthy (1970), and Reeder and others (1976) indicates that unless a positive pressure is maintained at the wellhead, entrainment of air in the injected water can effectively clog the well by reducing the hydraulic conductivity of the aquifer near the well bore. Pressures measured near the well head indicated that water flowing into the well entered under atmospheric-pressure conditions. Because a positive pressure was not maintained at the well head (the sound of water cascading inside the well was audible during the injection period), it is likely that air entrained in the injected water was responsible for clogging production well A during the first attempt at injection of ambient-temperature water.

Water at a temperature of approximately 10 °C was pumped from production well B at approximately 22.0 L/s and injected into production well A at approximately 8.0 L/s. The remaining 14.0 L/s from production well B was pumped to waste. Pumping to waste was necessary due to the large capacity of the pumps, which could only be adjusted by closing a series of valves. Closing the valves creates back-pressures in the above-ground piping that, for a pumping rate of 8.0 L/s, exceeds the designed safety standards of the valves. For pumping rates above 13 L/s, back-pressure was not severe and diverting water to waste in order to maintain a specific injection rate was not necessary.

Figure 14 illustrates the pressure changes in production well A, the upper and lower parts of the Franconia Formation, and in the Ironton and Galesville Sandstones at observation well AM2 for approximately one day of injection at 8.0 L/s.

Adjustment of the injection rate during the early part of testing took approximately 30 minutes. This is shown in figure 14 in the step-pressure changes in production well A. Pressures continued to rise in the aquifer until about 150 minutes into injection when pressure declines started in production well A and in the upper part of the Franconia Formation and the Ironton and Galesville Sandstones. These pressure declines are a result of well interference caused by production well B, which was pumping at approximately 22.0 L/s. Well-interference effects were observed in the observation well in the lower part of the Franconia Formation after approximately 300 minutes of injection. The pressure changes in the lower part of the Franconia Formation lag behind those in the upper part of the Franconia Formation and in the Ironton and Galesville Sandstones because (1) the lower part of the formation is cased off and, thus, there is no direct injection or withdrawal in this part of the aquifer and (2) the lower part of the Franconia Formation has a considerably lower hydraulic conductivity than the upper part of the Franconia Formation or the Ironton and Galesville Sandstones.

After 1,440 minutes of injection at 8.0 L/s the rate was increased to 18.9 L/s. Increasing the rate dropped back pressures in the above-ground piping substantially, which enabled withdrawals from production well B and injection into production well A to be equal. Figure 15 illustrates pressure changes in production well A for the injection period of 18.9 L/s. Pressures represent changes from the final pressure recorded after 1,440 minutes of injection at 8.0 L/s, as shown in figure 14.

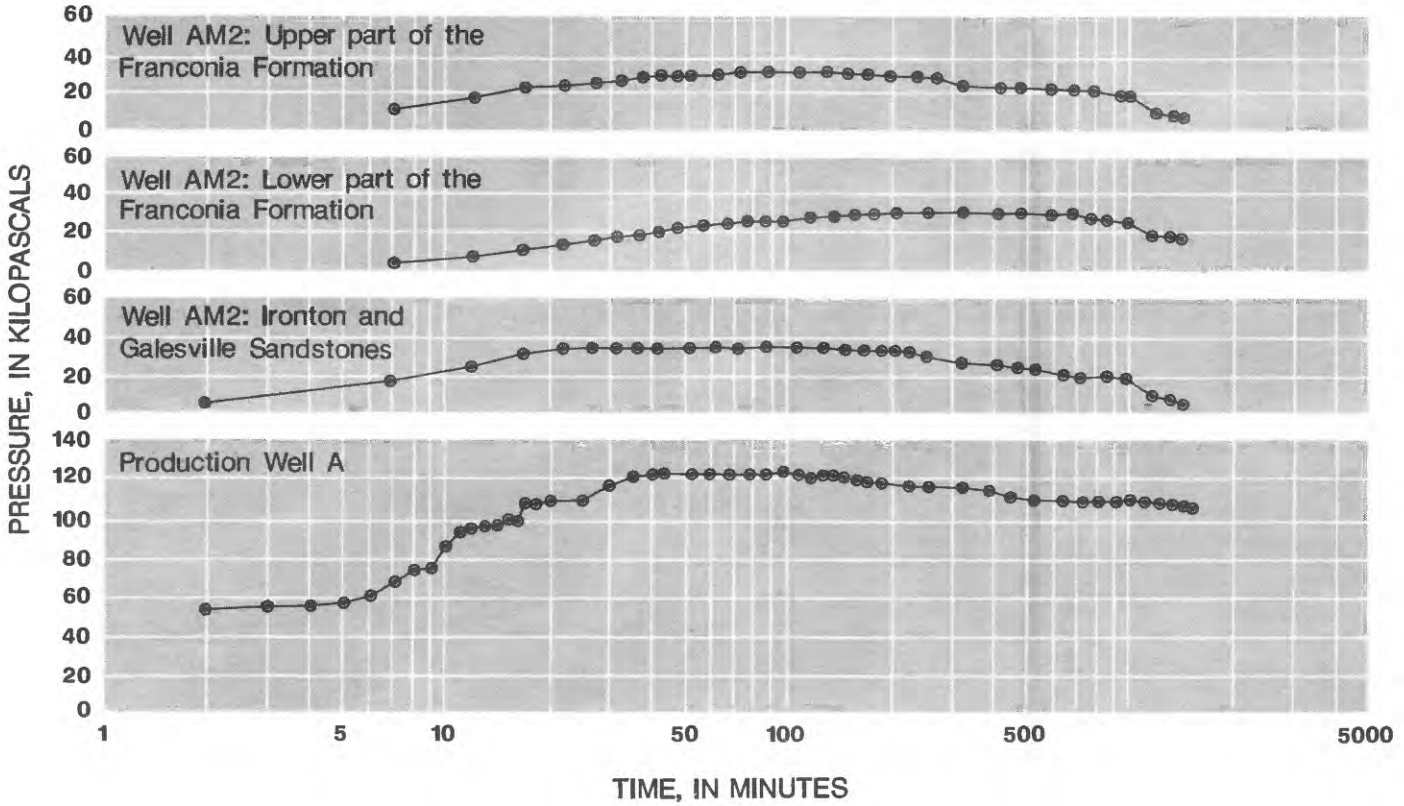

Figure 14.--Pressure changes for injection at 8.0 liters per second at observation well AM2 in the upper and lower part of the Franconia Formation and in the Ironton and Galesville Sandstones and in production well A.

It took approximately 30 minutes from the start of injection at 18.9 L/s to adjust the injection rate into production well A. Effects of the adjustment are illustrated in figure 15 by the large pressure-step increases in production well A during the early part of the injection. Following the adjustment period, the pressure continued to rise steadily for the next 20 minutes, which probably is a combination of the effects of a higher injection rate into production well A and overcoming the interference effects from production well B, in which the withdrawal rate was decreased from 22.0 to 18.9 L/s.

Pressures in production well A continued to increase. During the last 100 minutes of injection the rate of change of pressure started to increase, indicating potential clogging because of air entrained in the injection water. Therefore, after 400 minutes, injection was stopped before any further air entrainment clogging reduced the injection potential of the aquifer.

Water levels in production well A returned to within 0.30 m of preinjection levels after approximately 12 hours of recovery. Well rehabilitation consisted of pumping production well A continuously for approximately 18 hours, increasing the rate in three steps. Dissolved-oxygen levels were measured during redevelopment. The dissolved-oxygen concentration in the injection water before injection began was between 0.1 and 0.05 (mg/L) milligrams per liter; after redevelopment the concentration was between 0.5 and 0.1 mg/L. Figure 16 illustrates the pressure changes, pumping rate, duration, and dissolved-oxygen concentrations during redevelopment of production well A. Water levels were allowed to recover for approximately 8 days, at which time the water level in production well A was within 0.06 m of the preinjection level.

After 8 days of recovery, a second injection test was performed on production well A. To reduce the potential for air entrainment, water was injected through the pump-discharge column. A positive pressure of approximately 1,030 kilopascals (kPa) was maintained at the well head throughout the injection test, thus reducing the potential for air entrainment and subsequent clogging. Figure 17 shows the pressure changes in production well A and in observation well AM2 for the upper part of the Franconia Formation and for the Ironton and Galesville Sandstones for 8 days of injection at 18.6 L/s. From figure 17, it can be seen that most of the pressure build-up in production well A occurred within the first day of injection and that the rate of pressure change in well A and in the observation well was extremely low after 2 days of injection, which suggests that the aquifer approaches steady state quickly during injection. Figure 17 also indicates that redevelopment of production well A was successful and that aquifer characteristics near the well-bore were not seriously changed by air-entrainment clogging. It is likely that not all the injected air was removed from the aquifer during redevelopment and that values of hydraulic conductivity were lowered slightly near the well bore. However, interpretation of data from hot-water-injection testing should not be significantly affected.

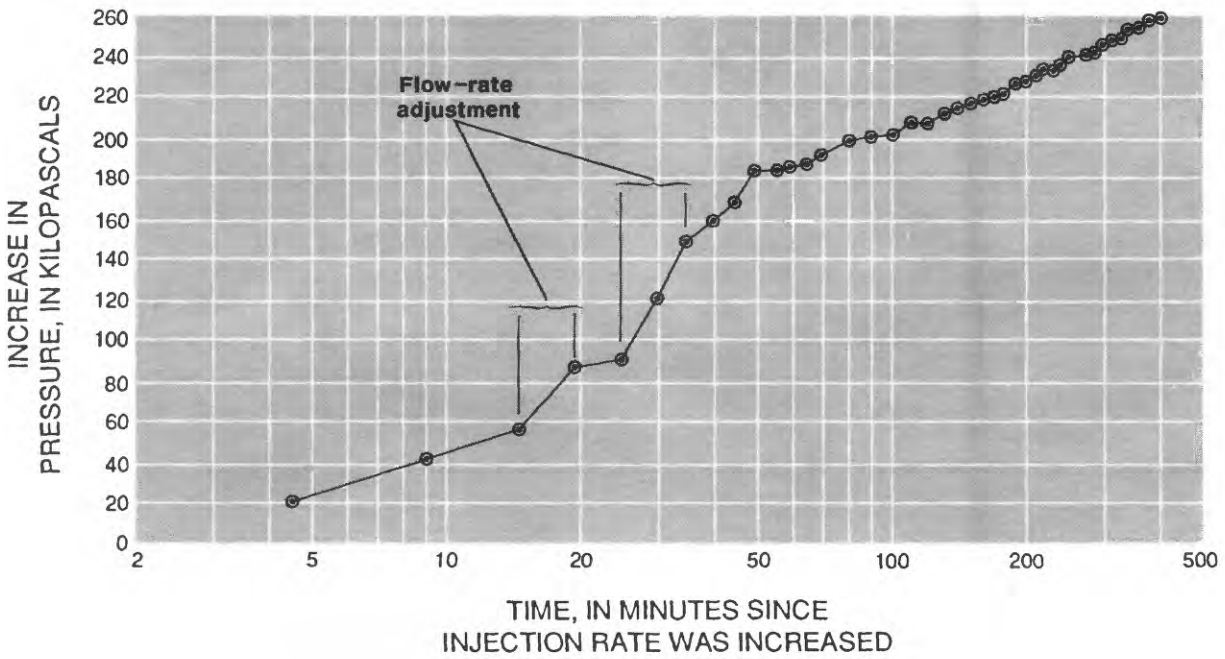

Figure 15.--Pressure changes in production well A at 18.9 liters per second after 1,440 minutes at 8.0 liters per second.

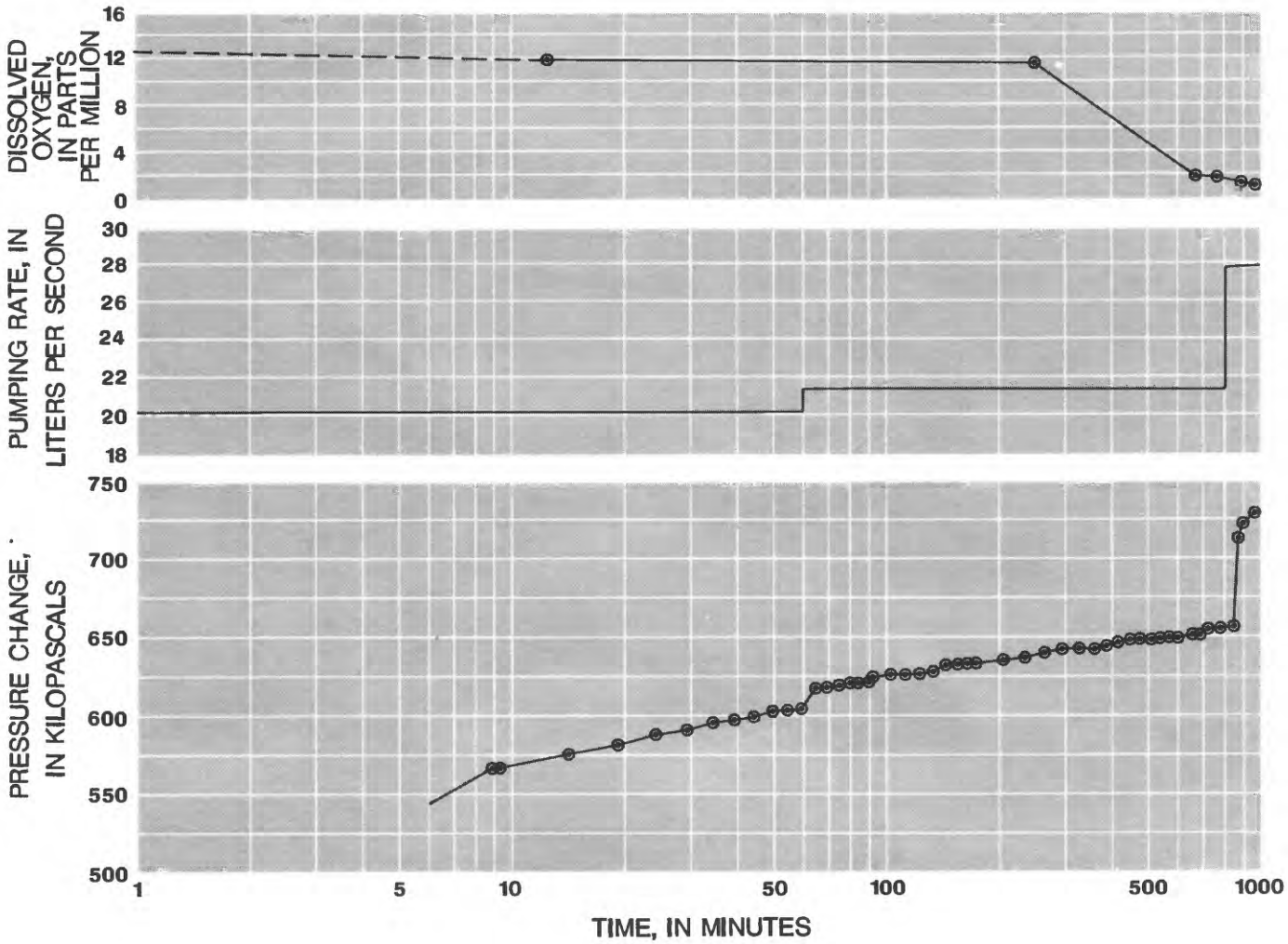

Figure 16.--Comparison of pressure change, pumping rate, and dissolved oxygen content during rehabilitation of production well A.

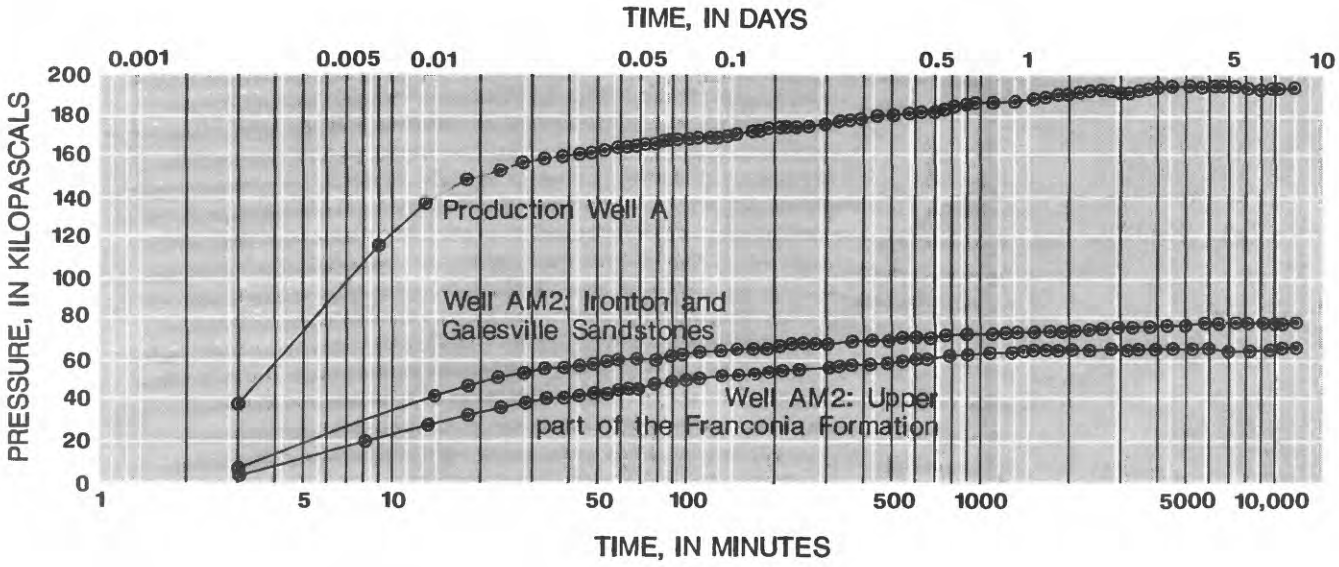

Figure 17.--Pressure changes for injection at 18.6 liters per second at observation well AM2 in the upper part of the Franconia Formation and in the Ironton and Galesville Sandstones and in production well A.

PRELIMINARY MODELING ANALYSIS

Two models have been constructed to analyze ground-water flow and thermal-energy transport. Early in the study, a preliminary two-dimensional, radial-flow, isotropic, nonisothermal, ground-water-flow and thermal-energy-transport model was constructed from available data. This model was used (1) for short-term sensitivity analyses of selected hydrogeologic and thermal characteristics of the aquifer, (2) to determine the potential for buoyancy-flow effects, (3) to develop a method to examine the efficiency of the aquifer for heat storage, and (4) to demonstrate how changes in cyclic injection/withdrawal rates and duration can affect aquifer efficiencies and production well temperatures.

The second model was a three-dimensional anisotropic, nonisothermal ground-water flow and thermal-energy transport model. This model was developed to more accurately represent field conditions and to simulate the doublet-well system and the short-term heat-injection testing. Both models use the same computer code.

Conceptual Model

A conceptual model of ground-water movement was developed from the field observations previously described and from water-level measurements in the Franconia-Ironton-Galesville aquifer and in the confining beds of the St. Lawrence and Eau Claire Formations. Figure 18 illustrates water levels from piezometers completed in the St. Lawrence and Eau Claire Formations confining beds, the upper and lower parts of the Franconia Formation, and the Ironton and Galesville Sandstones for monitoring wells AM1 and AM2 (see figures 12 and 3 for location and depth). The predominant hydraulic-head gradient is vertically downward, because hydraulic heads decrease with depth beneath the site.

Horizontal flow in the upper part of the Franconia Formation differs from horizontal flow in the Ironton and Galesville Sandstones. Because of the relatively low hydraulic conductivity of the lower part of the Franconia Formation, the Formation essentially acts as a confining layer for water in the Ironton and Galesville Sandstones. Water levels at sites A, B, and C indicate a gradient of 2.6×10^{-3} for the upper part of the Franconia Formation and a gradient of 7.0×10^{-4} for the Ironton and Galesville Sandstones. The direction of horizontal ground-water flow is from site C toward site B.

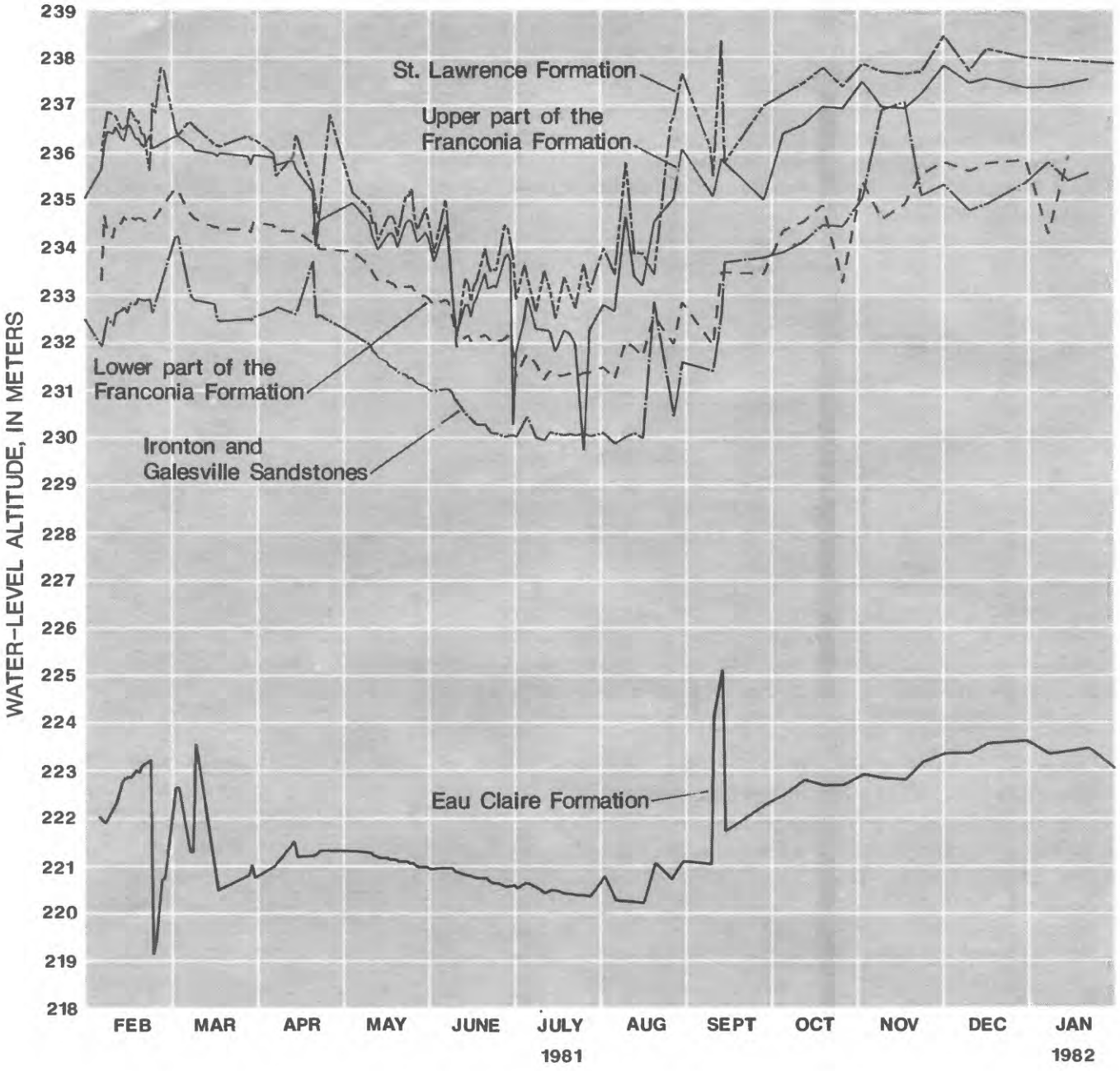

Figure 18.--Water-level measurements from February 1981 through January 1982 for the St. Lawrence, Franconia, and Eau Claire Formations and Ironton and Galesville Sandstones.

Average linear water velocities in the upper part of the Franconia Formation and in the Ironton and Galesville Sandstones may be determined from the equation (Freeze and Cherry, 1979),

$$V = \frac{K\Delta h}{\phi \Delta l} \qquad (15)$$

where:

V = the average linear velocity [L/T],

K = horizontal hydraulic conductivity [L/T],

$\frac{\Delta h}{\Delta l}$ = hydraulic gradient [L/L], and

ϕ = porosity [dimensionless].

Substituting the average values of horizontal hydraulic conductivity determined from the transmissivities in table 8 a porosity of 25 percent, and the hydraulic gradient determined from observation well measurements (fig. 18), the average linear velocity of water in the upper part of the Franconia Formation is 2 x 10 m per year; velocity in the Ironton and Galesville Sandstones is 1.3 x 10 m per year.

The thermal gradient increases with depth at a rate of approximately 0.5 °C per 30 m. Figure 19 illustrates a temperature profile for observation well AM1 for the St. Lawrence Formation through the Eau Claire Formation for a thermocouple lowered inside a 5.08-cm pipe and for thermocouples buried outside the 5.08-cm pipe. The variation in temperature at altitudes of approximately 100, 51, and 45 m is due to individual broken cables in the buried thermocouples.

Description of Numerical Modeling

The finite-difference ground-water flow and thermal-energy-transport model being used in this study was developed for waste-injection problems (Intercomp, 1976) and will be referred to in the report as the Survey Waste Injection Program (SWIP) code. The SWIP code considers ground-water flow and heat, and solute transport in a liquid-saturated porous medium; it contains both reservoir and well-bore modeling capabilities.

The major model assumptions include (Intercomp, 1976):

1. Three-dimensional, transient, laminar (Darcy) flow.

2. Fluid density as a function of pressure, temperature, and concentration.

3. Fluid viscosity as a function of temperature and concentration.

4. The injected fluid is miscible with the in-place fluids.

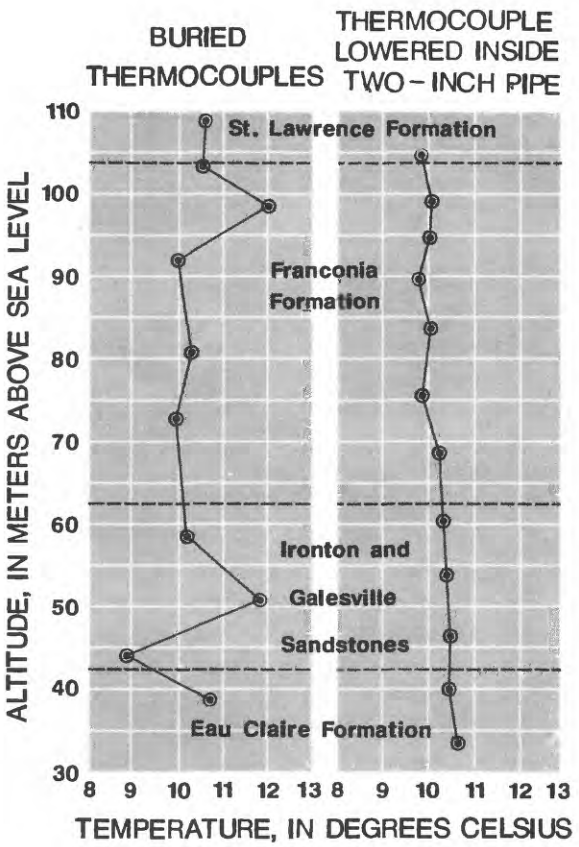

Figure 19.--Temperature profile for observation well AM1.

5. Aquifer properties vary with location.

6. Hydrodynamic dispersion is described as a function of fluid velocity.

7. The energy equation can be described as enthalpy in minus enthalpy out equals the change in internal energy of the system.

8. Boundary conditions allow natural water movement in the aquifer, heat losses to the adjacent formation, and the location of injection, withdrawal, and observation points anywhere within the system.

9. Thermal equilibrium exists within the simulation area.

Model Equations

The basic equation describing single-phase flow in a porous medium results from a combination of the continuity equation and Darcy's law in three dimensions and results in the basic flow equation (Intercomp, 1976, p. 3.4)

$$\nabla\cdot\left(\frac{\rho k}{\mu}(\nabla p - \rho g \nabla z)\right) - q' = \frac{\partial}{\partial t}(\phi\rho) \qquad (16)$$

where:

ρ = fluid density [M/L^3] (kg/m^3),

μ = fluid viscosity [M/L-T] (Pa-s),

k = intrinsic permeability [L^2] (m^2),

g = gravitational acceleration [L/T^2] (m/s^2),

z = spatial dimension in direction of gravity [L] (m),

p = pressure [$M/L\text{-}T^2$] (Pa),

q' = mass rate of flow per unit volume from sources or sinks [$M/T\text{-}L^3$] ($kg/s\text{-}m^3$),

t = time [T] (s),

ϕ = porosity [dimensionless], and

∇ = gradient operator (for an axially symmetric cylindrical coordinate system ∇ is: $\left(\frac{1}{r}\right)\left(\frac{\partial}{\partial r}\right) + \left(\frac{\partial}{\partial z}\right)$, where r is the radial dimension).

This equation may be combined with an energy balance defined as 'enthalpy in - enthalpy out = change in internal energy' to describe the transport of thermal energy in a ground-water system, as (Intercomp, 1976, p. 3.4):

$$\nabla\cdot\left(\frac{\rho k}{\mu}H(\nabla p - \rho g\nabla z)\right) + \nabla\cdot K\cdot\nabla T - q_L - q'H = \frac{\partial}{\partial t}\left[\phi\rho U + (1-\phi)(\rho C_p)_R T\right] \qquad (17)$$

where:

H = enthalpy per unit mass of fluid [E/M] (J/kg),

K = hydrodynamic thermal dispersion plus convection [E/T-L-t] (W/m-°C),

T = temperature [t] (°C),

q_L = heat loss across boundaries [E/T-L^3] (W/m^3),

U = internal energy per unit mass of fluid [E/M] (J/kg),

$(\rho C_p)_R$ = heat capacity of the aquifer matrix [E/L^3-t] (J/m^3-°C), and

C_p = specific heat of aquifer matrix [E/M-t] (J/kg-°C)

and all other terms are previously defined.

Equation 17 is a nonlinear system of coupled partial-differential equations that are solved numerically by discretizing the aquifer into three dimensions (or two dimensions for radial flow) and developing finite-difference approximations.

Finite-difference equations (Intercomp, 1976, p. 3.5) whose solution closely approximates the solution of equations 16 and 17 are, for the basic flow equation,

$$\Delta\left(T_W(\Delta p - \rho g\Delta z)\right) - q = \frac{V}{\Delta t}\delta(\phi\rho) \qquad (18)$$

and for the energy equation,

$$\Delta\left(T_W H(\Delta p - \rho g\Delta z)\right) + \Delta(T_C\Delta T) - q_L - q'H = \frac{V}{\Delta t}\delta\left[\phi\rho U + (1-\phi)(\rho C_p)_R T\right] \qquad (19)$$

where

$$\delta\chi = \chi^{n+1} - \chi^{n} \tag{20}$$

and

$$T_w = \frac{kA\rho}{\mu l} \tag{21}$$

$$T_c = \frac{KA}{l} \tag{22}$$

and where A is the area perpendicular to flow (that is, $\Delta x\Delta y$, $\Delta x\Delta z$, or $\Delta y\Delta z$), and l is the distance between grid block centers; all other terms are as previously defined.

The finite-difference operators are defined as

$$\Delta(T_w\Delta p) = \Delta_x(T_w\Delta_x p) + \Delta_y(T_w\Delta_y p) + \Delta_z(T_w\Delta_z p) \tag{23}$$

with the terms

$$\Delta_x(T_w\Delta_x p) = T_{w,i+0.5,j,k}\left(p^{n+1}_{i+1,j,k} - p^{n+1}_{i,j,k}\right) T_{w,i-0.5,j,k}\left(p^{n+1}_{i,j,k} - p^{n+1}_{i-1,j,k}\right) \tag{24}$$

where the subscripts x,y,z = the cartesian space coordinates,

i,j,k = grid block indices,

n = time level, t_n, and

all other terms as previously defined.

Finally, the thermal-conductance term, K, in equation 21 may be further defined as (Intercomp, 1976, p. 3.7)

$$K = \phi\left(\frac{\alpha u}{\phi}\right)(\rho C_p)_w + K_m \tag{25}$$

where:

α = the thermal dispersivity [L] (m),

ϕ = porosity [dimensionless]

u = volumetric flux (Darcy velocity) [L/T] (m/s),

$(\rho C_p)_w$ = heat capacity of water [E/L^3-t] (J/m^3-°C), and

K_m = molecular heat conductivity of porous media [E/T-L-t] (W/m-°C).

Description of Radial-Flow Model

As described earlier, the ATES system consisted of a doublet-well system. The steady-state flow field for a doublet-well system with well spacing equal to that of the ATES system (250 m) is shown in figure 20. The equipotentials indicate that the preliminary model assumption of radial flow is less exact with increasing distance from the center of either well bore. The interpretation of the preliminary model results in terms of representing the ATES doublet-well system will be related to the radial distance that heat will move away from the well for the period of simulation: that is, the farther the heat moves away from the well the less exact the assumption of radial flow. For the preliminary model simulations described in this report, all the injected heat was maintained within the boxed area around the injection well shown in figure 20. Figure 20 also shows the location of the preliminary model lateral boundary in relation to the doublet-well flow field.

Most of the injected heat, calculated by the preliminary model during sensitivity-analysis simulations, was concentrated within a radial distance of approximately 14 m from the injection well. None of the sensitivity-analysis simulations calculated movement of injected heat beyond approximately 17 m. The 17-m and 14-m radial distances from the well are shown in figure 21, which is an enlargement of the box area shown in figure 20. Comparison of the equipotentials for the doublet-well system and the 17-m model-computed radial extent of heat indicates that the preliminary model radial-flow assumption is fairly accurate for the sensitivity-analysis simulations. However, as indicated in the discussion of Buoyancy Flow, the sensitivity of certain properties may change with longer-term cycles (greater than 60 days).

Sensitivity Analysis

Approach

Sensitivity analyses were performed on the preliminary model for the hydraulic properties of hydraulic conductivity, porosity, and vertical anisotropy, and on the thermal properties of rock-thermal conductivity, rock-heat capacity, and thermal dispersivity. A radial-flow base model was constructed with data obtained from borehole-geophysical logs, analysis of core samples, inflatable-packer tests, from previous studies, and from laboratory values reported in text books. Base-model-hydraulic and thermal characteristics are presented in tables 9 and 10, respectively.

The purpose of the sensitivity analysis was to determine the relative importance of individual hydraulic and thermal characteristics in the computation of temperatures and aquifer-thermal efficiency in relation to the preliminary radial-flow model. This information could then be used to guide data collection and to adjust model-input properties during calibration of subsequent models, using data from the 24-day test cycles. Therefore, the simulation used in sensitivity analysis consists of 8 days of injection of water at a rate of 18.9 L/s and a temperature of 150 °C, 8 days of storage, and 8 days of withdrawal at a rate of 18.9 L/s; thus, composing a 24-day test cycle.

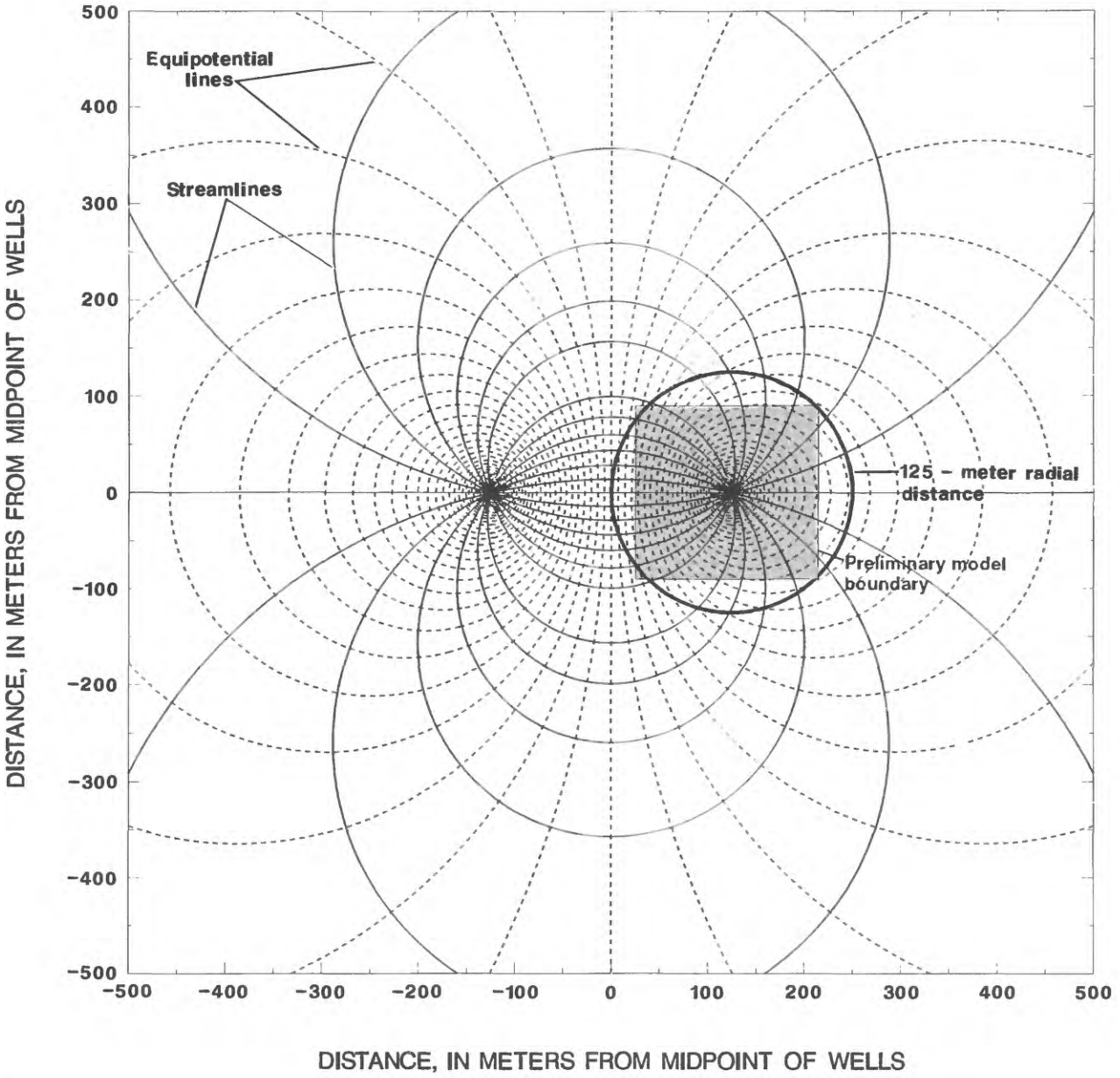

Figure 20.--Flow net showing a doublet-well system similar to the Aquifer Thermal-Energy Storage system and the preliminary model boundary.

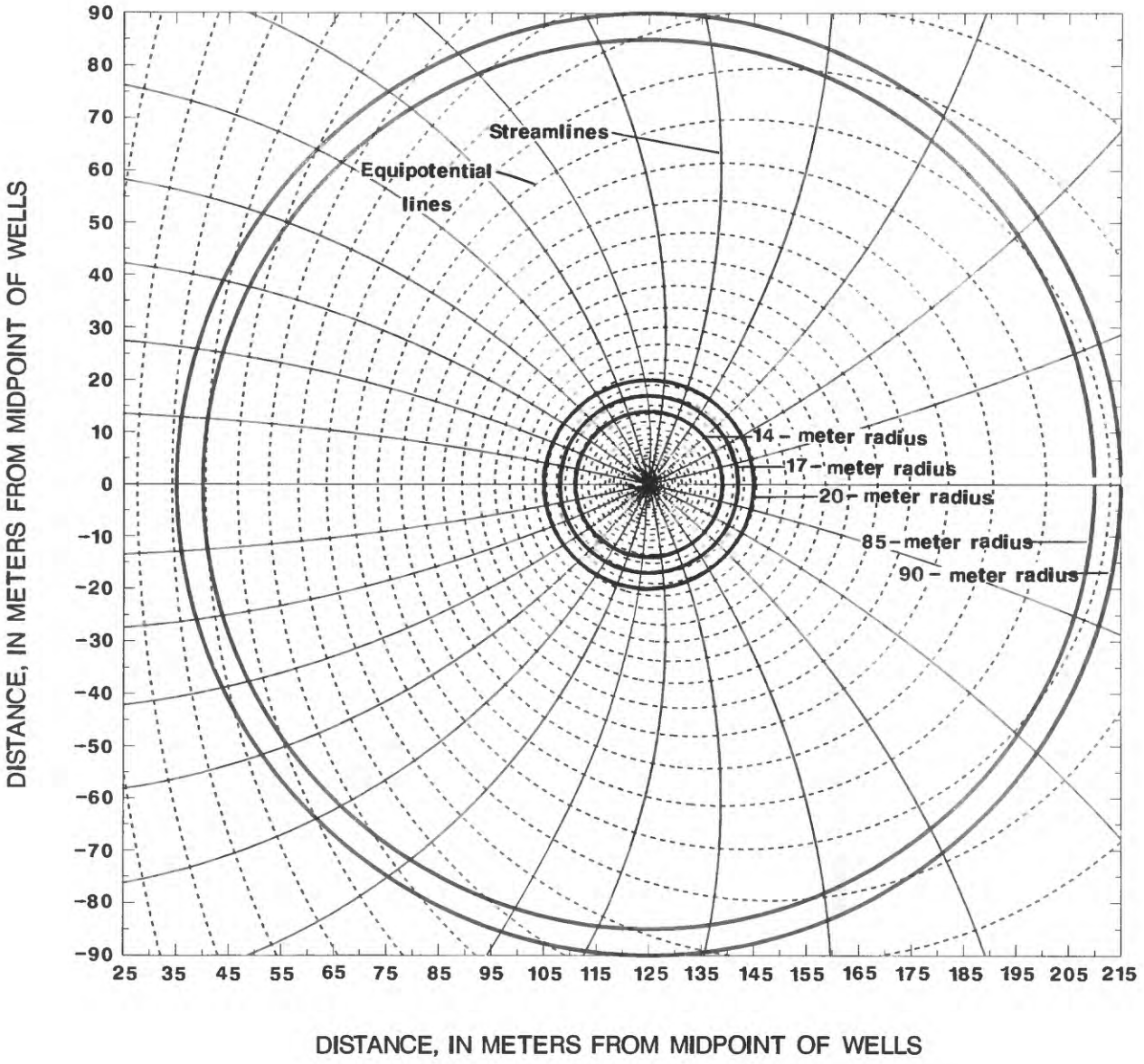

Figure 21.--Flow net within the preliminary model boundary for a doublet-well system similar to the Aquifer Thermal-Energy Storage system.

Table 9.--*Hydraulic zonation, thickness, and horizontal hydraulic conductivity determined from borehole geophysical logs, core samples, and inflatable packer-test data*

Hydraulic zone	Thickness (meters)	Horizontal hydraulic conductivity (meters per day)
Upper part of the Franconia Formation	13.7	0.6
Lower part of the Franconia Formation	24.4	.03
Ironton Sandstone	15.2	1.2
Galesville Sandstone	6.1	.3

Table 10.--*Summary of relevant system thermal properties*

Rock thermal conductivity (aquifer and confining beds)	=	2.20×10^{-5}	joules per meter per day per degree Celsius
Thermal dispersivity	=	3	meters
Rock-heat capacity	=	1.81×10^{6}	joules per cubic meter per degree Celsius

To determine the relative sensitivity of the model simulation to different values of selected properties, temperature versus time plots were constructed from model results and compared with similar plots for the base-model simulation. The temperatures represent a point within the Ironton and Galesville Sandstones at a radial distance of approximately 6.5 m from the injection well. Aquifer thermal efficiency was calculated as a percentage by dividing the total heat produced during withdrawal by the total heat injected. The aquifer thermal efficiency of the base simulation is 51.0 percent. The following discussion of individual properties is ordered from least to most sensitive in the model simulation.

Hydraulic and Thermal Properties

Ratio of Horizontal to Vertical Hydraulic Conductivity

In the radial-flow model, horizontal hydraulic conductivity (K_H) is equal in all horizontal directions. Therefore, the only anisotropy that can be simulated is the ratio of the horizontal to vertical hydraulic conductivity K_H/K_V.

The ratio of K_H to K_V was varied from an isotropic condition ($K_H/K_V = 1$) to K_H/K_V equal to 100. The base value of K_H/K_V is assumed to be 10 (Norvitch and others, 1973). Figure 22 shows that simulation of different values of K_H/K_V had negligible effect on model-computed temperatures. The calculated aquifer efficiencies are 50.7 percent for K_H/K_V equal to 1, and 50.9 percent for K_H/K_V equal to 100. Insensitivity of the model simulations to the ratio of K_H/K_V probably is due to the relatively low values of hydraulic conductivity. The ratio of K_H to K_V will be shown to be more important in the simulation of heat convection at the thermal front due to density differences between the warm injection water and the cooler ground water. The relation between the ratio of K_H to K_V and water-density differences is described in the section on Buoyancy Flow.

Rock-Thermal Conductivity

Values of rock-thermal conductivity were varied in the model according to approximate values given in Clark (1966) for sandstones comparable in composition to those in the Franconia-Ironton-Galesville aquifer. The reduction of rock-thermal conductivity with increase in temperature, as reported by Birch and Clark (1940), Sommerton and others (1965), and Clark (1966), is not accounted for in the SWIP code. This should not be a problem because the reduction of rock-thermal conductivity described by these authors is small for the injection temperature (150 °C) and is within the range described for sandstone aquifers (Clark, 1966) and used in the sensitivity analysis. Figure 23 shows the computed temperatures for different values of rock-thermal conductivity. The plots indicate a small divergence in the computed temperatures during storage, which is reflected in computed aquifer thermal efficiencies of 51.8 and 50.3 percent for the rock-thermal conductivities of 1.25×10^{-5} and 3.14×10^{-5} J/(m-d-°C), respectively. This divergence in temperature probably is due to the effects of the rock-thermal conductivity, which are small during injection in comparison to the effects of heat convection in the moving ground water. Therefore, the simulated effects of thermal conductivity are not observed until the storage period and remain constant through withdrawal.

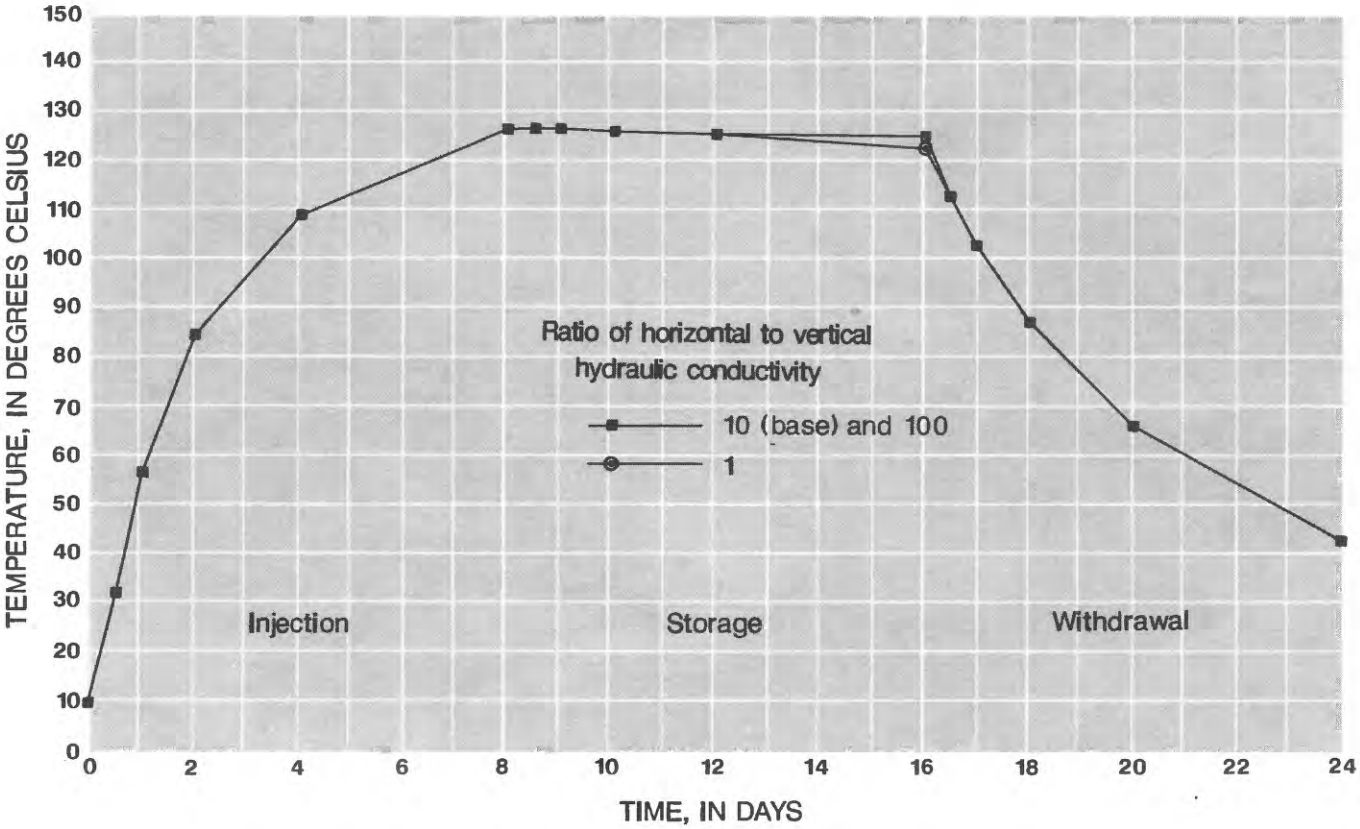

Figure 22.--Model-computed temperatures for different values of horizontal to vertical hydraulic conductivity.

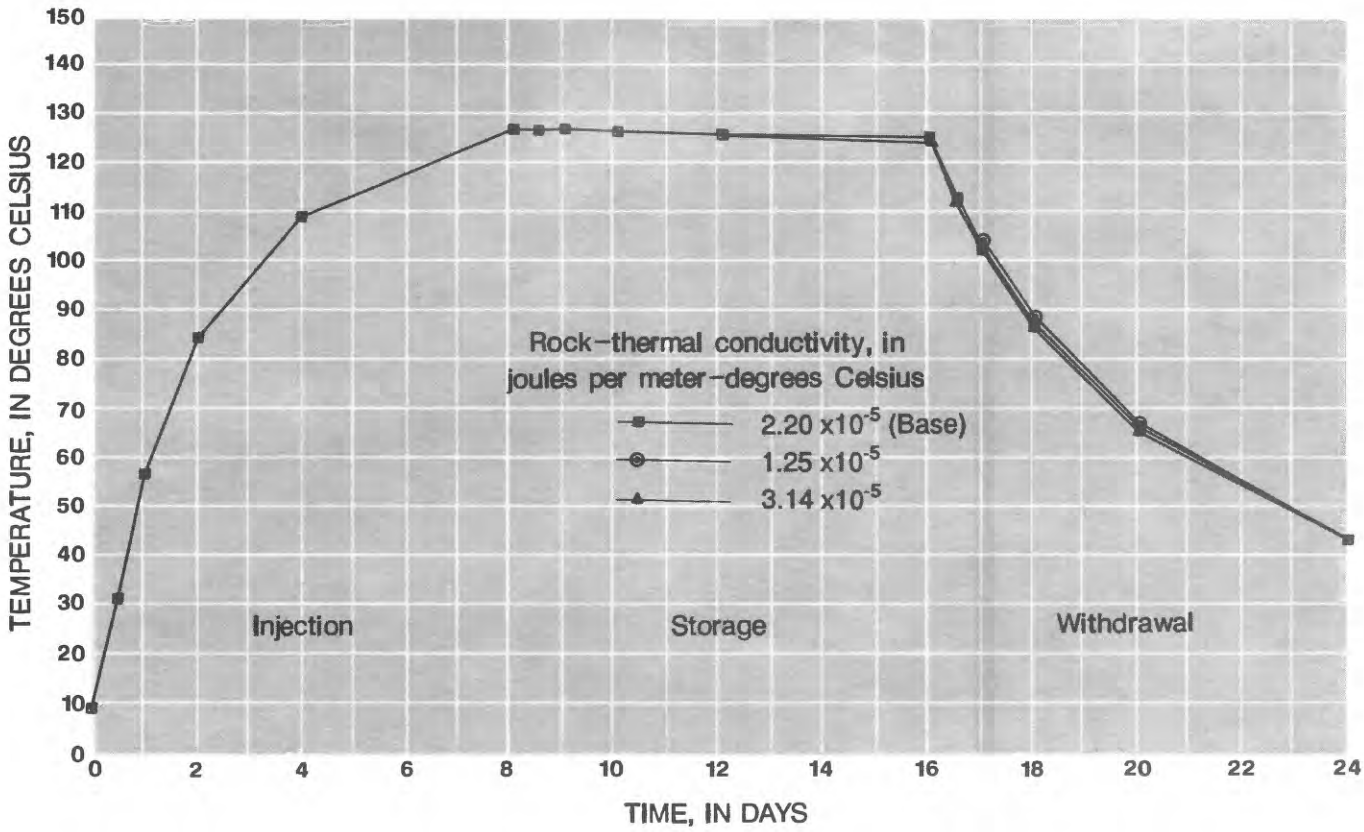

Figure 23.--Model-computed temperatures for different values of rock-thermal conductivity.

Horizontal Hydraulic Conductivity

Values of horizontal hydraulic conductivity (fig. 24) an order of magnitude greater than and less than the assumed base value (table 9) were simulated in the model with the ratio of K_H/K_V equal to 10. The lesser value resulted in computed temperatures and an aquifer thermal efficiency that differed only slightly from the base simulation. The greater value of hydraulic conductivity resulted in lower computed temperatures during storage and a calculated aquifer thermal efficiency of 49.5 percent (base value equals 51.0 percent). This is probably due to vertical convection resulting from the temperature-induced density differences between the natural and injected ground water. This effect is discussed in more detail in the section Buoyancy Flow. In brief, the density differences between the warmer injected water and the cooler water in the aquifer allows hot water to move to the top of the aquifer where heat can be lost to the upper confining layer or move laterally away from the production well.

Porosity

A range of porosity values was selected from published data (Clark, 1966; Norvitch and others, 1973); from the laboratory analysis of core samples; from natural gamma, gamma-gamma, and neutron borehole geophysical data; and from analyses of cores of the Franconia Formation and of the Ironton and Galesville Sandstones in southern Minnesota (Minnesota Gas Co., oral commun., 1980). The values ranged from 0.10 to 0.40. The median value, 0.25, was assumed to be the base value. Differences in model-calculated temperatures (fig. 25) for the value of porosity simulated were greatest during the injection period, which probably is due to the inverse proportionality of porosity to groundwater velocity. During injection/withdrawal, convection of heat by the moving ground water is the major mechanism of energy transport near the well where, for this analysis, the observation point is located. The greater the porosity the slower the heat front will move and, thus, the lower the temperature calculated at the observation point. Model-calculated aquifer efficiencies for the porosities of 0.10 and 0.40 were 51.5 and 50.1 percent, respectively.

An increase in porosity also increases aquifer (water + rock) heat capacity. The greater the aquifer heat capacity the more energy (heat) is required to raise an equal volume of aquifer one degree. This results in less heat, or a lower temperature moving away from the well. Similar effects are described in the next section, Rock-Heat Capacity.

Rock-Heat Capacity

Rock-heat capacity is the product of rock density and rock specific heat and is a measure of the ability of the rock to store heat. Ranges of heat capacity were obtained from Sommerton and others (1965) and calculated with data from Sommerton and others (1965), Clark (1966), Hellgeson and others (1978), and Robie and others (1978), and from methods described by Martin and Dew (1965). The base value for rock-heat capacity represents a sandstone with a composition similar to sandstones in the Franconia-Ironton-Galesville aquifer. The low value of rock-heat capacity represents a quartz-rich sandstone and the high value represents a clay-rich sandstone. The denser the rock, or the higher the specific heat, the greater the energy required to heat the rock. This is reflected in the model-computed temperatures in figure 26

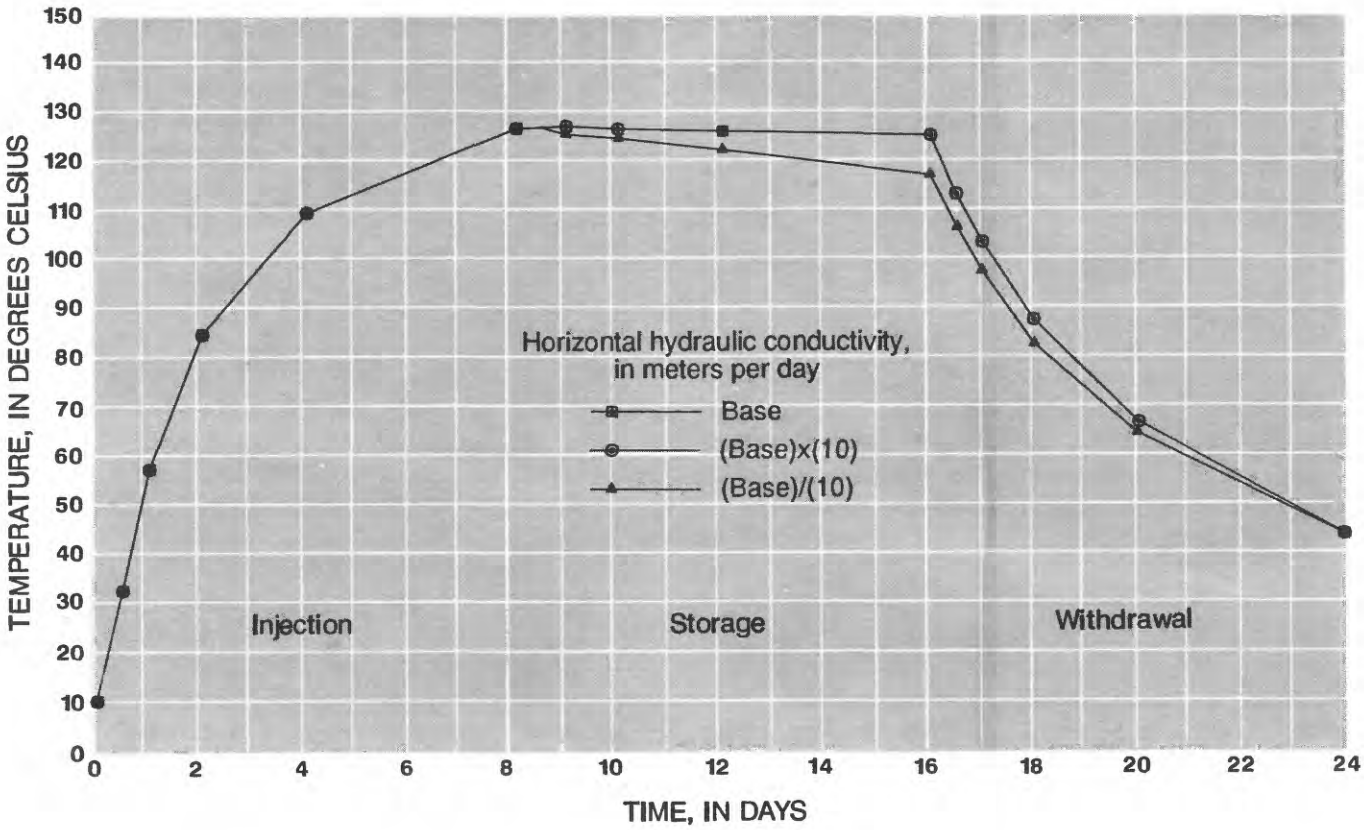

EXPLANATION

Horizontal Hydraulic Conductivity
[in meters per day]

Formation	Base	(Base)x(10)	(Base)/(10)
Upper part of the Franconia Formation	0.6	6	0.06
Lower part of the Franconia Formation	.03	.3	.003
Ironton Sandstone	1.2	12.	.12
Galesville Sandstone	.3	3	.03

Figure 24.--Model-computed temperatures for different values of horizontal hydraulic conductivity.

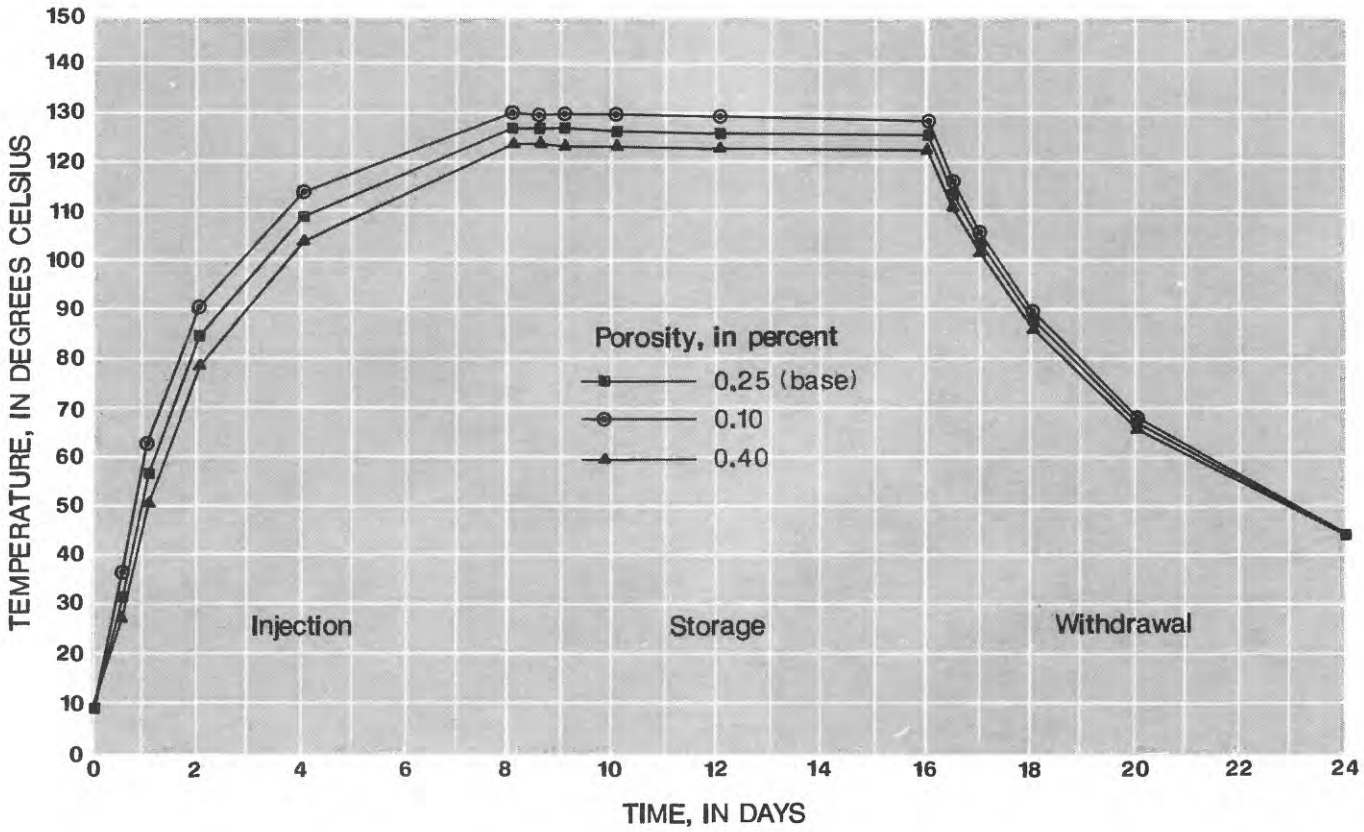

Figure 25.--Model-computed temperatures for different values of aquifer porosity.

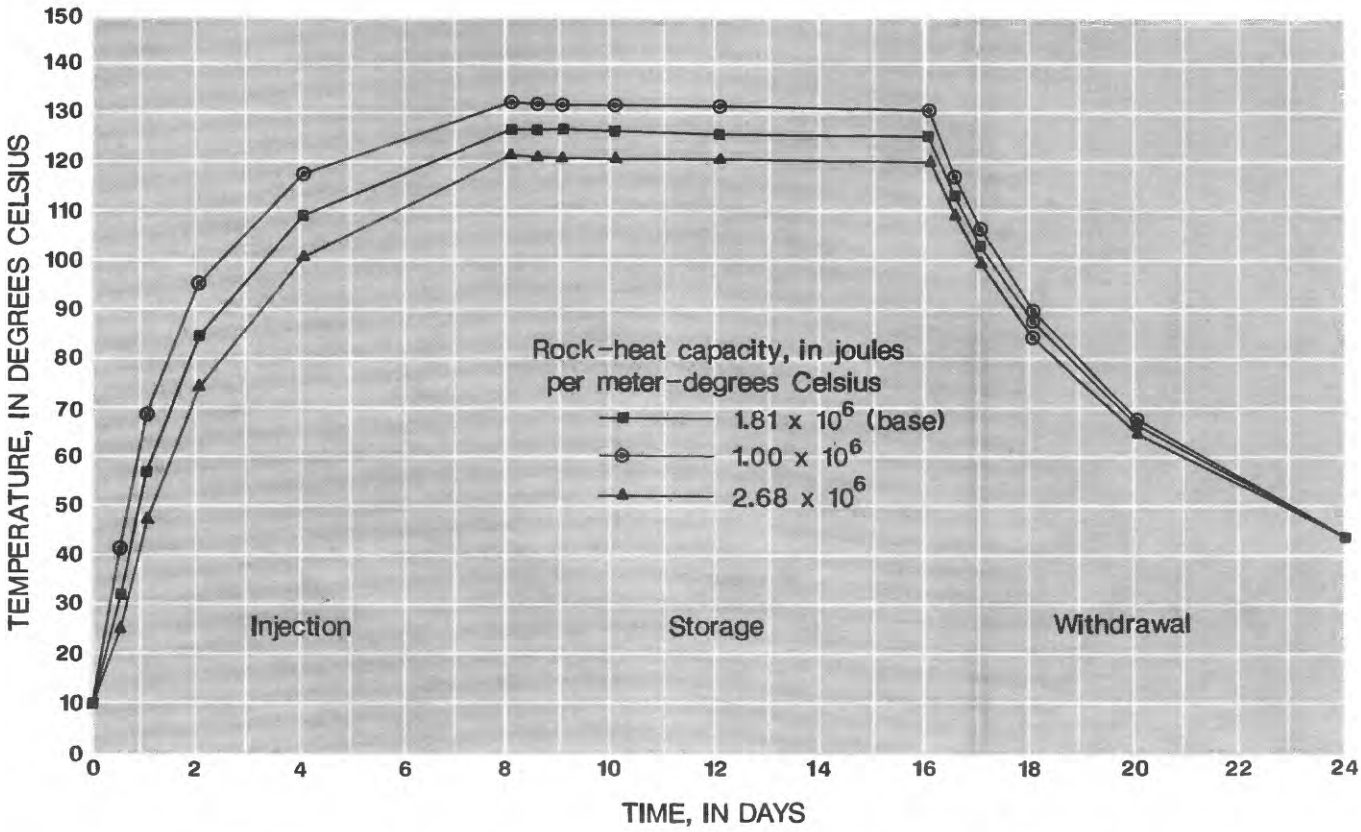

Figure 26.--Model-computed temperatures for different values of rock-heat capacity.

for the different values of rock-heat capacity. Lower temperatures are calculated for higher values of rock-heat capacity due to the energy required to heat the rock. Calculated aquifer thermal efficiencies for rock-heat capacities of 1.00×10^6 and 2.68×10^6 J/(m^3-°C) are 51.7 and 50.3 percent, respectively.

Thermal Dispersivity

The model was most sensitive to thermal dispersivity, which, unfortunately, is the most difficult property to measure in the ground-water-flow system. Although few data exist, Sauty and others (1979) conclude from heat-injection-tracer tests and model studies that thermal dispersivity probably is of the same order of magnitude as dispersivities measured by means of chemical tracers. Sauty and others (1979) also describe thermal dispersivity as a function of scale, suggesting a value of 0.1 m for a heat-storage radius of 10 m in isotropic aquifers. A base value of 3 m was assumed for sensitivity analysis.

In general, thermal dispersivity may be visualized as the dispersion of the thermal front, due to the length of the path a particle might take in going from one point in the aquifer to another point in the aquifer, as a function of the properties of the aquifer. The thermal front, defined for this report, is the transition zone between the warm injected water and the cooler water in the aquifer. Figure 27 shows a plan view of a hypothetical thermal front. It is important to note that the relative width of the thermal front can vary from point to point within the aquifer. When the particle path is more direct, the thermal dispersivity is smaller, the thermal front is thinner, and heated water moves past a given point faster. The longer the path, the larger the dispersivity, the wider the thermal front, and heated water moves past a given point slower. This is apparent in the very high temperature computed by the model early in the injection period, shown in figure 28, for a thermal dispersivity of 0.0 m and the much lower temperature computed for a thermal dispersivity of 6.0 m.

Thermal dispersivity also has the greatest effect on the model computed aquifer thermal efficiencies. A dispersivity of 0.0 m results in an efficiency of 66.8 percent, and a dispersivity of 6.0 m results in an efficiency of 43.4 percent.

Buoyancy Flow

Hellstrom and others (1979) describe the effects of thermal convection, termed buoyancy flow, due to the differences in density of the injected hot water and the cooler water in the aquifer. Their work was related to heat storage in shallow glacioalluvial aquifers, which generally have permeabilities higher than values reported for the Franconia-Ironton-Galesville aquifer. Figure 29 illustrates the effects of buoyancy flow. During early injection, the thermal front is approximately vertical. The thermal front is unstable because the hotter, lower-density water tends to rise convectively above the more dense cold water, resulting in thermal stratification in the aquifer and tilting of the thermal front. Heat losses from the aquifer to the confining units is roughly proportional to the areas of the upper and lower surfaces of the warm water region (fig. 29), (Hellstrom and others, 1979).

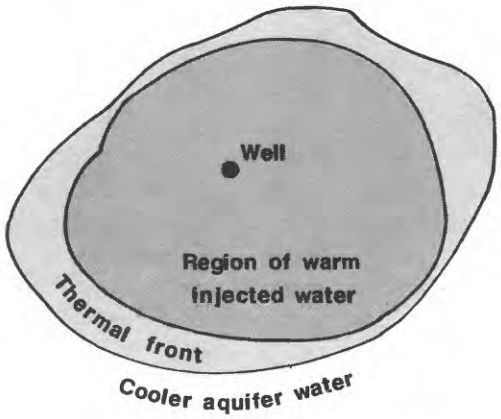

Figure 27.--Plan view of hypothetical heat front.

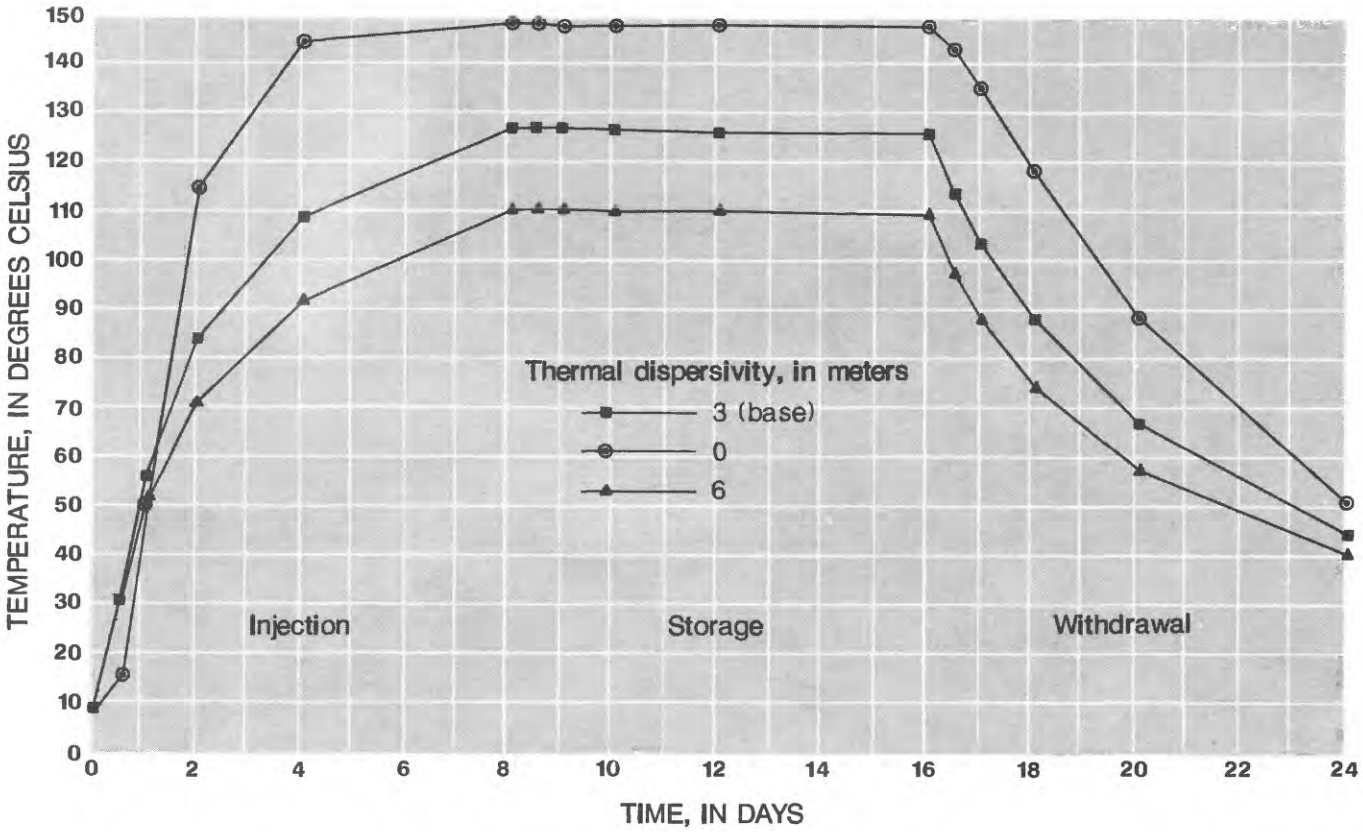

Figure 28.--Model-computed temperatures for different values of thermal dispersivity.

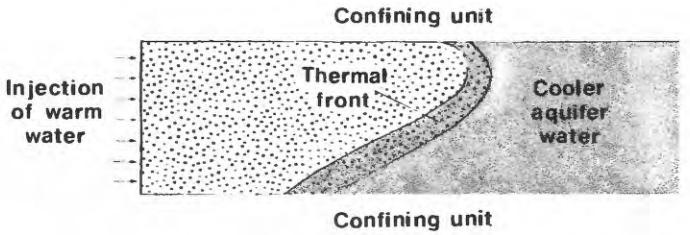

Figure 29.--Horizontal injection of warm water in an aquifer with excessive thermal stratification illustrating tilting of the thermal front or 'buoyancy flow.'

Since buoyancy flow tends to increase this region, it also increases the potential for heat loss. Excessive buoyancy flow may seriously reduce the efficiency of aquifer thermal storage.

To examine the potential for buoyancy flow and its possible effect on the thermal efficiency of the Franconia-Ironton-Galesville aquifer, the non-isothermal, isotropic, single-phase, radial-ground-water flow, thermal-energy-transport model was used to simulate the 24-day test cycle from which temperature versus depth plots were constructed for selected values of horizontal hydraulic conductivity (K_H) and the ratio K_H/K_V. As in previous simulations, the observation point for model-computed temperatures is 6.5 m radially from the injection well. The 24-day test cycle was simulated in the same way as in the sensitivity analysis with 8 days of injection of water at 18.9 L/s and 150 °C, followed by 8 days of storage, and 8 days of withdrawal at 18.9 L/s. To examine the effect of buoyancy flow due to natural convection and that due to forced convection during injection and withdrawal, vertical temperature profiles were constructed for the end of simulated injection, storage, and withdrawal periods.

Figure 30 illustrates temperature profiles at a radial distance of 6.5 m from the injection well for the base conditions (tables 9 and 10) used in the sensitivity analysis and with a K_H/K_V ratio equal to 10. At the end of simulated injection there is little evidence of buoyancy flow. The temperature profile illustrates vertical heat losses to the upper and lower confining layers and to the lower part of the Franconia Formation. The vertical and horizontal heat losses are apparent after the storage period, but tilting of the thermal front is small. At the end of withdrawal, thermal tilting is not apparent. It should be noted that there is some vertical convection, which can be observed by comparing the model-computed temperatures in the confining layers. At the end of the withdrawal period, the temperature within the upper confining bed, the St. Lawrence Formation, is warmer than the temperature in the lower confining bed, the Eau Claire Formation, even though the temperature in the Ironton and Galesville Sandstones is hotter than the temperature in the upper part of the Franconia Formation. It also should be noted that temperatures in the lower part of the Franconia Formation continued to increase during withdrawal, indicating that heat conduction from above and below is greater than forced convection from pumping into or out of this part of the aquifer. If heat injected or conducted to the lower part of the Franconia Formation is not recoverable, the efficiency of the aquifer thermal-storage system could be significantly reduced.

Figure 31 illustrates the model-computed temperature profile for conditions similar to those in figure 30 except that horizontal and vertical hydraulic conductivity are equal. The computed temperature profiles in figure 31 are similar to figure 30 except for a slightly larger tilt in the thermal front after the storage period and slightly higher temperatures in the upper confining bed (St. Lawrence Formation) and the lowermost point in the lower part of the Franconia Formation. This is because simulation of a larger vertical hydraulic conductivity allowed for easier vertical heat conduction resulting in greater thermal stratification and buoyancy flow. The small amount of heat lost due to greater buoyancy is reflected in a calculated aquifer thermal efficiency 0.2 percent lower than the aquifer thermal efficiency calculated for base conditions.

Property	Assumed base condition	
Ratio of horizontal to vertical hydraulic conductivity	10	
Rock thermal conductivity	2.2×10^{-5}	joules per meter per day per degree Celsius
Thermal dispersivity	3	meters
Rock-heat capacity	1.18×10^{6}	joules per cubic meter per degree Celsius
Porosity	0.25	
Horizontal hydraulic conductivity		
Upper part of the Franconia Formation	0.6	meters per day
Lower part of the Franconia Formation	0.03	meters per day
Ironton Sandstone	1.2	meters per day
Galesville Sandstone	0.3	meters per day

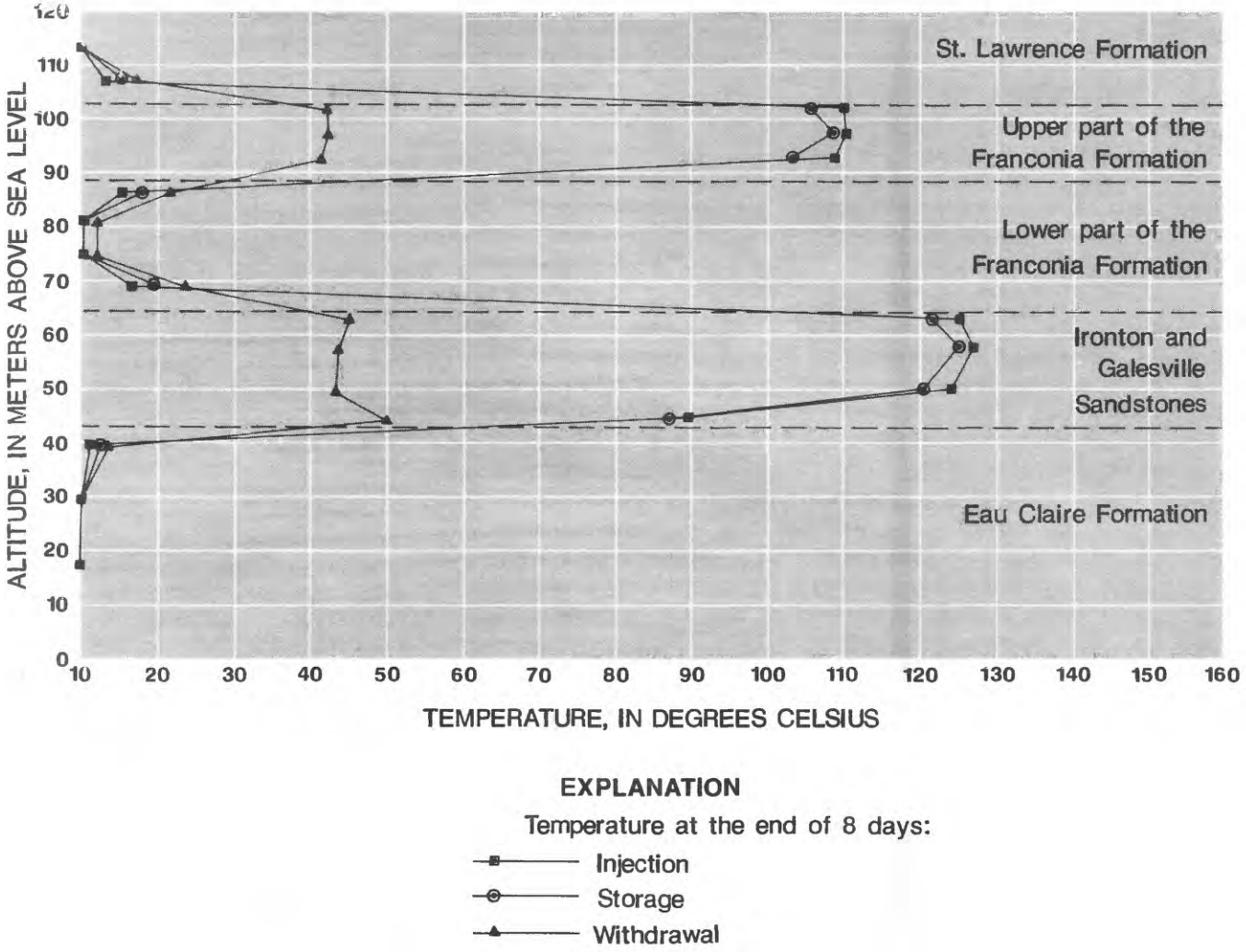

Figure 30.--Model-computed temperature profiles at the end of simulated injection, storage, and withdrawal for assumed base conditions.

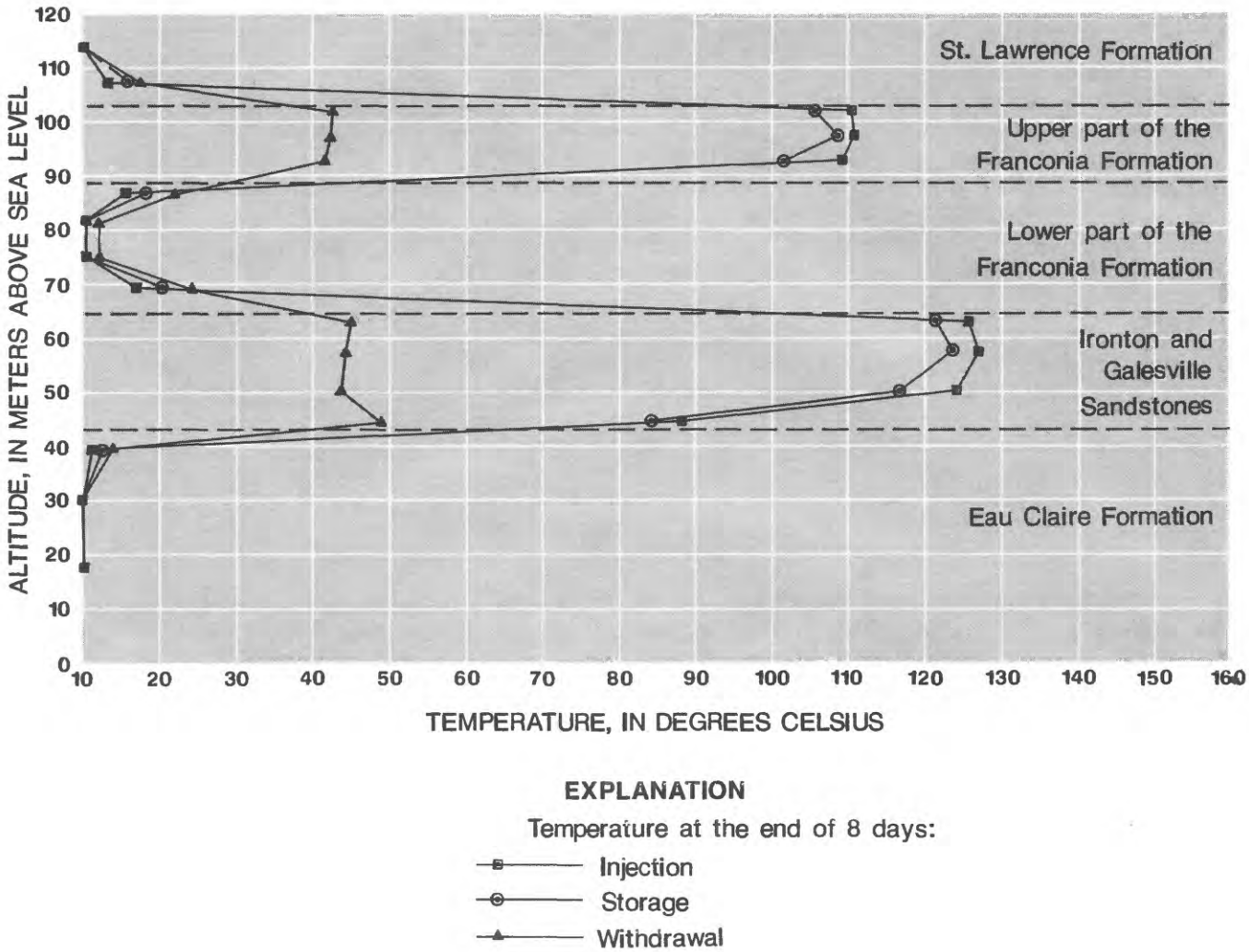

Figure 31.--Model-computed temperature profiles at the end of simulated injection, storage, and withdrawal for base conditions and horizontal equal to vertical hydraulic conductivity.
(Base conditions are referenced on Figure 30)

To examine further the effects of buoyancy flow within the possible range of hydraulic conductivity for the aquifer, hydraulic conductivity was simulated as 10 times the base values with K_H/K_V ratio equal to 10 (fig. 32). The computed temperature profiles at the end of the storage period are similar to those in figures 30 and 31 except in the Ironton and Galesville Sandstones in which the thermal front is moderately tilted. Also, computed temperatures are higher in the upper part of the Ironton and Galesville Sandstones during the withdrawal period than in the previous simulation. This resulted in greater heat loss to the lower part of the Franconia Formation and an aquifer thermal efficiency 1.3 percent lower than in the base simulation.

Figure 33 illustrates model-computed temperature profiles for hydraulic conductivities 10 times the base values and K_V equal to K_H. Buoyancy flow is evident in the thermal tilting produced in both the upper part of the Franconia Formation and in the Ironton and Galesville Sandstones at the end of the storage and withdrawal periods. The greater buoyancy flow resulted in an aquifer thermal efficiency 2.9 percent lower than in the base simulation.

It is important to note that the temperature in the lower part of the Franconia Formation continued to increase throughout the simulated test cycle for each of the assumed conditions. As stated earlier, losses to the lower part of the Franconia Formation may result in a significantly lower thermal efficiency of the aquifer. A method for possible reduction of heat loss to this part of the aquifer may be to screen only the permeable parts of the upper Franconia Formation and the Ironton and Galesville Sandstones and, thus, not inject hot water directly into the lower Franconia.

Finally, it must be noted that in simulations used to investigate buoyancy flow and tilting of the thermal front, only horizontal and vertical hydraulic conductivity were varied while other hydraulic and thermal properties were not. It is possible that for other values of porosity, thermal dispersivity, rock-heat capacity, and thermal conductivity different results may be obtained for simulations of buoyancy flow.

Aquifer Thermal Efficiency

The feasibility and success of an ATES system are determined by the amount of thermal energy that can be stored in and recovered from the aquifer. Aquifer thermal efficiency, expressed as a percent, is calculated as the total energy withdrawn divided by the total energy injected. For base values of hydraulic and thermal properties, the flow and energy-transport model calculated a thermal efficiency of 51.0 percent for simulation of short-term test cycles. Although the model is sensitive to values of certain hydraulic and thermal characteristics in terms of calculated temperature, simulation of different values of the properties resulted in only small differences in calculated thermal efficiency. Generally these differences were less than 2 percent, however, when thermal-dispersivity values were changed, differences in calculated thermal efficiencies were approximately 7 percent. In terms of estimating aquifer thermal efficiency, the model sensitivity analysis only indicates the possible range of thermal efficiency based on possible ranges in values of hydraulic and thermal properties. Better definition of these properties will improve model estimates of efficiency.

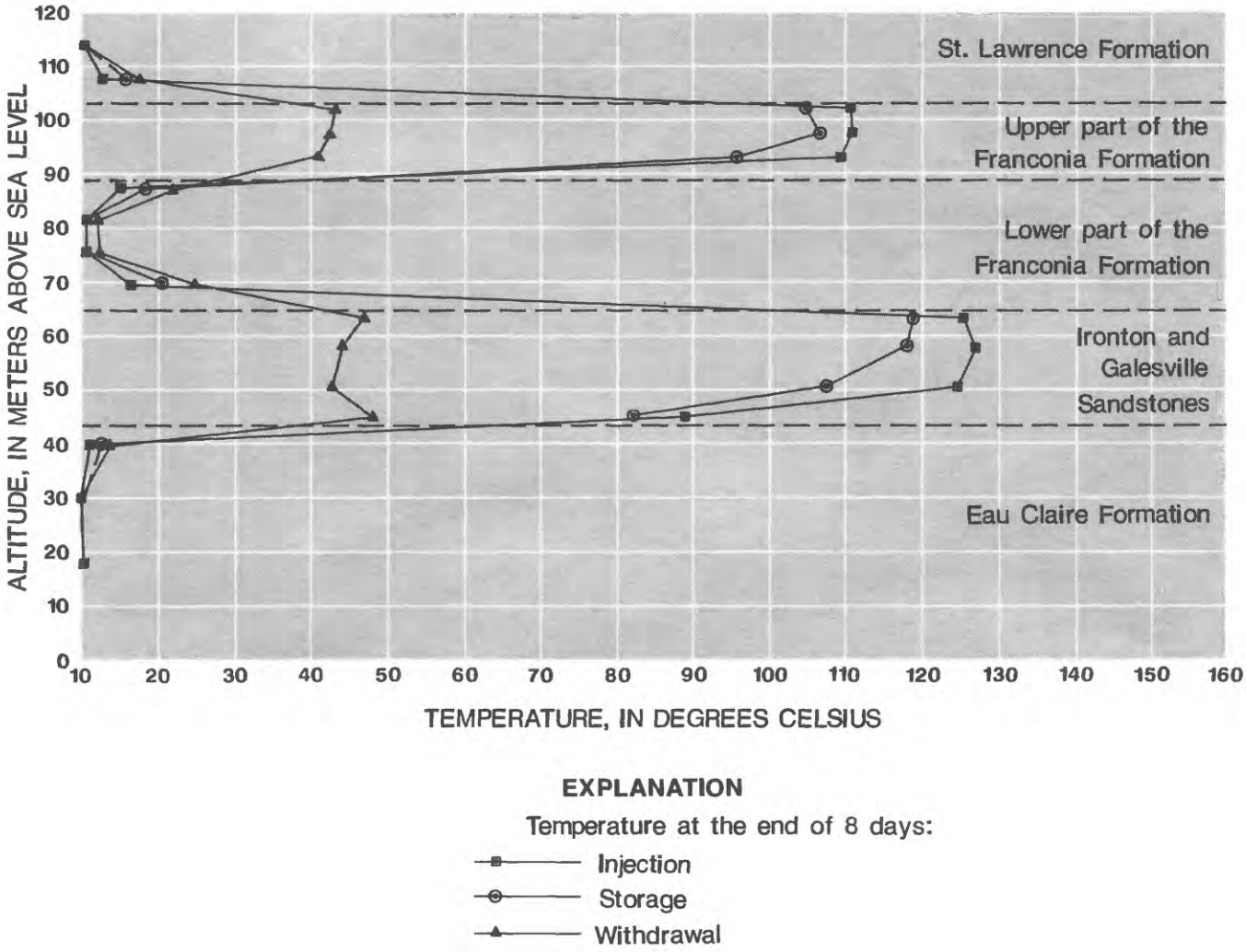

Figure 32.--Model-computed temperature profiles at the end of simulated injection, storage, and withdrawal for hydraulic conductivities equal to 10 times the base value.
(Base conditions are referenced on Figure 30)

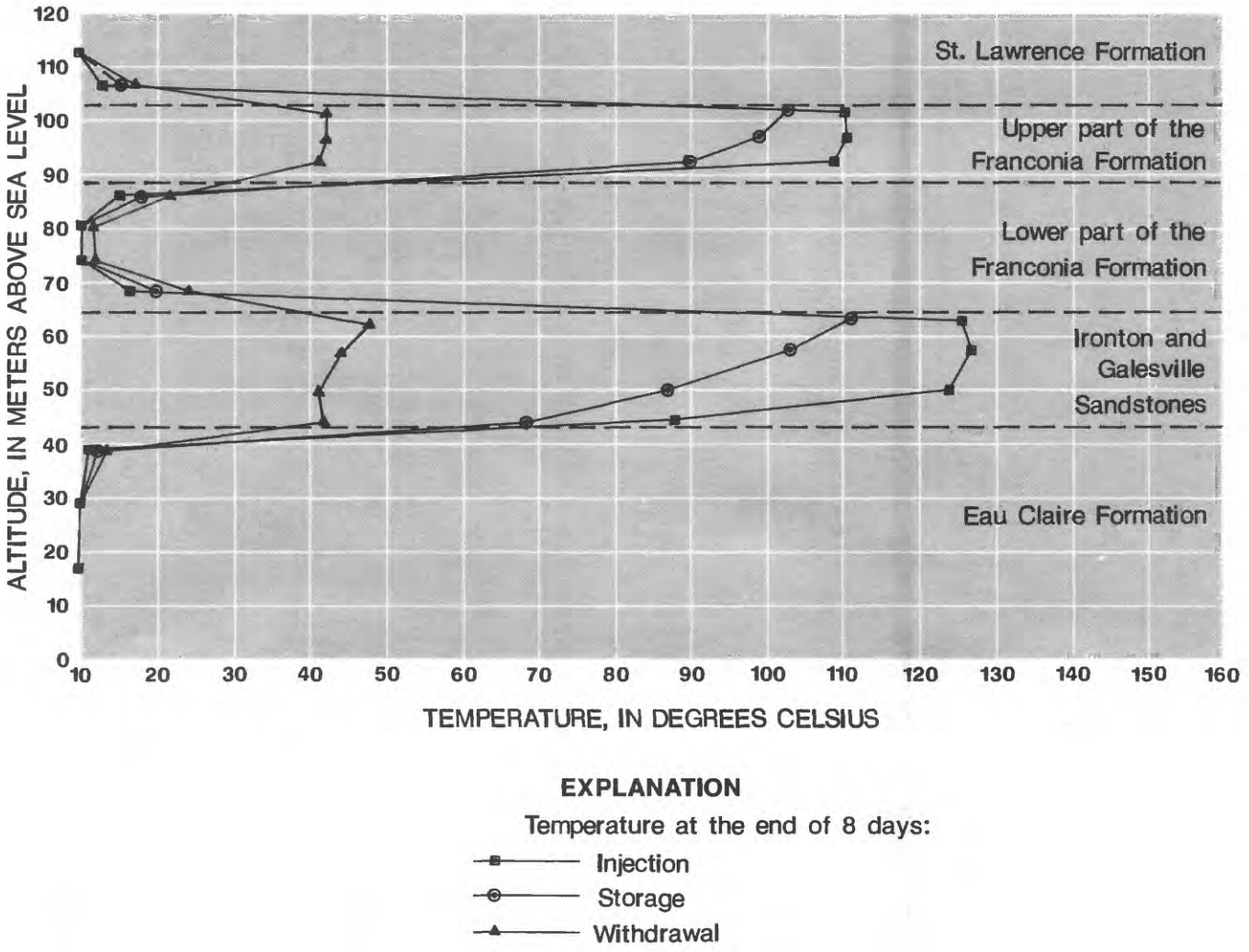

Figure 33.--Model-computed temperature profiles at the end of simulated injection, storage, and withdrawal for horizontal hydraulic conductivities equal to 10 times the base value and horizontal equal to vertical hydraulic conductivity.
(Base conditions are referenced on Figure 30)

The sensitivity analysis indicates which properties need to be defined more precisely in order to make the model estimate as accurate as possible. However, in addition to the physical properties of the aquifer system, there are also operational factors that will affect the thermal efficiency of the ATES system. These factors include temperature of injected water, rate of injection and withdrawal, and duration of injection, storage, and withdrawal. To test the effects of these factors on thermal efficiency, a series of model simulations were performed in which these factors were varied and the results compared. Base values of hydraulic and thermal properties were used in all these simulations.

Radial Flow Simulations

As described earlier, the ability of the preliminary radial-flow model to simulate the ATES doublet-well system is related to the radial distance that heat will move from the well for the period of simulation. Model-computed temperatures for the short-term-cycle simulations (fig. 34) indicate that injected heat was contained within a radial distance of approximately 20 m. This radial distance is shown in figure 21. Comparison of the equipotentials for the doublet-well system and the 20-m, model-computed, radial extent of heat indicates that the short-term-cycle simulations are representative of the doublet-well system.

The longer term simulations (figs. 35 to 38) indicate that heat will be contained within an 85-m radial distance for the 6-month injection periods and a 90-m radial distance for the 8-month injection periods. These two radial distances are plotted on figure 21. A comparison of the 85-m and 90-m radial distances with the equipotentials for the doublet-well system indicates that the preliminary model radial-flow assumption may not adequately represent the doublet-well system for the longer-term cycles. However, the usefulness of the results of the preliminary model long-term simulations is not affected because the purpose of the simulations is to describe how the operational factors of injection and withdrawal rates and duration can affect the aquifer efficiency. The aquifer efficiencies obtained from the long-term simulations are termed relative. Although they may not exactly represent efficiencies that would be obtained from the working ATES doublet-well system, they are comparable to each other and, thus, serve the intended purpose.

For purposes of this study, short-term testing cycles are defined as 8 days of injection at 18.9 L/s of 150 °C water, 8 days of storage, and 8 days of withdrawal at 18.9 L/s for a total cycle of 24 days. Figure 34 shows a plot of model-computed well-bore temperatures versus time for five sequential 24-day cycles as simulated by the base radial-flow model. Also indicated at the end of each 24-day cycle is the aquifer thermal efficiency. The plot indicates that for the short-term uniform cycles the aquifer thermal efficiency tends to increase with successive cycles. This is because injected water must heat up the aquifer from its initial ambient temperature of approximately 10 °C. At the beginning of subsequent injections, the aquifer is warmer due to residual heat that was not completely recovered from the previous cycle. The graph also indicates that the aquifer thermal efficiency will approach a maximum value after several cycles. For the simulation depicted in figure 34, the maximum aquifer efficiency probably will be between 60 and 65 percent.

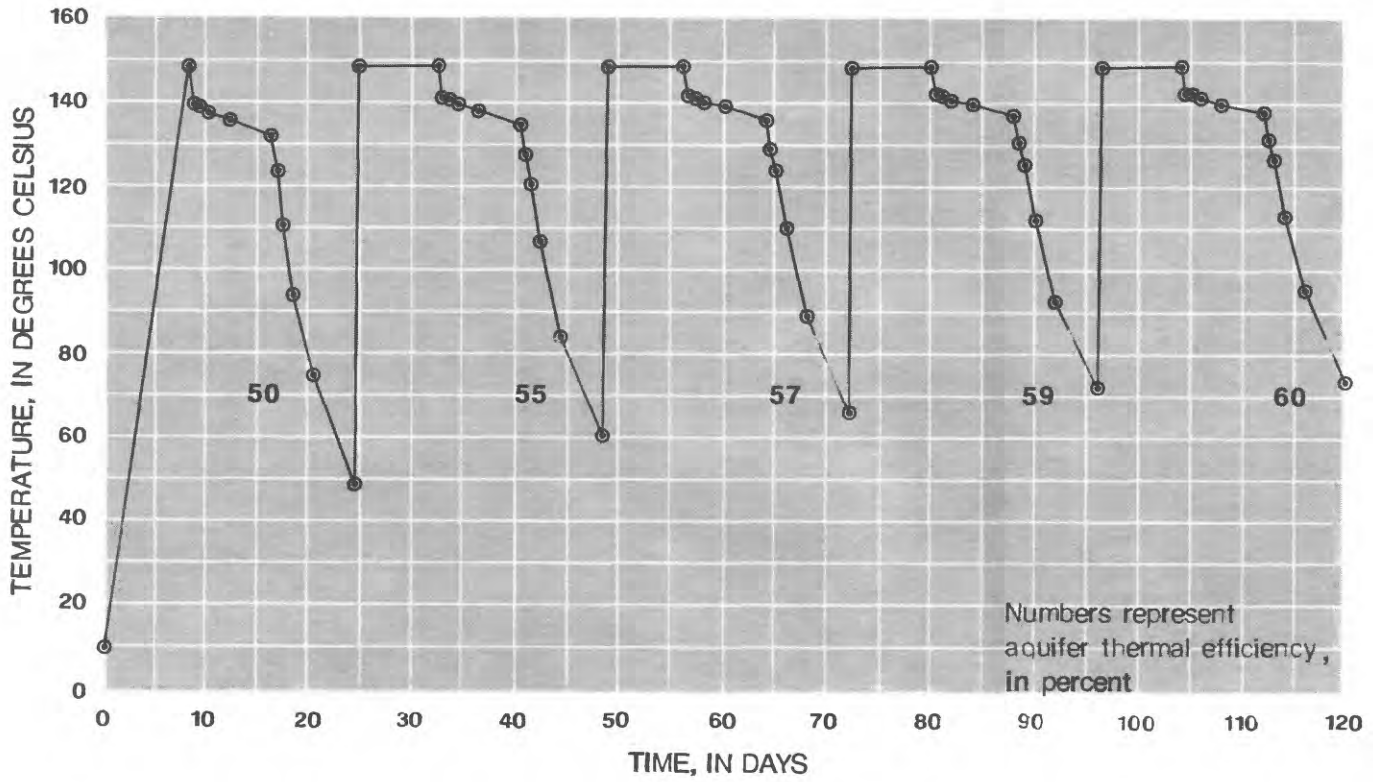

Figure 34.--Model-computed well-bore temperatures and aquifer thermal efficiencies for five sequential 24-day test cycles.

A working ATES system would not operate on the short-term (24 day) test cycles, but rather on yearly cycles based on seasonal thermal-energy surplus and demand. Figure 35 shows model-computed well-bore temperatures and relative thermal efficiencies for five continuous 1-year cycles of 8 months of injection at 18.9 L/s and 150 °C and 4 months of withdrawal at 18.9 L/s. The model conditions are similar to those previously described for the five 24-day cycles. Relative aquifer thermal efficiencies range from 34 to 39 percent and well-bore temperatures at the end of withdrawal range from approximately 80 to 105 °C.

Figure 36 shows model-computed well-bore temperatures and relative aquifer thermal efficiencies for conditions similar to those shown in figure 35 except that the withdrawal rate is 37.7 L/s. The relative aquifer thermal efficiency ranges from 51 to 59 percent and the well-bore temperature at the end of each cycle ranges from approximately 55 to 78 °C.

Figure 37 shows model-computed well-bore temperatures and relative aquifer thermal efficiencies calculated for five continuous 1-year cycles each consisting of 6 months of injection at 18.9 L/s and 150 °C and 6 months of withdrawal at 18.9 L/s. Relative aquifer thermal efficiency at the end of each cycle ranges from 52 to 61 percent and the well-bore temperature at the end of each cycle ranges from approximately 46 to 78 °C.

Figure 38 shows model-computed well-bore temperatures and relative aquifer thermal efficiencies calculated for conditions similar to figure 37 except that the withdrawal rate is 37.8 L/s. Relative aquifer thermal efficiencies are the highest of any of the simulations and range from 73 to 84 percent. This simulation also produces the lowest well-bore temperatures at the end of each cycle, ranging from approximately 27 to 45 °C. To summarize, figures 35 through 38 illustrate relative aquifer thermal efficiencies and well-bore temperatures based on 1-year cycles with hypothetical injection/withdrawal rates and periods. It is obvious from a comparison of the graphs that operational methods that increase aquifer thermal efficiency also lower well-bore temperatures at the completion of each cycle. Thus, for a working ATES system, a required minimum well-bore temperature may also limit the aquifer thermal efficiency. The simulations shown in figures 34 through 38 also demonstrate one method for developing an optimization scheme for a working ATES system by use of a calibrated ground-water-flow and thermal-energy-transport model.

Three-Dimensional Model

Analysis of aquifer-test data described earlier indicates the upper Franconia and Ironton-Galesville parts of the aquifer are areally anisotropic and at an angle of approximately 30 degrees between the major axis of transmissivity and the axis between the two wells. Although the anisotropy may be considered to be small (less than 3:1), its effect on the movement and direction of heat flow for these particular hydrologic conditions is not known. Reducing the problem to one of radial-flow would neglect this anisotropic effect. The potential errors introduced in the radial-flow assumptions were examined earlier in this report in the section describing the radial-flow model. Based on that discussion, it was decided to construct a three-dimensional model to more accurately represent field conditions and simulate the

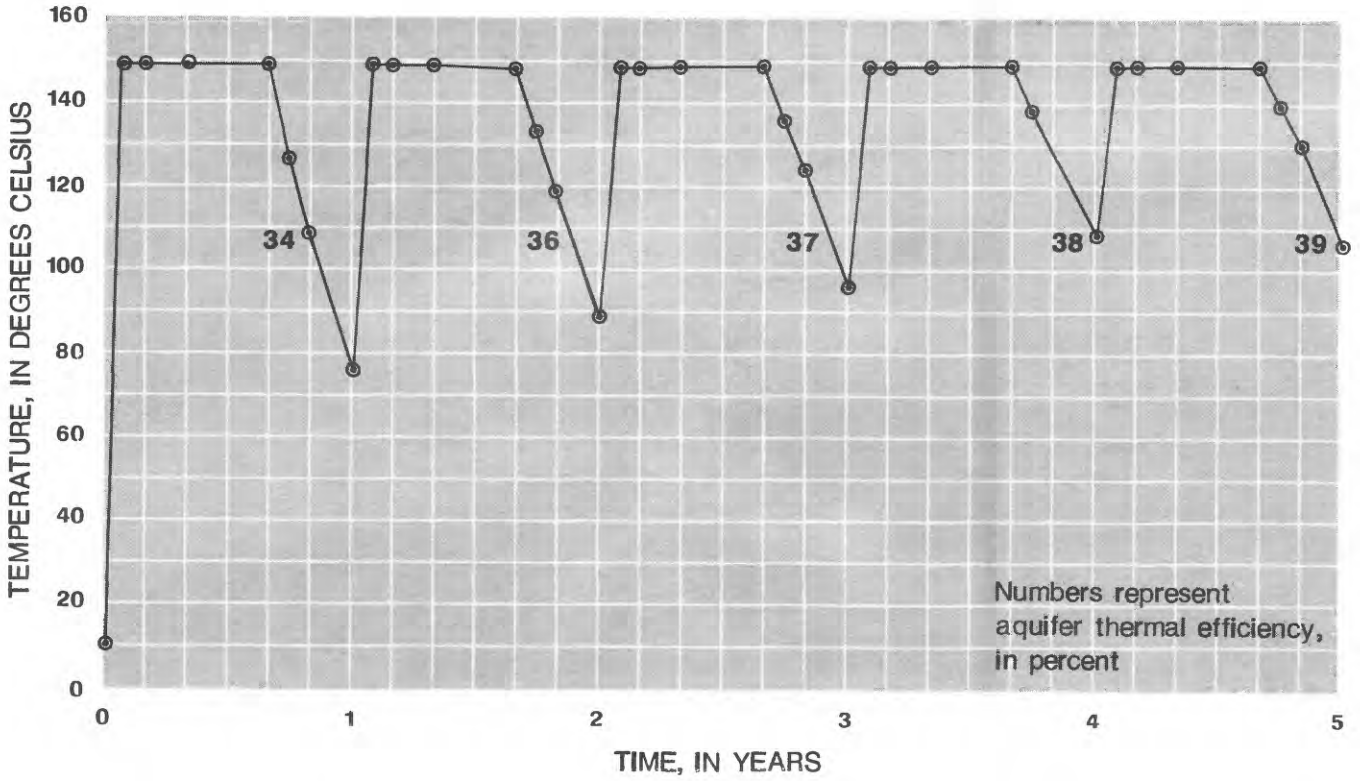

Figure 35.--Model-computed well-bore temperatures and aquifer thermal efficiencies for five sequential 1-year cycles each consisting of 8-months injection at 18.9 liters per second and 4-months withdrawal at 18.9 liters per second.

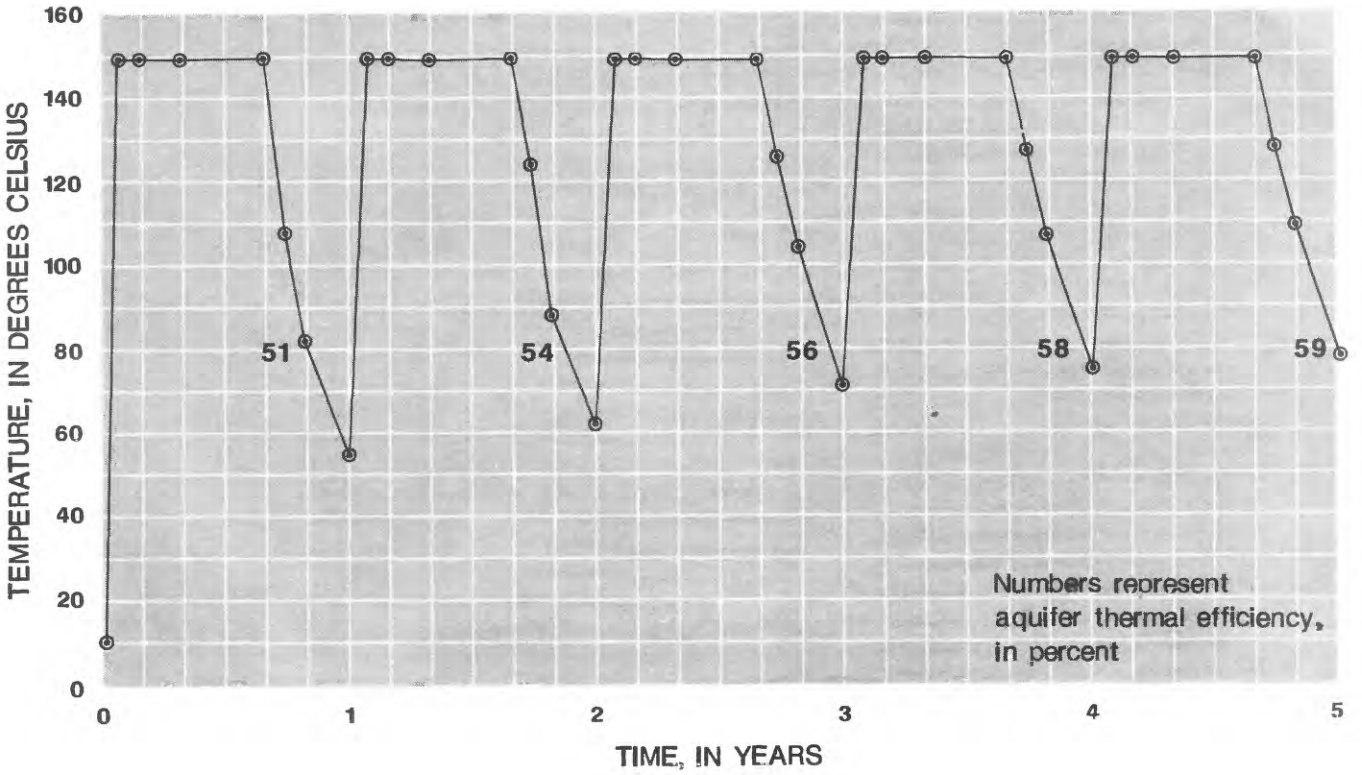

Figure 36.--Well-bore temperatures and calculated aquifer relative efficiencies for five hypothetical 1-year cycles of 8-months injection at 18.9 liters per second of 150 degrees Celsius water and 4-months of withdrawal at 37.7 liters per second.

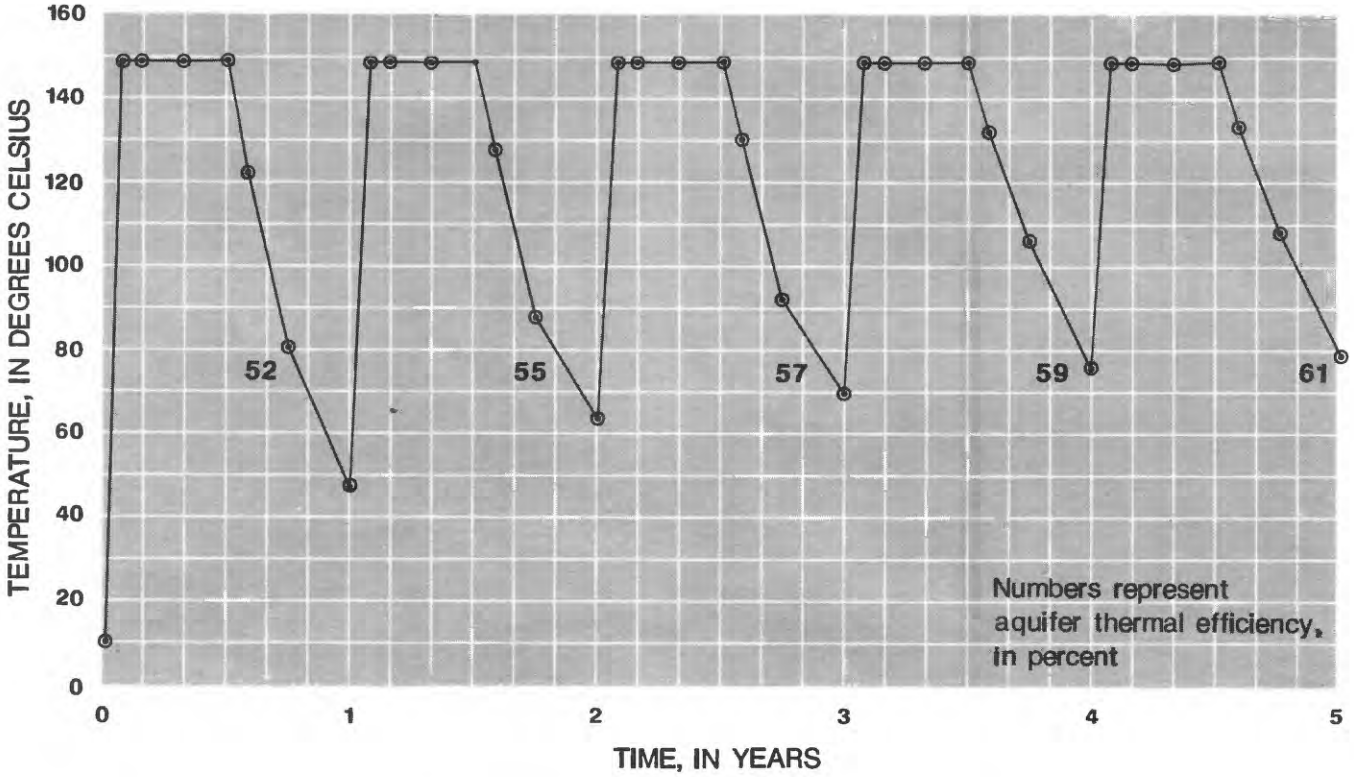

Figure 37.--Well-bore temperatures and calculated aquifer relative efficiencies for five hypothetical 1-year cycles of 6-months injection at 18.9 liters per second of 150 degrees Celsius water and 6-months of withdrawal at 18.9 liters per second.

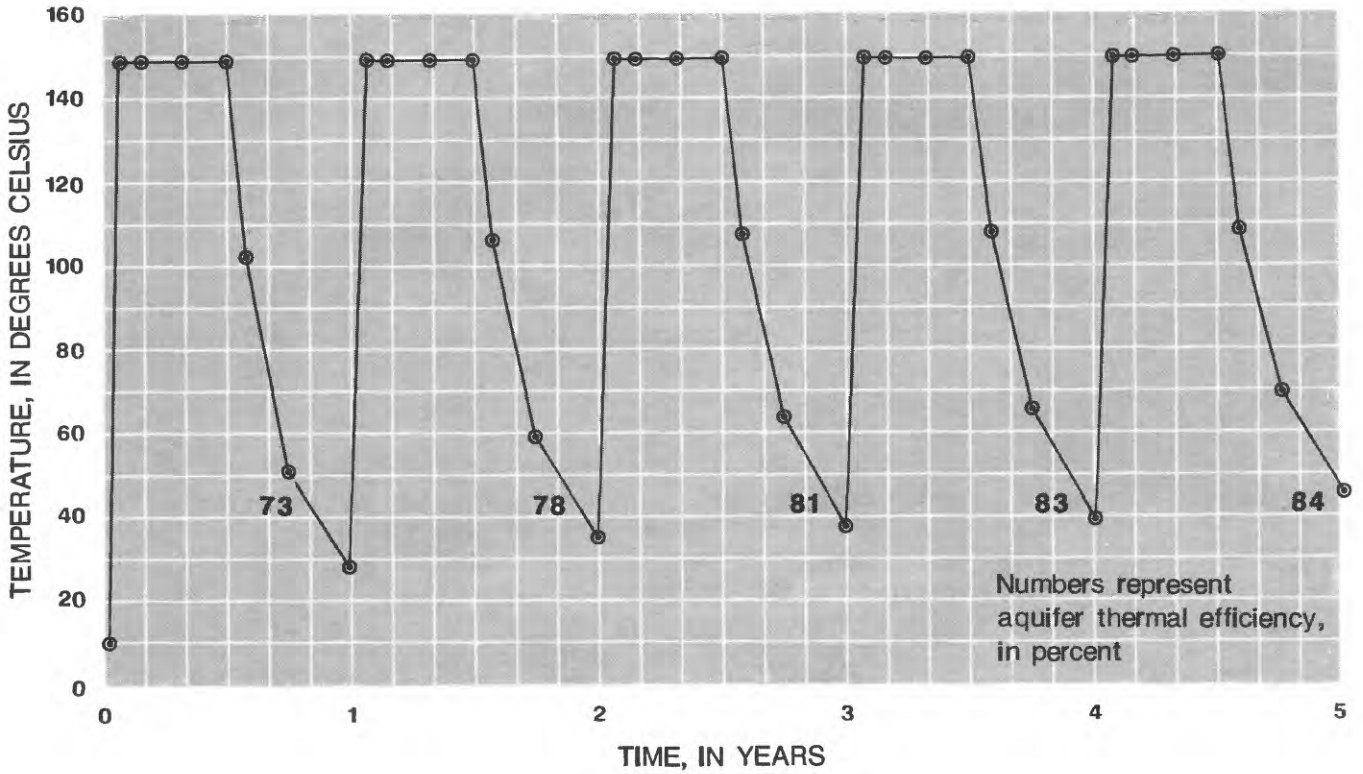

Figure 38.--Well-bore temperatures and calculated aquifer relative efficiencies for five hypothetical 1-year cycles of 6-months injection at 18.9 liters per second of 150 degrees Celsius water and 6-months withdrawal at 37.8 liters per second.

ATES short-term tests. This section of the report describes the construction and calibration of the isothermal hydraulic-flow part of the model that incorporates the effects of anisotropy.

Finite-Difference Grid Design

The area around the ATES doublet-well system that can be modeled is severely limited by (1) constraint on the finite-difference grid spacings inherent in the model solution techniques, (2) the fact that the axes of aquifer anisotropy and the axis on which the doublet wells are located are not aligned, and (3) the large cost of running the model for large three-dimensional problems. Miller and Voss (1986) describe an analytical solution for steady flow in an isothermal, anisotropic, doublet-well system. They describe a method to simplify and reduce the simulated region to a computationally economical size while retaining the main physical attributes of the flow and energy-transport regime. The procedure begins with an analytical solution for flow in an isotropic, isothermal, doublet-well system and modifies the solution for the effects of anisotropy and the nonalignment of principal directions of hydraulic conductivity with the doublet-well axis.

Bear (1972, p. 320) gives the analytical solution for a two-dimensional flow field around a doublet-well system in an infinite, isotropic, isothermal, confined aquifer where one well is withdrawing water and the other is injecting water, both at the same rate. In terms of the velocity potential, Φ, and stream lines, Ψ, the solution can be written:

$$\Phi = \frac{Q}{4\pi b} \ln \frac{(X_B + d_B)^2 + Y_B^2}{(X_B - d_B)^2 + Y_B^2} \tag{26}$$

Since $\Phi = K\phi$ it follows that (26a)

$$\phi = \frac{Q}{4\pi Kb} \ln \frac{(X_B + d_B)^2 + Y_B^2}{(X_B - d_B)^2 + Y_B^2} \tag{26b}$$

finally $T = Kb$ therefore

$$\phi = \frac{Q}{4\pi T} \ln \frac{(X_B + d_B)^2 + Y_B^2}{(X_B - d_B)^2 + Y_B^2} \tag{26c}$$

$$\Psi = \frac{Q}{4\pi b} \tan^{-1}\left(\frac{-2Y_B d_B}{X_B^2 + Y_B^2 - d_B^2} \right) \tag{27}$$

where:

X_B, Y_B = orthogonal coordinates [L] (m),

d_B = one-half distance between two wells [L] (m),

Q = rate of flow of source and sink [L^3/t] (m^3/s),

T = aquifer transmissivity, [L^2/t] (m^2/s),

b = aquifer thickness, [L] (m),

K = aquifer hydraulic conductivity, [L/T] (m/s), and

ϕ = equipotential, [L] (m).

The first step involves describing the isotropic coordinate system X_B, Y_B, in terms of a rotated coordinate system X_i, Y_i, and θ, where θ is the angle between the X_i and X_B axes. Taking the inverse transform and expressing it in matrix notation,

$$\begin{bmatrix} X_B \\ Y_B \end{bmatrix} = \begin{bmatrix} \cos\theta & \sin\theta \\ -\sin\theta & \cos\theta \end{bmatrix} \begin{bmatrix} X_i \\ Y_i \end{bmatrix} \tag{28}$$

The next step is to take the transformation from an anisotropic to an equivalent isotropic coordinate system described by Freeze and Cherry (1979) as:

$$X_i = X_f \tag{29}$$

$$Y_i = Y_f \left(\frac{K_{xf}}{K_{yf}} \right)^{1/2} \tag{30}$$

where X_f, Y_f are the true field coordinates in the anisotropic system, and K_{xf}, K_{yf} are the respective maximum and minimum values of horizontal hydraulic conductivity, where K_{xf} is aligned in the X_i direction. For the case where the thickness of the confined aquifer is constant, equation 30 may be written in terms of transmissivity as:

$$Y_i = Y_f \left(\frac{T_{xf}}{T_{yf}} \right)^{1/2} \tag{31}$$

Substituting 29, 30 and 31 into 28 and solving for X_B and Y_B yields

$$X_B = X_f \cos\theta + Y_f \left(\frac{T_{xf}}{T_{yf}} \right)^{1/2} \sin\theta \tag{32}$$

$$Y_B = -X_f \sin\theta + Y_f \left(\frac{T_{xf}}{T_{yf}} \right)^{1/2} \cos\theta \tag{33}$$

which are the coordinates of the isotropic flow-field solution expressed in an anisotropic nonaligned field-coordinate system. As described by Miller and Voss (1986) one further correction to the values of θ and d_B is necessary in order to express them in terms of the true distance between the wells, d_f, and the true field angle, θ_f, from the maximum transmissivity direction to the well axis. This expression is

$$d_B = \left(\frac{T_{xf}}{T_{yf}} \right)^{1/2} \left(\frac{d_f \sin\theta_f}{\sin\theta} \right) \tag{34}$$

where θ is described by

$$\theta = \tan^{-1} \left((\tan\theta_f) \left(\frac{T_{xf}}{T_{yf}} \right)^{1/2} \right) \tag{35}$$

The values of X_B,Y_B and d_B described by equations 32, 33, and 34, respectively, can be substituted into equations 26 and 27 for a description of equipotentials and streamlines in an anisotropic system where the major axis is not aligned with the doublet-well axis.

Figures 39 and 40 illustrate the flow net for the solution to equations 26 and 27 for the Ironton and Galesville Sandstones and the upper part of the Franconia Formation, respectively. It was generated using the average horizontal hydraulic-conductivity data in table 9 and for rates of 15.1 L/s for the Ironton and Galesville Sandstones and 3.8 L/s for the upper part of the Franconia Formation. The equipotentials and streamlines illustrated in figures 39 and 40 are the steady-state solution to the two-dimensional isothermal flow in a homogeneous, confined, infinite, anisotropic aquifer that has no regional hydraulic gradient. For practical purposes, the Franconia-Ironton-Galesville aquifer may be treated as infinite, because it has no lateral boundaries within several miles (Kanivetsky, 1979). The regional gradient, as discussed earlier in this report, has been estimated as less than 10^{-3}, which here is taken to be negligible. As described earlier, the Ironton and Galesville Sandstones are effectively confined above by the lower part of the Franconia Formation, because the transmissivity of the lower part of the Franconia Formation is approximately one order of magnitude less than the transmissivity of Ironton and Galesville Sandstones. The upper part of the Franconia Formation also is confined below by the lower part of the Franconia Formation.

The finite-difference model grid was aligned with the principal axes of transmissivity, with the horizontal-coordinate direction being the direction of the maximum transmissivity. The origin of the field coordinate system shown in figures 39 and 40 was arbitrarily chosen to be halfway between the wells.

A finite-difference grid for a ground-water-flow model generally is constructed with cells as large as possible to reduce computer storage requirements and computation time while maintaining adequate discretization in space. The maximum cell size is determined by the nature of the finite-difference approximation of the ground-water flow and(or) transport equations. For the solution of transport equations, large cell dimensions may cause oscillations in the distribution of the transported quantity in space. In order to remedy this, Intercomp (1976) suggests restrictions on the selection of cell sizes based on the approximate value of the hydrodynamic dispersivity. The restriction is that the cell size should be less than twice the value of dispersivity.

Although it is possible to construct a finite-difference grid that would encompass the entire area illustrated in figures 39 and 40 and would accurately simulate the doublet-well system, the number of resulting cells and corresponding calculations would be too costly to model with the SWIP code. However, the flow-net analysis described previously makes it possible to reduce the modeled area and simulate flow only in the area around the injection well, the flow region of greatest concern where energy transport is most prominent. Flow outside this region is represented with prescribed fluxes at model boundaries determined by flow-net analysis.

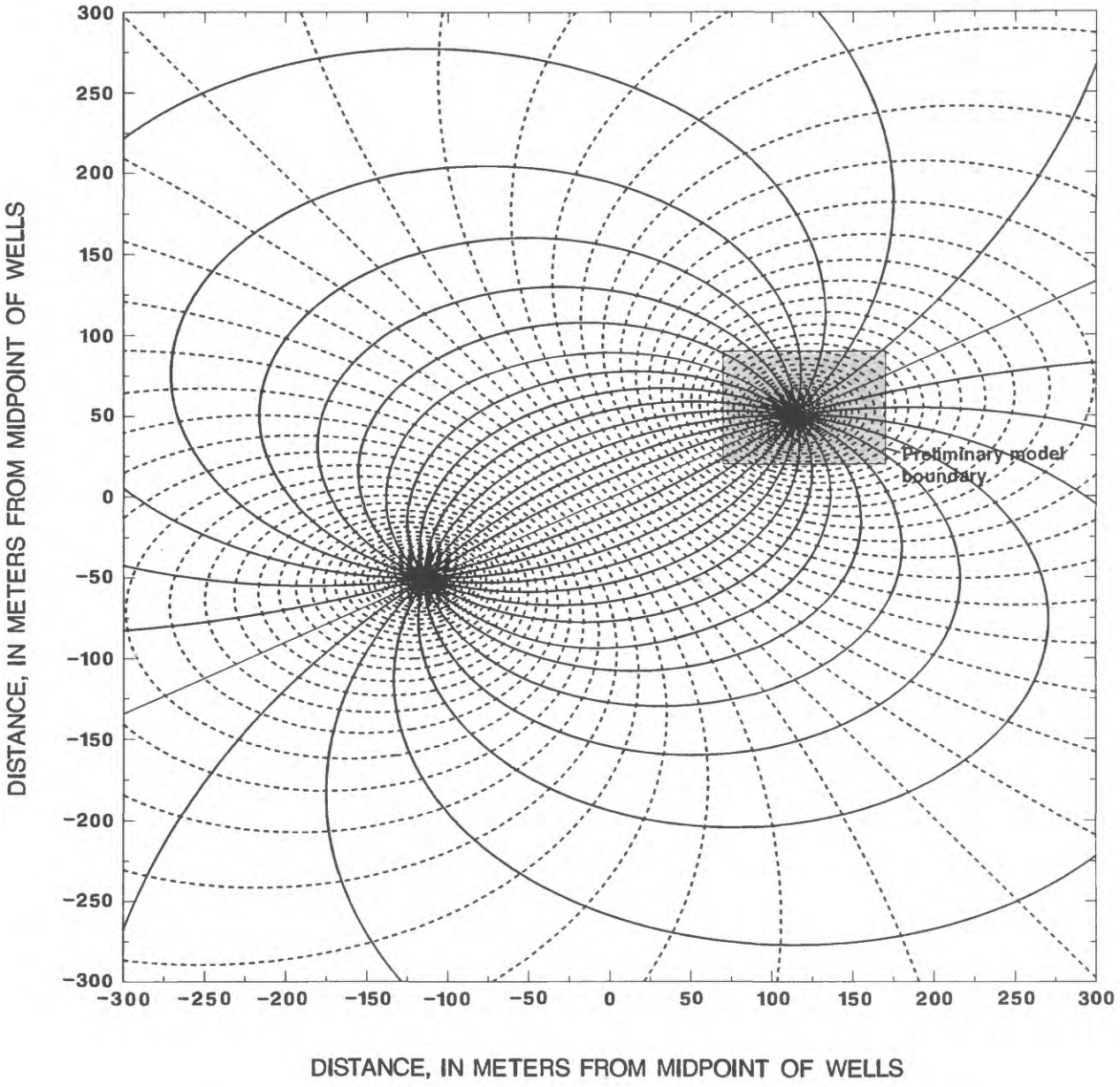

Figure 39.--Flow net for the Ironton and Galesville Sandstones for the Aquifer Thermal-Energy Storage doublet-well system showing the modeled area near production well A.

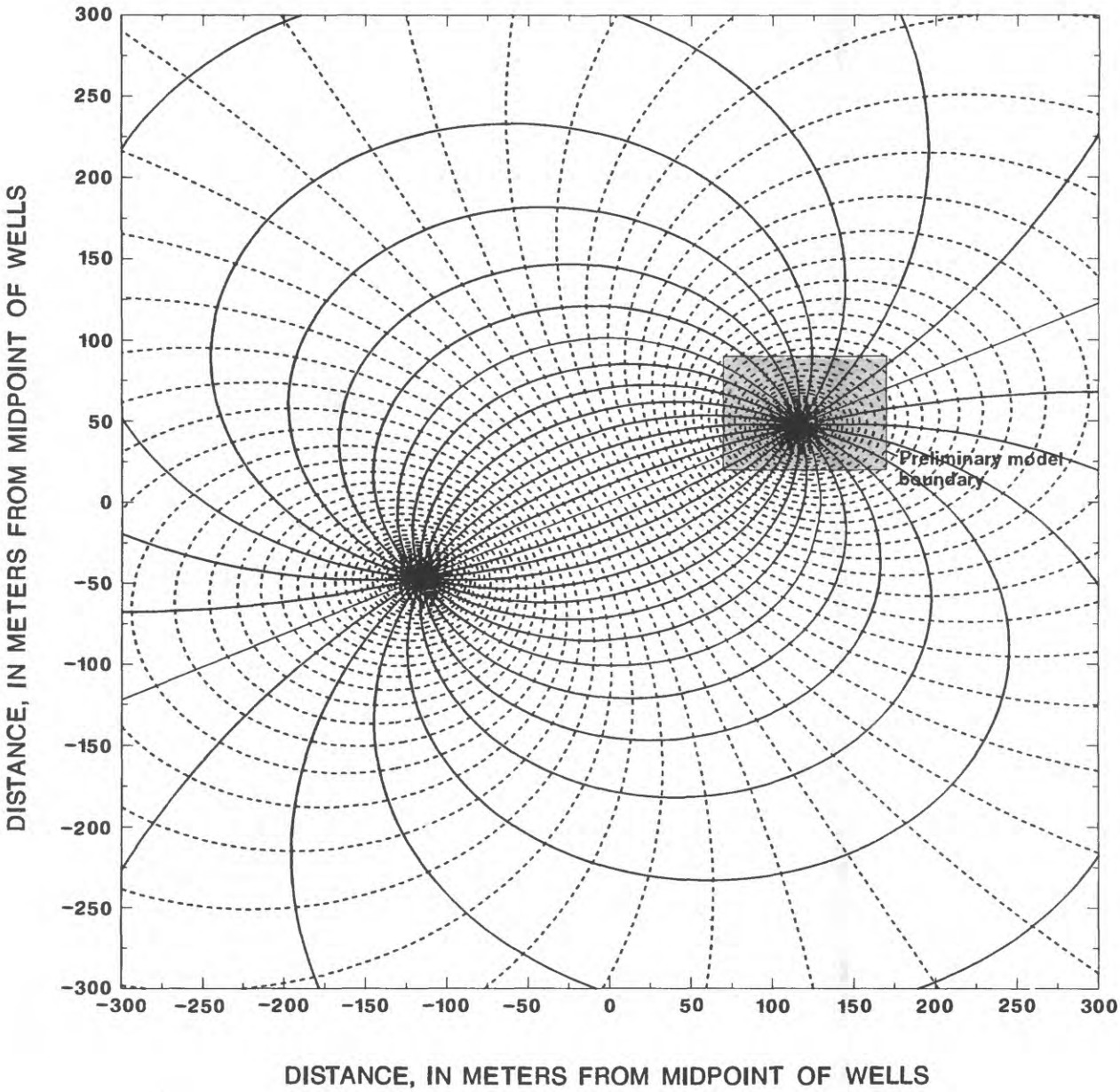

Figure 40.--Flow net for the upper part of the Franconia Formation for the Aquifer Thermal-Energy Storage doublet-well system showing the location of the modeled area near production well A.

Figures 41 and 42 illustrate an enlargement of the boxed flow field around the injection well shown in figures 39 and 40, respectively. Because of restrictions on grid size for solution accuracy and stability based on a central-difference-space and backward-difference-time solution method used in the SWIP code (Intercomp, 1976), a variable grid of 22 rows and 27 columns was designed. Cell sizes range from 0.3 m x 0.3 m in the center of the grid at the injection well to a maximum of 4.6 m x 4.6 m, increasing in all directions equally by a factor of 1.5 or less. The model grid covers about 4,800 m^2 and has 594 cells per layer. A three-dimensional view of the finite-difference grid is illustrated in figure 43.

Vertical grid spacings were selected to correspond with the 4 hydraulic zones in the aquifer and with the overlying and underlying confining beds. Table 11 summarizes the vertical grid spacing by model layer number shown in figure 43, the thickness of the layer, and the corresponding hydrogeologic unit. The lateral boundaries of the model correspond to the 10-m equipotential for the Ironton and Galesville Sandstones (fig. 41) and to the 2.9-m equipotential for the upper part of the Franconia Formation (fig. 42). These are internal model boundaries and require specified flux rates if they are to behave as though they were located in the flow field shown in figures 39 and 40.

Table 11.--***Layer number, thickness, and corresponding hydrogeologic unit of vertical grid spacing for the three-dimensional model***

Layer	Thickness (meters)	Hydrogeologic unit
1	7.6	St. Lawrence Formation (confining bed)
2	13.7	Upper part of the Franconia Formation (aquifer)
3	24.4	Lower part of the Franconia Formation (confining bed)
4	15.2	Ironton Sandstone (aquifer)
5	6.1	Galesville Sandstone (aquifer)
6	30.5	Eau Claire Formation (confining bed)

Flux Calculation at Model Boundaries

The correct boundary fluxes may be determined based on an analysis of the flow net for steady-state conditions. The total flow crossing an equipotential is equal to the injection rate and is thus known, also, equal-portion flow occurs in each streamtube. Therefore, assuming quasi-steady flow, the distribution of fluxes along an equipotential is known for any injection history.

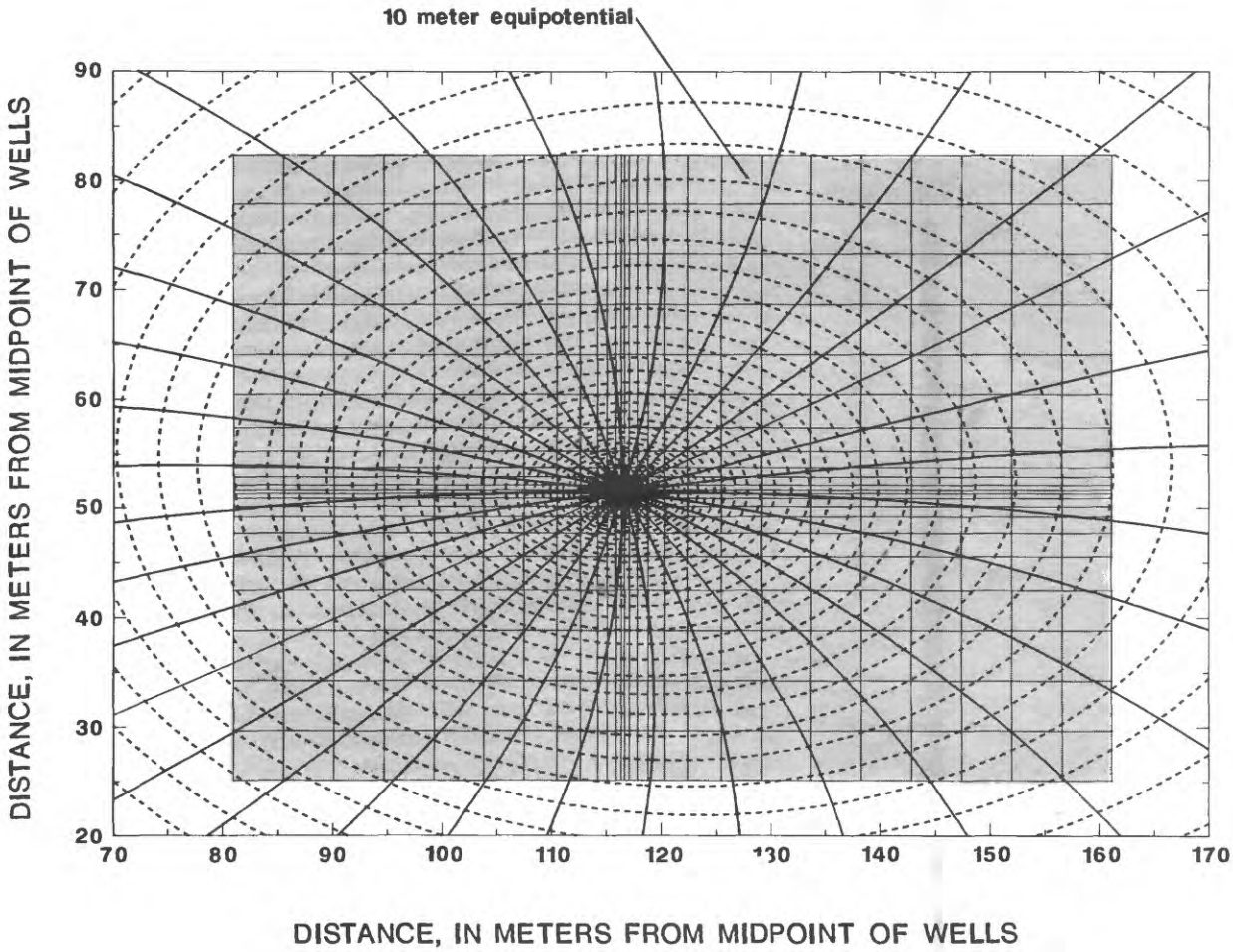

Figure 41.--Model grid superimposed over flow net for the Ironton and Galesville Sandstones near the injection well.

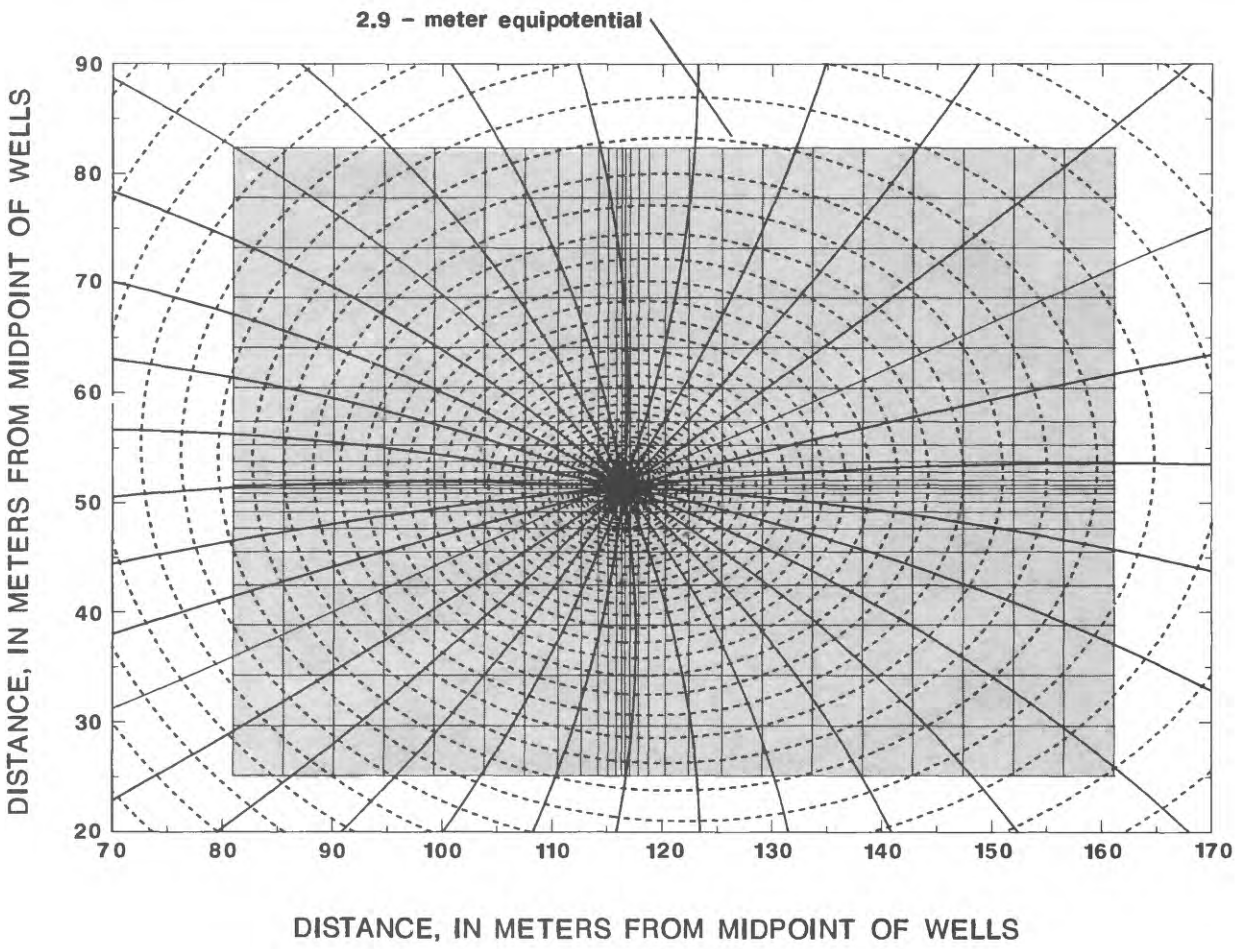

Figure 42.--Model grid superimposed over flow net for the upper part of the Franconia Formation near the injection well.

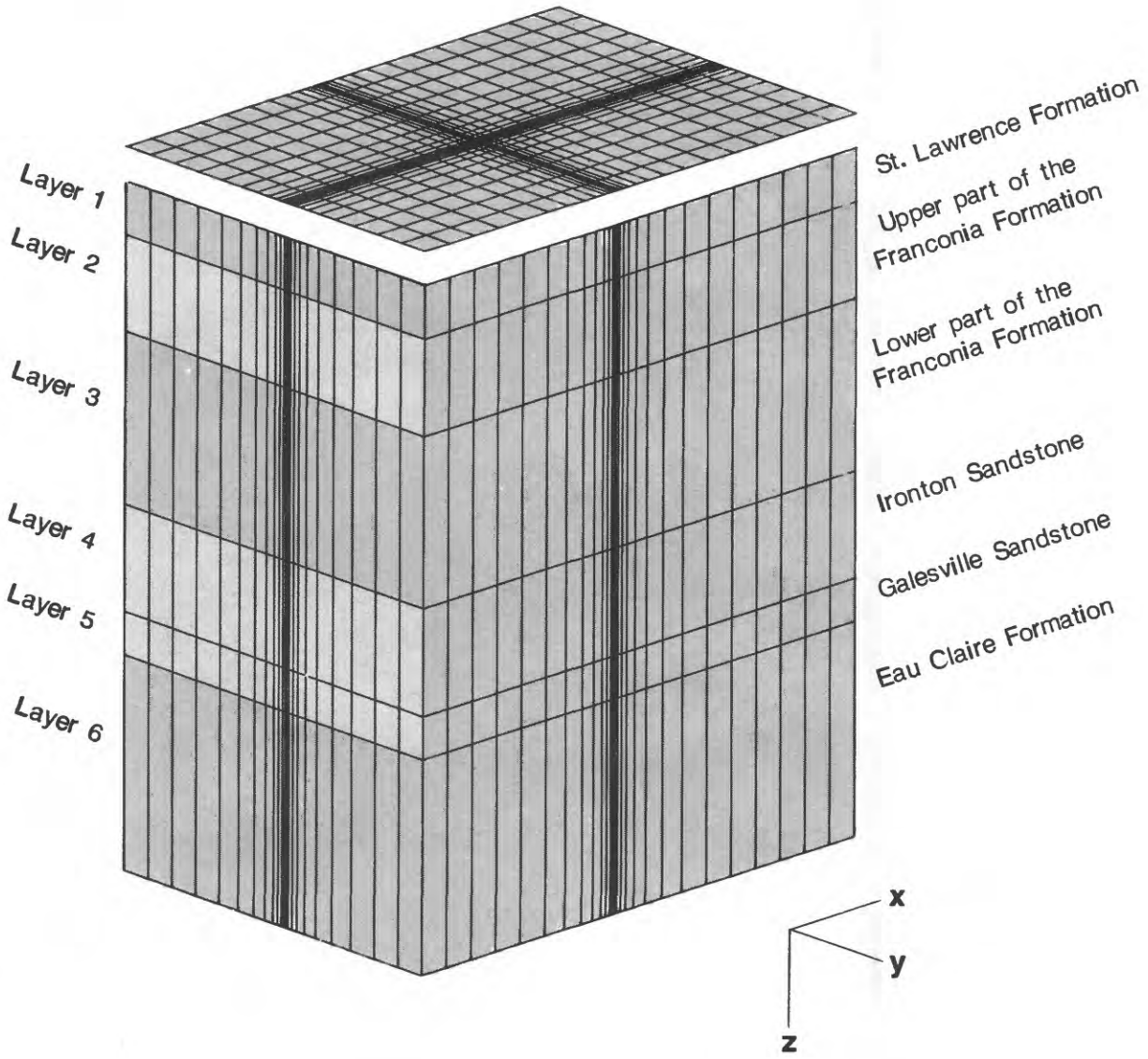

Figure 43.--Finite-difference grid with variable grid spacing.

One form of boundary-flux specification allowed by the SWIP code Intercomp, (1976, p. 3.13) code is:

$$ew_{ij}(t) = \alpha_{ij}V(P_I - P_{ij}^{n+1}) \quad (36)$$

where:

ew_{ij} is the fluid influx rate at boundary cell i,j [L^3/T] (m^3/s),

α_{ij} is a constant factor that gives the fraction of the entire grid boundary that cell i,j represents [dimensionless],

V is an aquifer flux coefficient [$L^3/T\text{-}(M/L\text{-}T^2)$] ($m^3/s\text{-}Pa$),

P_I is a fixed pressure at some distance outside the aquifer model boundary [$M/L\text{-}T^2$] (Pa),

P_{ij}^{n+1} is the pressure in boundary cell i,j at time of the (n+1)th time step [$M/L\text{-}T^2$] (Pa).

For an infinite aquifer, P_I is maintained at the initial system pressure before pumping. For simulation of the doublet-well system, the initial pressure (P_{ij}) is maintained at all times along a locus somewhere between the wells. In a homogeneous isotropic aquifer this locus would be the perpendicular bisector of the well axis. However, in the anisotropic Franconia-Ironton-Galesville aquifer, the locus is not along a line perpendicular to the well axis, but rather along a line at an oblique angle to the well axis (see figures 39 and 40). Thus the coefficient, V, is calculated with equation 36 for an equipotential by letting: P_I equal initial pressure, α_{ij}=1 (representing the entire boundary, ew_{ij} equal the steady injection rate, and P_{ij}^{n+1} equal the steady-state pressure at the equipotential. Values of V were calculated for the 10-m equipotential shown in figure 38 for the Ironton and Galesville Sandstones and the 2.9-m for the upper part of the Franconia Formation, as 12.6 and 3.8 m^3/d-kPa, respectively. Noting that the 32 streamtubes illustrated in figures 41 and 42 all have equal rates of flow, values for α_{ij} were determined around the model boundary for each model layer based on the number of streamtubes that each boundary cell intersects. The respective equipotential boundaries were simulated by the model with the flux boundaries illustrated in figure 44.

Model Calibration for Isothermal Conditions

Data from an 8-day, ambient-temperature injection test at 18.9 L/s were used for model calibration. Table 12 summarizes the hydraulic data by model layer used for isothermal calibration. Pressure changes in production well A and observation well AM2 are compared to model-computed values in figure 45.

The data shown in figure 45 indicate that model results approximate the field-test data, and that the boundary fluxes are adequately described by equation 36. Model results also indicate that the method of apportioning flow at the model boundary by flow-net analysis reasonably represents the doublet-well flow field in the anisotropic aquifer. Based on the flow-net analysis

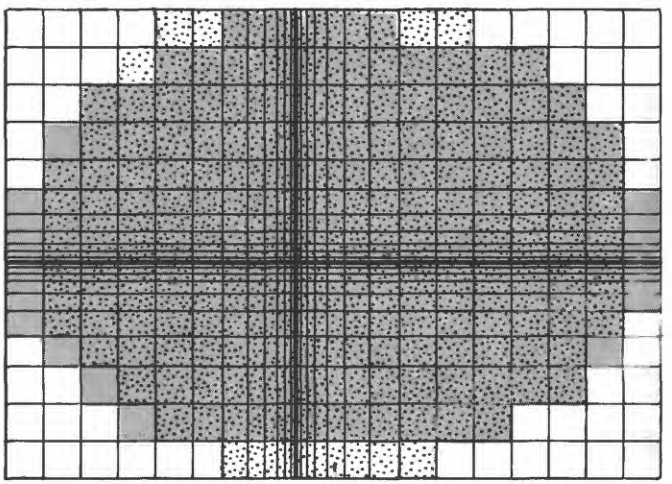

EXPLANATION

Model area:

Layers 1–3

Layers 4–6

Figure 44.--Location of lateral internal flux boundaries for model layers 1 to 3 and 4 to 6.

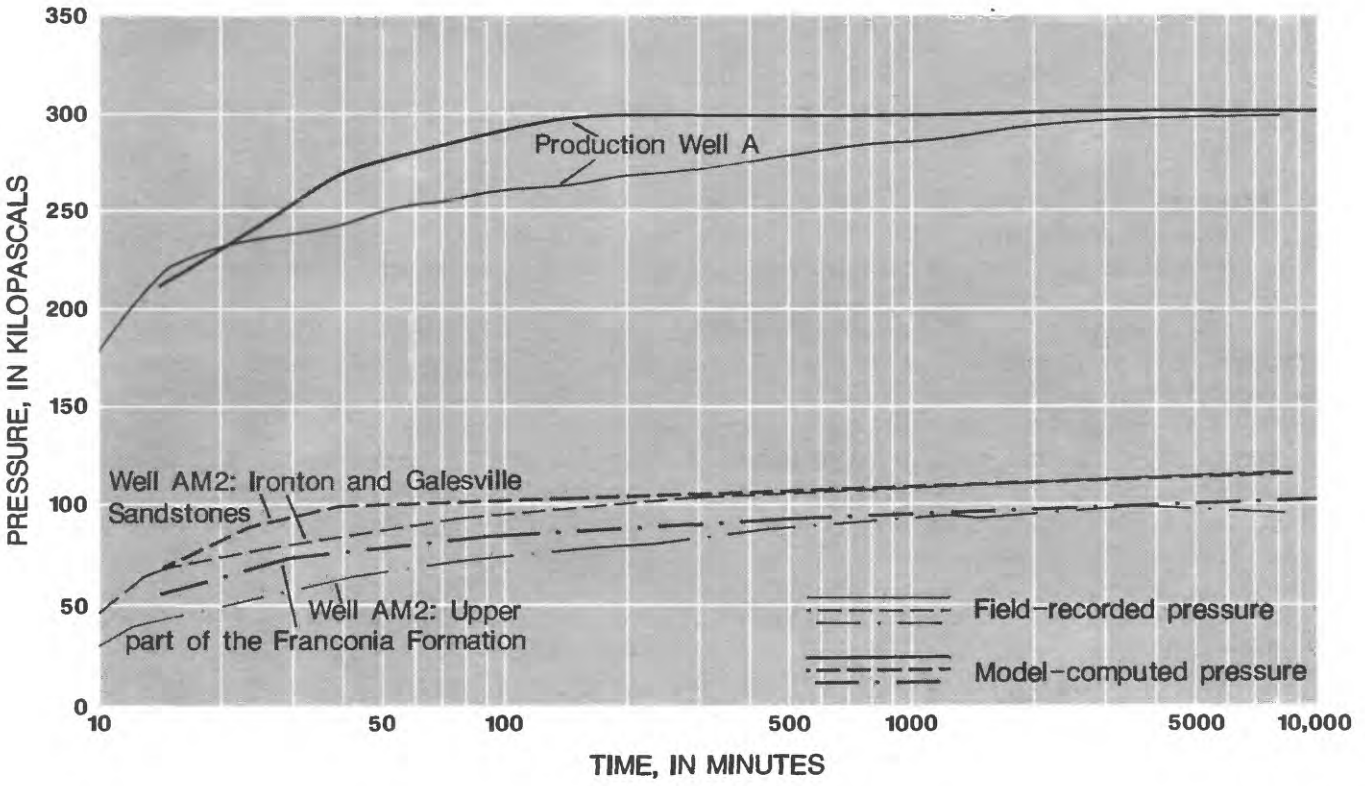

Figure 45.--Model-computed and field-recorded pressure changes in production well A and observation well AM2.

Table 12.--*Hydraulic data by model layer*

Model layer	Hydraulic conductivity in meters per day K_x	K_y	K_z	Porosity (percent)
1	0.003	0.003	0.00003	26.8
2	2.89	1.71	.222	28.2
3	.03	.03	.0003	27.3
4	5.78	2.51	.380	25.2
5	1.45	.628	.095	25.6
6	.003	.003	.00003	31.6

of various conditions of injection and withdrawal, the lateral extent of the finite-difference grid around the injection well can be varied. The system can be modeled in an economical and yet physically meaningful manner.

Application of the model to nonisothermal simulations, with boundary fluxes determined from isothermal flow-net analysis, is predicated on the assumption that the equipotential near the boundary does not change significantly in shape due to temperature changes during hot-water injection. To examine this assumption, 8 days of injection of 150 °C water at 18.9 L/s was simulated using the isothermal calibrated model. Equipotentials in the Ironton and Galesville Sandstones were constructed from computed pressure data and compared with the equipotential from the flow-net analysis (fig. 46). The temperature along the model boundary was approximately 38 °C. Figure 46 shows that the shape and position of the 10-m equipotential for simulated hot-water injection to be similar in shape and position to that derived from the flow-net analysis of the injection of ambient-temperature water. It may be that injection and withdrawal rates will not remain constant at the planned 18.9 L/s rate during hot-water testing, due to limitations of the above-ground piping and the need for system maintenance. However, the rates are not expected to fluctuate more than about 3 percent, or 0.6 L/s. Although it is possible to account for transient changes in the injection/withdrawal rates, with the SWIP Code it is not possible to redefine the boundary-fluxes condition to accommodate these rate changes to determine the sensitivity of model computed heads to changes in injection/withdrawal rates. Two different 24-day test cycles at injection/withdrawals rates of 15.8 and 22.1 L/s were simulated and compared with computed heads for an injection/withdrawal rate of 18.9 L/s. All three simulations had flux-boundary conditions determined for an injection/withdrawal rate of 18.9 L/s.

Table 13 summarizes the model-computed head-change data in wells AM2 and AM3 for the injection/withdrawals rates of 15.8 and 22.1 L/s. The values represent the computed change in head for the respective rate as compared to the computed head for the 18.9 L/s rate. Negative values indicate lower computed heads and positive values higher computed heads. The grid locations chosen for comparison correspond to the approximate locations of monitoring wells AM2 and AM3, which will be used for model calibrations.

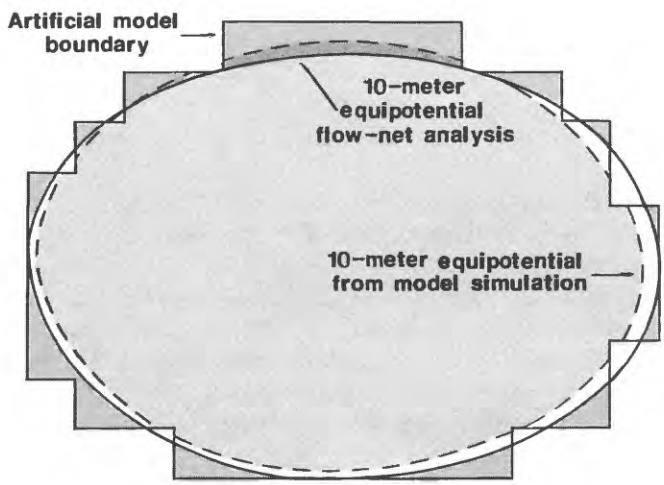

Figure 46.--Comparison of shape of lines of equipotential after 8 days of injection of ambient temperatures and 150 degrees Celsius water at 18.9 liters per second.

Table 13.--*Difference in computed heads for injection/withdrawal rates of 15.8 and 22.1 liters per second as compared to 18.9 liters per second for a flux-boundary condition determined for 18.9 liters per second*

Well number	Computed head change, in meters			
	Rate of 15.8 liters per second		Rate of 22.1 liters per second	
	Injection	Withdrawal	Injection	Withdrawal
AM2	-2.88	-1.85	+2.87	+1.86
AM3	-2.38	-1.92	+2.40	+1.91

The model-computed head changes in table 13 indicate that large head differences may be computed by the model if the model boundary-flux conditions are not determined by a representative rate. The results also suggest that head differences may directly correlate to changes in flow rate regardless of flow direction. The head-change results indicate that the model boundary fluxes are valid for at least relatively short injection periods. It will be necessary, however, to increase the model region if the shape of the equipotentials near the internal model boundary is affected by temperature during longer simulated periods of injection.

SUMMARY

In May 1980, the University of Minnesota began an ATES (Aquifer Thermal-Energy Storage) study on the St. Paul campus. The ATES system uses a doublet-well design with an injection/withdrawal-well spacing of approximately 250 m. Hot water (150 °C) will be injected into the deep (180 to 240 m) Franconia-Ironton-Galesville aquifer, a consolidated sandstone. The aquifer is confined above by the St. Lawrence Formation, a dolomitic sandstone, and below by the Eau Claire Formation, a shale. Short-term testing will consist of 8 days of injection at 18.9 L/s of 150 °C water, 8 days of storage, and 8 days of withdrawal of heated water at 18.9 L/s.

Monitoring-well locations were determined by using an analytical one-dimensional radial-flow model. Temperature and pressure within the aquifer and the overlying and underlying confining layers are measured at four monitoring wells, two at distances of 7 m and two at distances of 14 m. During testing, pressure at 22 points and temperatures at 56 points are recorded automatically by a central data logger and stored on magnetic tape.

Methods to determine the hydraulic characteristics of the aquifer included packer testing, borehole-geophysical logging, core sampling, step-drawdown tests, constant-rate aquifer tests, laboratory tests on core samples for permeability and effective porosity, and ambient-temperature water-injection testing. Packer-test results indicate that the aquifer can be divided into four zones based on values of relative horizontal hydraulic conductivity. Aquifer tests indicate the aquifer is anisotropic. Major and minor

transmissivities are 101.5 and 44.6 m^2/d, respectively, for the Ironton and Galesville Sandstones and 40.0 and 24.0 m^2/d, respectively, for the upper part of the Franconia Formation. The average effective porosity for the Franconia-Ironton-Galesville aquifer ranges from 25 to 31 percent and the average storage coefficient is 4.5×10^{-5}.

Results of ambient-temperature water-injection tests indicate that the aquifer approaches steady-state conditions within one day for an injection rate of approximately 19 L/s.

A preliminary radial-flow model for ground-water flow and thermal-energy transport was constructed using a code developed for waste injection problems. Vertically the model consists of 6 layers ranging from approximately 6-m to 30-m thick, which simulate the aquifer and the confining layers.

Sensitivity analysis was performed on the preliminary radial-flow and thermal-energy-transport model for hydraulic conductivity , porosity, the ratio of horizontal hydraulic conductivity (K_H) to vertical hydraulic conductivity (K_H), rock-thermal conductivity, rock-heat capacity, and thermal dispersivity. Each simulation consisted of 8 days of injection at 18.9 L/s of 150 °C water, 8 days of storage, and 8 days of withdrawal at 18.9 L/s for one complete 24-day cycle. Individual model properties were varied from the assumed base values and plots of model-computed temperature versus time were constructed at a radial distance of approximately 6.5 m from the well bore. The resultant curves then were compared with each other and with those for other model properties to determine model sensitivity in terms of calculated temperature and aquifer thermal efficiency. Model results indicate that hydraulic and thermal properties may be ranked in terms of increasing model sensitivity as follows: ratio of K_H to K_V, rock-thermal conductivity, hydraulic conductivity, porosity, rock-heat capacity, and thermal dispersivity.

The preliminary radial-flow and thermal-energy-transport model was used to study the potential effects of thermal convection, termed buoyancy flow, that are due to density differences between the cooler ambient-temperature ground water and the heated injection water. Eight-day injection of 150 °C water at 18.9 L/s, storage, and withdrawal at 18.9 L/s were simulated. Values of hydraulic conductivity and the ratio of horizontal to vertical hydraulic conductivity were individually varied by an order of magnitude. Vertical profiles of temperature were constructed at the end of injection, storage, and withdrawal at a radial distance of 6.5 m. Tilting of the thermal front caused by buoyancy flow was not apparent in the temperature profiles at the end of injection, storage, or withdrawal for the assumed base values of hydraulic and thermal properties. The simulation of horizontal hydraulic conductivity at 10 times the base value and K_V equal to K_H resulted in significant tilting of the thermal front at the end of storage and withdrawal, indicating the importance of accurate data collection and analyses for these two hydraulic properties.

The preliminary radial-flow and thermal-energy-transport model also was used to examine the effects on aquifer thermal efficiency of hypothetical test cycles that consist of various periods and rates of injection and withdrawal of hot water. Simulations consisted of five injection/withdrawal cycles of 1-year durations each representing a total of 5 years of system operation. In all simulations, injection was 18.9 L/s of 150 °C water. Aquifer thermal

efficiency was calculated as total energy withdrawn divided by total energy injected. The least-efficient cycle simulated consisted of 8 months of injection at 18.9 L/s and 4 months of withdrawal at 18.9 L/s. The aquifer efficiency computed at the end of the fifth cycle was 39 percent and the final well-bore temperature was 105 °C. The most efficient simulation consists of 6-months injection at 18.9 L/s and 6-months withdrawal at 37.8 L/s. The computed efficiency after 5 cycles was 84 percent, and the final well-bore temperature was 45 °C.

A three-dimensional, nonisothermal, ground-water flow and thermal-energy-transport model was constructed to account for the anisotropic characteristics of the Franconia-Ironton-Galesville aquifer. The model consists of 27 columns, 22 rows, and 6 layers and covers about 4,800 m^2. The six model layers represent the four hydraulic zones in the aquifer and the upper and lower confining layers.

Equipotentials and streamlines from a flow-net analysis of a doublet-well system in an infinite, isotropic aquifer were modified to account for field conditions. The modifications of the radial flow model include rotation of coordinate axes and transposition from an isotropic to an anisotropic condition.

Examination of a flow net for the Ironton and Galesville Sandstones indicates that approximate symmetry is not available to reduce the size of the finite-difference model grid, and that a model of the entire doublet-well system would be costly. An alternative method is to design a model grid for an area near the injection well where significant transport occurs, and to specify water fluxes at an internal model boundary to simulate the effect of the remaining flow field.

A method for calculating water flux in the midst of the flow field combined with known steady-state equipotentials was used to calculate model-boundary fluxes. The model boundary then was subdivided into individual equal-flux segments, and water flux at each boundary cell was computed based on the number of stream tubes that intersect each cell.

The validity of model-boundary fluxes determined from flow-net analyses was tested by simulation of an ambient-temperature injection test. The model satisfactorily simulated field-reported pressure changes observed in two piezometers for 8 days of ambient-temperature injection at 18.9 L/s. Applicability of the model boundary fluxes to non-isothermal flow was examined by simulating 8 days of injection of 150 °C water at 18.9 L/s and comparing the resultant 10-m equipotential with that from flow-net analysis. The shape and location of the equipotentials were not significantly changed for the period of simulation and, thus, the fluxes across the boundary were considered to be adequate for representation of the large-scale flow field. The finite-difference grid and the boundary fluxes can be modified to simulate other injection/withdrawal conditions for the doublet-well system as needed.

REFERENCES CITED

Bear, J., 1972, Dynamics of fluids in porous media: Elsevier, New York, 764 p.

Birch, F., and Clark, H., 1940, The thermal conductivity of rocks and its dependence upon temperature and composition: American Journal of Science, v. 238, no. 9, p. 614-635.

Clark, S.P., 1966, Handbook of physical constants: Geological Society of America Memoir 97, 587 p.

Cooper, H.H., Jr., 1963, Type curves for nonsteady radial flow in an infinite leaky artesian aquifer *in* Bentall, Ray, ed., Shortcuts and special problems in aquifer tests: U.S. Geolgical Survey Water Supply Paper 1545-C, p. C48-C55.

Czarnecki, J.B., 1983, Fortran computer programs to plot and process aquifer pressure and temperature data: U.S. Geological Survey Water-Resources Investigations Report 85-4051, 49 p.

Czarnecki, J.B., and Craig, R.W., 1985, Computer notes--a program to calculate aquifer transmissivity from specific-capacity data for programmable calculators: Groundwater, v. 23, no. 5, p. 667-672.

Freeze, A.R., and Cherry, J.A., 1979, Ground water: Englewood Cliffs, New Jersey, Prentice-Hall Inc., 604 p.

Foxworthy, B.L., 1970, Hydrologic consideration and artificial recharge through a well in Salem Heights area of Salem, Oregon: U.S. Geological Survey Water-Supply paper 1594-F.

Foxworthy, B.L., and Bryant, C.T., 1967, Artificial recharge through a well tapping basalt aquifers at the Dalles, Oregon: U.S. Geological Survey Water-Supply Paper 1594-E, 55 p.

Gringarten, A.C., and Sauty, J.P., 1975, A theoretical study of heat extraction from aquifers with uniform regional flow: Journal of Geophysical Research, v. 80, no. 35, p. 4956-4962.

Guyton, W.F., 1946, Artificial recharge of glacial sand and gravel with filtered river water at Louisville, Kentucky: Economic Geology, v. XLI (6), p. 644-658.

Harrill, J.R., 1970, Determining the transmissivity from water-level recovery of step-drawdown tests: U.S. Geological Survey Professional Paper 700-C, p. C212-213.

Hausz, W., 1974, Heat storage in wells: Institute of Gas Technology Symposium, April 17, 1974, Chicago, Illinois, 8 p.

Hellgeson, H.C., Delaney, J.M., Nesbitt, H.W., and Bird, D.K., 1978, Summary and critique of the thermodynamic properties of rock forming minerals: American Journal of Science, v. 278-A, 229 p.

Hellstrom, G., Tsang, Chin-Gu, and Claesson, Johan, 1979, Heat storage in aquifers. Buoyancy flow and thermal stratification problems: Lund University, Sweden, p. 70.

Intercomp Resources Development and Engineering, Inc., 1976, A model for calculating effects of liquid waste disposal in deep saline aquifers: U.S. Geological Survey Water-Resources Investigations Report 76-61.

Kanivetsky, R., 1979, Hydrogeologic map of Minnesota, bedrock hydrogeology: Minnesota Geological Survey State Map Series, Map S-2, 1 pl.

Kazmann, R.G., 1971, Exotic uses of aquifers: Proceedings of American Society of Civil Engineers, v. 97 (IR3), p. 515-522.

Lawrence Berkeley Laboratory, 1978, Thermal Energy Storage in aquifers: Lawrence Berkeley Laboratory Publication LBL, Report 8431.

Labadie, J.W., and Helweg, O.J., 1975, Step-drawdown test analysis by computer: Ground Water, v. 13, no. 5, p. 438-444.

Leggette, R.M., and Brashears, M.L., Jr., 1938, Ground-water for air conditioning on Long Island, New York: Transactions of the American Geophysical Union, p. 412-418.

Lohman, S.W., 1972, Ground-water hydraulics: U.S. Geological Survey Professional Paper 708, 70 p.

Martin, W.L. and Dew, J.N., 1965, How to calculate air requirements for forward combustion: Petroleum Engineer, February 1965.

Mercer, J.W., Faust, C.R., and Miller, W.J., 1980, Review of simulation techniques for aquifer thermal energy storage (ATES), Battelle Pacific Northwest Labs., PNL-3769, p. 183.

Meyer, C.F., and Todd, D.K., 1973, Conserving energy with heat storage wells: Environmental Science and Technology, v. 7, no. 6, p. 512-516.

Meyer, C.F., Todd, D.K., and Hare, R.C., 1976, Role of heat storage wells in future U.S. energy systems: General Electric TEMPO, GE76TMP-27A.

Miller, R.T., 1984, Anisotropy of the Ironton-Galesville Sandstones near a thermal-energy-storage well, St. Paul, Minnesota: Groundwater, v. 22, no. 5, p. 532-537.

Miller, R.T., and Voss, C.I., 1986, Finite-difference grid for a doublet well in an anisotropic aquifer: Groundwater, v. 24, no. 4, p. 490-496.

Molz, F.J., Warman, J.C., and Jones, T.E., 1978, Aquifer storage of heated water: Part I-A field experiment: Ground Water, v. 16, no. 4, p. 234-241.

Norvitch, R.F., Ross, T.G., and Brietkrietz, Alex, 1973, Water resources outlook for the Minneapolis-St. Paul Metropolitan Area, Minnesota: Metropolitan Council of the Twin Cities, 219 p.

Norvitch, R.F. and Walton, M.S., eds., 1979, Geology and hydrologic aspects of tunneling in the Twin Cities area, Minnesota: U.S. Geological Survey Miscellaneous Map Series, Map 1157, 7 sheets.

Papadapulos, I.S., 1966, Nonsteady flow to a well in an infinite anisotropic aquifer: International Association of Scientific Hydrology, Proceedings of Dubrovinik Symposium, v. 1, publ. no. 73, p. 21-31.

Reeder, H.O., Wood, W.W., Ehrlich, G.G., and Sun, R.J., 1976, Artificial recharge through a well in fissured carbonate rock, West St. Paul, Minnesota: U.S. Geological Survey Water-Supply Paper 2004, 80 p.

Robie, R.A., Hemmingway, B.S., and Fisher, J.R., 1978, Thermodynamic properties of minerals and related substances at 298.15 ^{o}K and 1 Bar (105 pascals) pressure and at higher temperatures: U.S. Geological Survey Bulletin 1452, 456 p.

Rorabaugh, M.I., 1953, Graphical and theoretical analysis of step-drawdown tests of artesian wells: ASCE Proceedings, Hydrology Division, v. 79, Dec., 13 p.

Sauty, J.P., Gringarten, A.C., and Landel, P.A., 1979, The effects of thermal dispersion on injection of hot water in aquifers *in* Proceedings of Second Invitational Well Testing Symposium, Lawrence Berkeley Laboratory, Berkeley, California: p. 122-131.

Sniegoki, R.T., 1963, Problems in artificial recharge through wells in the Grand Prairie Region, Arkansas: U.S. Geological Survey Water-Supply Paper 1615-F, 25 p.

Sommerton, W.H., Mehta, M.M., and Dean, G.W., 1965, Thermal alteration of sandstones: Journal of Petroleum Technology, May, p. 589-593.

Theis, C.V., 1935, The relation between the lowering of the piezometric surface and the rate and duration of discharge of a well using ground-water storage: American Geophysical Union Transaction, v. 16, p. 519-524.

Theis, C.V., Brown, R.W., and Meyer, R.R., 1963, Estimating the transmissivity of aquifers from the specific capacity of wells. Methods for determining permeability, transmissivity and drawdown: U.S. Geological Survey Water-Supply Paper 1536-I, p. 331-341.

Tsang, C.F., 1979, A review of current aquifer thermal energy storage projects: Lawrence Berkeley Laboratory, LBL-9834, 21 p.

Walton, M., 1981, The University of Minnesota aquifer thermal-energy storage system *in* Proceedings of the mechanical, magnetic, and underground energy storage, 1981 Annual Contractors Review: U.S. Department of Energy, August 24-26, 1981, Washington D.C.

Werner, D., and Kley, W., 1977, Problems of heat storage in aquifers: Journal of Hydrology, v. 34, p. 35-43.